UNIVERSITY OF CALIFORNIA, SAN DIEGO

Isolation and Characterization of Neuronal Substrates of the Ubiquitin Proteasome System

A dissertation submitted in partial satisfaction of the requirements for

the degree Doctor of Philosophy

in

Biology

by

Jeffrey McCartney Keil

Committee in charge:

Professor Gentry Patrick, Chair
Professor Michael Burkart
Professor Randolph Hampton
Professor Terunaga Nakagawa
Professor Yimin Zou

2011

The dissertation of Jeffrey McCartney Keil is approved, and it is acceptable in quality and form for publication on microfilm and electronically:

_____

_____

_____

_____

_____

Chair

University of California, San Diego

2011

DEDICATION

To my loving parents, Richard and Mary, who made this all possible.

EPIGRAPH

You could tell by the way he talked, though, that he had gone
to school a long time. That was probably what was wrong with him.

John Kennedy Toole (A Confederacy of Dunces)

TABLE OF CONTENTS

LIST OF FIGURES

Chapter I

Chapter II

Chapter III

LIST OF TABLES

Chapter I

ACKNOWLEDGEMENTS

I am grateful to have found Gentry Patrick as a mentor. His outlook on science has shaped my development as a biologist, and has kept me from giving up even when I felt I could give no more. His ever optimistic outlook on science and his willingness to allow his students to explore a project on their own helped me mature as a scientist.

I feel incredibly fortunate to have worked in a lab with such wonderful and supportive people. I would like to thank all the members of the Patrick lab past and present. Special thanks to Tim Foley, Lindsay Schwarz, and Stevan Djakovic for assistance with materials and protocols without which I would have never accomplished any of this. Thanks to the Zhouxin Shen from the Briggs lab and Jeff Savas from the Yates lab for the fantastic mass spec collaborations.

Most importantly, I need to give an immeasurable thanks to the wonderful friends and family who have been with me along the way. Without their encouragement and support, I would have surely succumbed to the abyss that is graduate school.

Chapter I, in part, contains material previously published in Keil, JM, Shen Z, Briggs SP, Patrick GP**.** (2010). Regulation of STIM1 and SOCE by the ubiquitin proteasome system (UPS). *PloS One*. 5(10):e13465

Chapter II, in part, contains material previously published in Keil, JM, Shen Z, Briggs SP, Patrick GP**.** (2010). Regulation of STIM1 and SOCE by the ubiquitin proteasome system (UPS). *PloS One*. 5(10):e13465.,

Chapter III, in part, contains material previously published in Keil, JM, Shen Z, Briggs SP, Patrick GP**.** (2010). Regulation of STIM1 and SOCE by the ubiquitin proteasome system (UPS). *PloS One*. 5(10):e13465.,

VITA AND PUBLICATIONS

2003	Bachelor of Science, The University of Illinois, Urbana-Champaign
2003-2004	Research Technician, The University of Illinois, Urbana-Champaign
2004-2011	Graduate Student, University of California, San Diego
2011	Doctor of Philosophy, University of California, San Diego

Keil JM, Shen Z, Briggs SP, Patrick GN. Regulation of STIM1 and SOCE by the Ubiquitin Proteasome System (UPS). *PLoS One*. 2010 Oct 18;5(10):e13465

ABSTRACT OF THE DISSERTATION

Isolation and Characterization of Neuronal Substrates of the Ubiquitin Proteasome System

by

Jeffrey McCartney Keil

Doctor of Philosophy in Biology

University of California, San Diego, 2011

Professor Gentry Patrick, Chair

The covalent attachment of ubiquitin to proteins is one of the most common regulatory mechanisms in mammalian cells. It regulates numerous cellular processes through a combination of proteolytic and non-proteolytic forms of ubiquitination. In a neuronal context, the UPS has long been implicated in a variety of neurological disorders,

and more recently, in normal neuronal function. Given the potential importance of the UPS in a neuronal framework, a logical step towards better understanding the scope of its function in neurons would involve an examination of the neuronal targets of the UPS. This research began with a large-scale identification of ubiquitinated, neuronal proteins. Using transgenic, His-6-ubiquitin tagged mice, in combination with denaturing nickel-affinity chromatography, we were able to specifically enrich for large amounts of ubiquitinated proteins. We identified over 385 unique proteins, of which 278 passed stringent filters of potential false-positives. With an approximate proteome of 1200 proteins, we concluded that at least 25% of all synaptic proteins were ubiquitinated at a detectable level. Following the screen, I conducted a more in-depth analysis of the more interesting targets. One of the more promising candidates identified was stromal interaction molecule I (STIM1). Characterization of neuronal STIM1 revealed that it was expressed throughout development with stable levels of expression in mature neurons. Furthermore, subpopulations of STIM1 were identified on the surface of hippocampal neurons. Ectopically expressed STIM1 rapidly redistributed into punctate clusters in response to thapsigargin (TG)-induced store-depletion. Proteasome inhibitors significantly increase surface STIM1 levels and peak Ca2+ influx upon TG-induced SOCE. Additionally, overexpression of POSH, an E3 ligase, leads to a decrease in STIM1 surface populations. Together, these results provide compelling evidence for previously undescribed roles of the ubiquitin-proteasome system (UPS) in the regulation of STIM1 and SOCE function. Examination of neuronal Rac1-GEF, kalirin-5, reveals that its stability is affected by CamKII and PP1/2 activity, in a proteasome-dependent

manner. The role of kalirin-5 in the brain is yet unknown, but UPS-mediated regulation may provide a platform from which to pursue future studies.

Chapter I

Isolation and Identification of Novel, Synaptic Substrates of the Ubiquitin Proteasome System

INTRODUCTION

Since its discovery, the ubiquitin-proteasome system (UPS) has been shown to play a critical role in eukaryotic cells. Both degradative and non-degradative forms of ubiquitination have been implicated in a myriad of cellular processes. Depending on the topology of the ubiquitin chain, changes in protein stability, interaction, and localization can be effected (Hochstrasser, 2006). In a neuronal context, the UPS has long been implicated in a variety of neurological disorders. More recently, it has been shown to play a key role aside from neuronal dysfunction (Patrick, 2006; Yi and Ehlers, 2007). The UPS is critical for both the proper function of developing neurons, as well as synaptic viability and plasticity in mature neurons. Given the emerging importance of UPS in a neuronal framework, a logical step towards better understanding the scope of this interplay would involve an examination of the neuronal targets of the UPS.

Protein modification via the covalent attachment of ubiquitin is one of the most common regulatory processes in mammalian cells (See Review by Pickart, 2004) (Pickart, 2004). Classically, ubiquitination is a process whereby target proteins can be marked for degradation by the proteasome. It is a multi-step enzymatic process, using three classes of enzymes (E1s, E2s, and E3s), and involves the sequential transfer of ubiquitin from these enzymes to a lysine residue on the target protein. Both degradative and non-degradative forms of ubiquitination have been implicated in a myriad of cellular processes. Depending on the topology of the ubiquitin chain, changes in protein stability, interaction, and localization can be effected (Hochstrasser, 2006). Specificity of the ubiquitination reaction depends on the later steps of the ubiquitination process. There are a significant but limited number of ubiquitin-carrier enzymes (E2s), and a much larger

number of ubiquitin ligases (E3s). Thus, the ubiquitination enzymes form a hierarchical cascade, where the substrate specificity of the overall ubiquitination reaction depends on the specific E2s and E3s that pair up to ubiquitinate the substrate. In a neuronal context, the UPS has long been implicated in a variety of neurological disorders. More recently, it has been shown to play a key role in normal neuronal function (Patrick, 2006; Yi and Ehlers, 2007). The UPS is critical for both the proper function of developing neurons, as well as synaptic viability and plasticity in mature neurons (DiAntonio, 2004; Patrick, 2006). Several studies have identified key synaptic proteins in mammals that are regulated in a UPS-dependent manner (Colledge et al., 2003; Ehlers, 2003; Hoogenraad et al., 2007; Lee et al., 2008; Pak and Sheng, 2003; Yao et al., 2007). Given the emerging importance of the UPS in a neuronal framework, a logical step towards better understanding the scope of its function in neurons an at synapses would involve an examination of the neuronal targets of the UPS.

Modern mass spectrometry approaches have provided tractability regarding detection and mapping of covalent modifications from large, complex mixtures of proteins. Of the nearly 300 different types of post translational modifications (PTMs), mass spectrometry is one of the few ways poised to identify a large portion of them (Witze et al., 2007). Phosphorylation , acetylation, and more recently, ubiquitination, have become common modifications sought out in mass spectrometry screens. Identifying ubiquitinated residues can be especially challenging. One of the many caveats pertains to the signature Gly-Gly dipeptide created following tryptic digest of the ubiquitin's C-terminus(Marotti et al., 2002), and the fact that cleavage can be suppressed at Gly-Gly-coupled lysines(Peng et al., 2003b). After parsing out identification errors

resulting from tryptic anomalies, the next hurdle to overcome when identifying endogenous ubiquitinated proteins is abundance. For any given protein, the relative abundance of the modified species is only a fraction of the total amount(Peng, 2008) . This issue is partially overcome as mass spectrometry-based technologies achieve subfemtomolar sensitivity(Yates, 2004). However, for proper identification of most ubiquitinated proteins, enrichment strategies must be employed. Typically, these include the use of ubiquitin-binding proteins or epitope-tagged ubiquitin that is overexpressed in the organism of interest(Kirkpatrick et al., 2005a). Peng et al. 2003, describe a method using 6xHis-ubiquitin expressing yeast and liquid chromatography coupled to tandem mass spectrometry (LC/LC-MS/MS) to perform one of the first large-scale screens for ubiquitinated proteins(Peng et al., 2003b). The 6xHis-tagged ubiquitin allowed them to utilize denaturing conditions, and thus greatly limit the amount of non-specific hits. Moreover, parallel analysis of untagged yeast lysates established the background levels of endogenous proteins capable of complexing the nickel-affinity beads. In addition, the chromatography step of LC/LC-MS/MS was spread out over 120 hours, thus allowing for a longer analysis time and a greater number of peptides to be sequenced.

As mentioned earlier, neuronal proteomics provides a valuable platform from which to examine both normal neuronal physiology, as well as neuronal dysfunction. Specifically, the so-called neuronal communication-centers, or synapses, are of particular interest. Pocklington et al., 2006 outlined four major reasons for examining the proteins that comprise the synapse:

I. *It is the most important structure for communication between nerve cells.*

II. *The neurotransmitter receptors and signal transduction machinery within the synapse respond to patterns of electrical activity and instigate biochemical changes in the nerve cell and in so doing modify the brain in response to behavioural experience.*
III. *Synapse proteins correspond to many human disease genes and drug targets for therapeutics that modulate cognitive illnesses.*
IV. *Synapse proteomic studies have compiled a first draft of the protein composition of the synapse, revealing an unexpectedly high degree of molecular complexity. (Pocklington et al., 2006a)*

Synaptic proteomics often utilize purified synaptic preparations, or synaptosomes(Carlin et al., 1980; Cheng et al., 2006; Cho et al., 1992; Collins et al., 2005; Pocklington et al., 2006b; Schrimpf et al., 2005; Whittaker et al., 1964). These artificial organelles, derived from differential density gradient centrifugation, contain complete pre- and post-synaptic terminals, along with mitochondria and synaptic vesicles. Mass spectrometry analyses of the mammalian synaptosome, estimate synaptic proteome at approximately 1100 proteins(Grant, 2006; Schrimpf et al., 2005). As the number of potential proteins to be identified increases, so does the amount of separation and enrichment needed to isolate the post-translationally modified species(Witze et al., 2007). To provide the best possible opportunity to identify the majority of ubiquitinated proteins in the mammalian synapse, a strategy similar to Peng et al., 2003 would need to be employed(Peng et al., 2003b). Transgenic expression of tagged-ubiquitin within a mammalian system, combined with tandem LC- MS/MS approaches will provide the respective enrichment and sensitivity

required to map the synaptic ubiquitinome. In 2001, Tsirigotis et al. developed a tractable mammalian expression system. Similar to the yeast system, a 6xHis-tagged ubiquitin was expressed under the human UbC promoter in a number of tissues, including the brain(Tsirigotis et al., 2001).

Any large-scale screen for ubiquitinated proteins has a number of downstream caveats. Assuming that non-specific hits are minimized, remaining issues such as ubiquitin-site fidelity, ubiquitin topology, and target abundance still must be overcome(Peng, 2008). Although there may be a preferred site, ubiquitination is often promiscuous, with proteins containing multiple lysines capable of accepting ubiquitin (Danielsen et al., 2010). It is of great interest to know the topology of a particular ubiquitin chain, as this informs the fate of the protein. In addition to a N-terminal amine group, there are seven lysines on ubiquitin available for chain elongation – K6, K11, K27, K29, K33, K48, K63(Kirkpatrick et al., 2006; Pickart and Eddins, 2004; Xu and Peng, 2008). The classic poly-ubiquitin linkage, K48, typically marks a protein for degradation by the proteasome (Li and Ye, 2008). K63-linked polyubiquitination, well-established as a regulatory mechanism in NF-κB signaling, plays a greater role in non-proteasomal processes, such as trafficking, protein-protein interactions, and autophagy(Hayden and Ghosh, 2008; Ikeda and Dikic, 2008; Tan et al., 2008; Wooten et al., 2008). Identifying the type of ubiquitin linkage, or chain topology, can be intensive in terms of both cost and time. There are strategies involving the use of linkage specific antibodies and stable isotope labeling of internal linkage standards, but these are not always practical for large-scale screens (Denis et al., 2007; Flick et al., 2004; Newton et al., 2008). In an attempt to maximize the number of substrates identified, while

balancing issues of cost and feasibility, we utilized a genetic and proteomic approach that combines aspects of the aforementioned strategies listed above. As a result, we have isolated and identified a large cohort of novel neuronal substrates of the UPS.

RESULTS

Identification of ubiquitinated proteins from synaptic enriched rat brain fractions

In order to better understand the capacity of UPS function at synapses we developed a genetic and proteomic approach to isolate and identify ubiquitinated proteins (Fig. 1A). Crude washed synaptosomal membrane fractions (P2') were isolated using standard differential and density gradient fractionation methodologies (Carlin et al., 1980; Cho et al., 1992) from whole brain tissues of mice expressing a hexahistidine-tagged ubiquitin GFP fusion transgene under the human UbC promoter (Tg-Ub mice). Cleavage of the fusion protein by endogenous enzymes produced moderate to high levels of the epitope-tagged ubiquitin that is detected both in monomeric form and conjugated to cellular proteins (Tsirigotis et al., 2001). Compared to other synaptic fractions examined, P2 synaptosomal lysates provided an optimum level of synaptic enrichment, while still producing a significant amount of total protein (data not shown). To isolate ubiquitinated proteins from the Tg-Ub synaptosomal fractions we used nickel affinity chromatography under denaturing conditions. Similar fractions from non-transgenic mice were used to control for non-specific binding of proteins to NiNTA resin. Eluted proteins were then precipitated, solubilized, digested and then subjected to tandem mass spectrometry (LC-MS/MS) (See methods section for complete details of the mass spectrometry methods). The raw data was extracted and searched using Spectrum Mill (Agilnet). The resulting MS/MS spectra were filtered and searched against the International Protein Index mouse protein database (version 3.14). To verify that the purification methods were efficient we resolved a sample of the eluted proteins on SDS-PAGE and probed the blot with anti-ubiquitin antibodies. While similar amounts of

ubiquitin immunoreactivity were found in the lysates from non-transgenic and Tg-Ub samples, we observed ubiquitin immunoreactivity (monomeric and conjugated forms) primarily in Tg-Ub samples purified by nickel-affinity chromatography (Fig. 1B). Any non-specific binding would be accounted for downstream following the LC-MS/MS.

Using the spectral abundance of each identified protein from non-transgenic and Tg-Ub samples, we calculated the normalized Tg/WT spectral ratio. Figure 2 is a graphical plot depicting the Tg/WT spec ratio plotted against percent peptide coverage. We considered identified proteins with greater than 10% peptide coverage and a Tg/WT spec ratio greater than 2 to be a synaptic candidate ubiquitinated protein (synCUP) (Fig. 2). Several identified proteins with these criteria have been reported to be ubiquitinated in the literature (Fig. 2 and data not shown). Indeed, the protein identified with the highest Tg/WT spec ratio was ubiquitin, which further corroborated our isolation, identification, and group assignment strategies (Fig. 2). Initially, 911 non-redundant proteins were identified by LC-MS/MS. After filtering out proteins identified in a reverse database lookup, as well as duplicate entries, a total of 385 distinct proteins were identified by the screen; filtering out any target with less than 10% peptide coverage or a Tg/WT below 2, resulted in 279 synaptic ubiquitinated proteins. Functional classification of the top 279 proteins reveals that a wide variety of processes overlap with the ubiquitin proteasome system (Fig. 3). Candidate proteins were classified according the DAVID functional ontology analysis(Huang da et al., 2009a; Huang da et al., 2009b). Table 2 lists the top 40 proteins, as ranked by Tg/WT spectral ratio. At the time of the screen, over half of the top 40 had previously been identified as ubiquitinated (data not shown). Both mono and polyubiquitinated proteins were readily identified in the screen. Smad4

(number 2 on the Top 40), has been shown to be mono-ubiquitinated by a number of groups (Wang et al., 2008)(Table 1). More recently, the O-GlcNAase, OGT (#12), was shown to be polyubiquitinated and degraded by the proteasome(Daou et al., 2011). STIM1, the focus of research expounded upon in Chapter 2, resides at number 35 on the list (Table 2). A complete list of unfiltered, non-redundant proteins can be found in Table 3. Most of the hits, either due to matches found in the reverse database or because of low spectral occurrence (i.e. less than 2 hits), are suspect. However, it is also possible that the population of ubiquitinated species of those particular proteins is incredibly low.

The initial screen for ubiquitinated proteins did not readily inform the type or context of ubiquitination. The ultimate goal when studying the role of the ubiquitin proteasome system in neuronal function is to place ubiquitination within a neuronal-specific activity or developmental paradigm. The most tractable paradigm, in terms of UPS function, is the proteasome-dependent stability of neuronal substrates. Simply looking for a change in ubiquitinated proteins or protein levels in the context of proteasome function is relatively straightforward. Application of any number of commercially available, validated proteasome inhibitors to neurons prior to isolation of ubiquitinated proteins, in theory, should allow for the identification of potential targets of the proteasome. Moreover, it is of great interest to know what type of ubiquitination is occurring. Since targeting of ubiquitinated proteins requires non-K63-linked chains of 4 or more ubiquitins, which are also often K48-linked, then strategies isolating proteasomal-dependent targets can be quite informative(Pickart, 2004). Regarding type of ubiquitination, there are a number of methods that can be coupled with mass spectrometry to identify number and linkage type (see review by (Peng, 2008). One

simple method, using the ubiquitin binding properties of the 19S cap of the proteasome (S5A) allows for purification of poly-ubiquitin proteins that are presumably destined for proteasomal degradation (Deveraux et al., 1994; Glickman et al., 1999; Layfield et al., 2001). Also, the use of rat primary cortical cultures as the source of ubiquitinated material made it possible to directly perturb the cells, and thus examine possible contextual effectors of ubiquitination. Beginning with very basic perturbations, either vehicle alone or proteasome inhibition (MG-132), we prepared P2 fractions and precipitated poly-ubiquitinated proteins using GST-S5A affinity purification. Precipitates were analyzed via Mudpit LC-MS/MS, a mass spectrometry technique that is useful for identifying proteins from large, complex mixtures(Delahunty and Yates, 2007; Washburn et al., 2001). As expected, immunoblot analysis of the lysates and precipitates revealed that a marked increase in total poly-ubiquitin conjugates did not translate into a difference in ubiquitin conjugates isolated by S5A affinity purification (Fig. 4, left panels). Between the two conditions, there was no difference in total lysates, as determined by the non-proteasomal target GluR1 immunoblot, or silver stain (Fig. 4, middle and right panels). Moreover, the total amount of protein precipitated appeared similar, as indicated by both silver stain and ubiquitin immunoblots of S5A eluates (Fig. 3, left panel). This suggests that the S5A beads were saturated in both conditions, and the total amount of ubiquitinated proteins identified by mass spectrometry should be similar. Therefore, any difference between individual ubiquitinated species identified should indicate which proteins are rapidly turned over by the proteasome.

Table 4 lists the top 50 hits obtained via the directed screen for synaptic, proteasomal dependent, poly-ubiquitinated proteins. The list is sorted by spectrum count,

an approximation of abundance. Polyubiquitin is in the top 2 for both lists, demonstrating the efficacy of the screen for isolating polyubiquitinated proteins. Moreover, the MG-132 inhibited samples showed higher spectrum (more than double) counts for polyubiquitin and other ubiquitin complexes (Table 4). Unfortunately, examination of other proteins did not reveal much difference between treatments. A scatterplot of the top 150 targets identified within MG-132 and DMSO treated samples shows a high degree of overlap between the two treatments. A linear regression model was fit to the data, and the P-value, testing the null hypothesis that the slope of the line is zero, and thus there is no correlation between the two, was less than 10^{-16} (Fig. 5). With only one round of isolation and identification, no significance can be applied to the results, and thus all observations are predominantly qualitative. What the data does suggest is that the purification scheme works, in that it can efficiently isolate poly-ubiquitinated proteins. In both treatments, over a 1000 different proteins were identified that had greater than 2 spectral hits (data not shown). There is a great chance that a vast majority of these are true, polyubiquitinated proteins. Due to what is undoubtedly a large, endogenous baseline of polyubiquitinated proteins, this particular method experiences rapid saturation and subsequent loss of precision. Accordingly, no major differences between mock or proteasome-inhibited samples could be identified. Examination of global changes in proteasomal-dependent poly-ubiquitination will require a more quantitative and precise approach.

DISCUSSION

In this study, we developed and implemented methodologies to identify neuronal substrates of the ubiquitin proteasome system (UPS). The initial impetus behind the series of screens that were performed was to understand the scope and composition of ubiquitinated species at the synapse. Accordingly, knowledge of specific UPS substrates should provide platforms from which studies on both normal neuronal physiology and dysfunction could be conducted. Both screens identified a large number of potential substrates of the UPS. The initial screen, employing a genetic and proteomic approach, was indiscriminate in terms of the types of ubiquitinated proteins identified. Both mono and poly-ubiquitinated proteins were precipitated; and presumably, all types of ubiquitin linkages were also present in ratios corresponding to their endogenous proportions. As a result, downstream analysis of individual targets was not as informed as would be the case with more directed screens. Indeed, both mono and poly-ubiquitinated targets, such as STIM1 and Kalirin-7, respectively, were validated in secondary analyses (Fig. 5A and Fig. 18A). The unfiltered, non-redundant proteins numbered over 900 (data not shown), and the estimated synaptic proteome is 1100 proteins(Schrimpf et al., 2005). It should be noted that over 500 of these proteins only had a single spectral hit. Thus, many of these peptides could merely be the result of non-specific binding or improper matches to the protein database. An optimistic conclusion is that the vast majority of synaptic proteins are ubiquitinated. This is actually a reasonable assertion, when viewed from a cellular housekeeping point of view. The UPS is a major quality control pathway within the cell, and at some level, most proteins will undergo ubiquitin mediated degradation eventually.

Even with the conservative estimate of 279 ubiquitinated proteins out of 1100, the scope of the ubiquitin proteasome's role in neuronal function is unquestionable. Indeed, recent work has begun to crystallize the importance the UPS plays in neuronal function and plasticity (Bingol and Sheng, 2011) (Mabb and Ehlers, 2010; Patrick, 2006).

The functional diversity of proteins identified within the screen was large. Kinase/phosphatase pathways represented one of the largest functional groups to appear in the screen, with nearly 13% of all filtered targets falling within this category (Fig 3). Neuronal function depends on the balance of phosphorylation and de-phosphorylation of synaptic proteins (Lee, 2006; Lisman, 1985; Mansuy and Shenolikar, 2006; Wayman et al., 2008). Regulating the stoichiometry of kinases and phosphatases through regulated proteolysis is one way to affect this balance. Moreover, non-proteolytic regulation of kinase/phosphatase cascades has also been shown (Skaug et al., 2009). This data suggests there is likely a large, dynamic interplay between the ubiquitin proteasome system and phosphorylation with regards to neuronal function.

Another functional group that contained a number of promising targets was the actin cytoskeleton group (Fig 3). Actin cytoskeletal dynamics are of great importance in neurobiology because they comprise the structural determinants for synaptic function and plasticity (Cingolani and Goda, 2008; Dent et al., 2010; Dillon and Goda, 2005). The underlying molecular basis for neuronal actin regulation is not yet fully known. Regulation of effectors of actin dynamics, either in terms of stability or function, presents an attractive avenue for future target-based studies. In addition to actin itself, various actin regulators, such as Kalirin, neural specific F-actin binding protein, and various RhoGEFs were identified as candidate ubiquitinated proteins (Lee and Dominguez,

2010). The connection between the UPS and the actin cytoskeleton is examined in greater detail in chapter 3. From this mass spectrometry screen, the major conclusion that can be drawn is that there are a number of effectors of neuronal cytoskeleton dynamics which may be ubiquitinated.

With only one round performed, this screen does leave a bit of doubt regarding the fidelity of the entire list. To date, all targets that have been examined in greater detail have proven to indeed be ubiquitinated. As mentioned earlier, both mono and poly-ubiquitinated substrates have been validated. There would be no reason to assume preference for either type of modification. In either case, thorough downstream investigations and validation will be required. Until replicates are obtained, the most prudent use of the putative targets will focus on the top 300, as they have relatively high sequence coverage and Tg/WT ratios (Table 3). As a first approximation, this screen was quite successful. It provided a large list from which to work, and also highlighted many of the shortcomings of screens of this type. Future screens could benefit by increasing the specificity of the purification and identification. Additional information pertaining to linkage location, type, and abundance on potential targets would ease downstream investigations greatly. In fact, recent screens for ubiquitinated proteins have employed novel methods using linkage specific antibodies and isotopically-labeled internal standards to isolate and quantify ubiquitinated proteins and prospective modified sites (Newton et al., 2008; Xu et al., 2010).

In an attempt to remedy some of the drawbacks of the first screen, we tested an approach that was intended to identify a specific type of ubiquitinated protein – namely, K48-linked poly-ubiquitin conjugated proteins. Given the fact that the initial screen

suggests there is widespread neuronal ubiquitination, we wanted to establish a method that could also uncover context-specific ubiquitination. As such, we also used primary cultures, which were amenable to various perturbations. Using GST-S5A, we were able to efficiently purify poly-ubiquitinated proteins from rat neuronal cultures (Fig. 4). Unfortunately, the poly-ubiquitinated proteins identified by LC-MS/MS did not vary between treatments (Table 4 and Figure 5). The problem that we encountered was two-fold: (a) the GST-S5A beads were saturated at a relatively low amount of total protein, and (b) the baseline levels of ubiquitinated proteins were so high that proteasome inhibition alone could not uncover proteasome-dependent, ubiquitinated substrates. Although it was expected that the beads would be saturated, we assumed that a cohort of proteins would accumulate in a proteasome-dependent manner at levels above other proteins. It must also be noted that if proteasome inhibition cannot enrich for detectable differences in poly-ubiquitinated proteins, then it suggests that other perturbations will certainly not overcome the signal-to-noise present with this method. Newer methods employing internal isotopic standards would allow for a more quantitative comparison of treatments. However, overcoming the saturating levels of poly-ubiquitinated proteins will likely require scaling up the purification.

Chapter I, in part, contains material previously published in Keil, JM, Shen Z, Briggs SP, Patrick GP**.** (2010). Regulation of STIM1 and SOCE by the ubiquitin proteasome system (UPS). *PloS One*. 5(10):e13465.

MATERIALS AND METHODS

Detailed mass spectrometry methodology (Screen 1)

Protein pellets were solubilized in 100uL of 1% RapiGest (Waters) and 50mM NH_4HCO_3 (pH8). The proteins were reduced and alkylated using 2 mM Tris(2-carboxyethyl)phosphine (Fisher, AC36383) at 95°C for 5 minutes and 5 mM iodoacetamide (Fisher, AC12227) at 37°C in dark for 30 minutes, respectively. The proteins were digested with 1 ug trypsin (Roche, 03 708 969 001) overnight. HCl was added to the mixture to precipitate RapiGest (pH1.4). Sample was incubated at 4°C overnight and then centrifuged at 16.1Kg for 15 minutes. Supernatant was collected and passed through a 0.22uM spin filter. The cleared solution was subject to Nano-LC-MS/MS analysis.

Automated 2D nanoflow LC-MS/MS analysis was performed using LTQ tandem mass spectrometer (Thermo Electron Corporation, San Jose, CA) employing automated data-dependent acquisition. An Agilent 1100 HPLC system (Agilent Technologies, Wilmington, DE) was used to deliver a flow rate of 300 nL min^{-1} to the mass spectrometer through a splitter. Chromatographic separation was accomplished using a 3 phase capillary column. Using an in-house constructed pressure cell, 5um Zorbax SB-C18 (Agilent) packing material was packed into a fused silica capillary tubing (200µm ID, 360 um OD, 20 cm long) to form the first dimension RP column (RP1). A similar column (200µm ID, 5 cm long) packed with 5 um PolySulfoethyl (PolyLC) packing material was used as the SCX column. A zero dead volume 1µm filter (Upchurch, M548) was attached to the exit of each column for column packing and connecting. A fused silica capillary (100µm ID, 360 um OD, 20 cm long) packed with 5um Zorbax SB-C18

(Agilent) packing material was used as the analytical column (RP2). One end of the fused silica tubing was pulled to a sharp tip with the ID smaller than 1μm using a laser puller (Sutter P-2000) as the electro-spray tip. The peptide mixtures were loaded onto the RP1 column using the same in-house pressure cell. Peptides were first eluted from RP1 column to SCX column using a 0 to 80% acetonitrile gradient for 150 minutes. Then the peptides were fractionated by the SCX column using a series of 8 salt gradients (20mM, 30mM, 40mM, 50mM, 60mM, 80mM, 100mM, 1M ammonium acetate for 20 minutes), followed by high resolution reverse phase separation using an acetronitrile gradient of 0 to 80% for 120 minutes.

Spectra were acquired on LTQ linear ion trap tandem mass spectrometers (Thermo Electron Corporation, San Jose, CA) employing automated, data-dependent acquisition. The mass spectrometer was operated in positive ion mode with a source temperature of 150 ^{o}C. As a final fractionation step, gas phase separation in the ion trap was employed to separate the peptides into 3 mass classes prior to scanning; the full MS scan range was divided into 3 smaller scan ranges (300-800, 800-1100, and 1100-2000 Da) to improve dynamic range. Each MS scan was followed by 4 MS/MS scans of the most intense ions from the parent MS scan. A dynamic exclusion of 1 minute was used to improve the duty cycle.

The raw data was extracted and searched using Spectrum Mill (Agilnet, version A.03.02). MS/MS spectra with a sequence tag length of 1 or less were considered as poor spectra and discarded. The rest of the MS/MS spectra were searched against the IPI (International Protein Index) mouse protein database (version 3.14). The enzyme parameter was limited to full tryptic peptides with a maximum miscleavage of 1. All

other search parameters were set to SpectrumMill's default settings (carbamidomethylation of cysteines, +/- 2.5 Da for precursor ions, +/- 0.7 Da for fragment ions, and a minimum matched peak intensity of 50%). A concatenated forward-reverse database was constructed to calculate the in-situ false discovery rate (FDR). A total of 3,031 IPI proteins from the forward database were identified, while 102 proteins (3% protein FDR) from the reverse database were identified. Proteins with the same set or subsets of unique peptides were grouped into protein groups to minimize protein redundancy. There were 911 and 26 protein groups (3% FDR) identified from forward and reverse database, respectively.

Table 1. Filtering Criteria for autovalidation of database search results.

mode	Protein score	1+ peptide	2+ peptide	3+ peptide
Protein Details	>20	>9, >50%	>9, >50%	>11, >50%
Peptide	NA	>13, >50%	>13, >50%	>15, >50%

Detailed mass spectrometry methodology (Screen 2)

Sample Preparation

The precipitate was resuspended in 8 M Urea with ProteasMAX (Promega, Madison, WI, USA) per the manufacturer's instruction. The samples were subsequently reduced by 20 minute incubation with 5mM TCEP (*tris*(2 carboxyethyl)phosphine) at room temperature and alkylated in the dark by treatment with 1mM 2-Chloroacetamide for 20 additional minutes. The proteins were digested over-night at 37 degrees with Sequencing Grade Modified Trypsin (Promega, Madison, WI, USA) and the reaction was stopped by acidification.

Multidimensional Protein Identification Technology (MudPIT) and LTQ Orbitrap Mass Spectrometry

The protein digest was pressure-loaded onto a 250--μm i.d capillary packed with 2.5cm of 10-μm Jupiter C18 resin (Phenomenex, Torrance, CA, USA) followed by an additional 2.5cm of 5-μm Partisphere strong cation exchanger (Whatmann, Clifton, NJ). The column was washed with buffer containing 95% water, 5% acetonitrile, and 0.1% formic acid. After washing, a 100--μm i.d capillary with a 5-μm pulled tip packed with 15 cm 4-μm Jupiter C18 resin (Phenomenex, Torrance, CA, USA) was attached to the filter union and the entire split-column (desalting column–filter union–analytical column) was placed inline with an Agilent 1200 quaternary HPLC (Palo Alto, CA) and analyzed using a modified 5-step separation described previously(Washburn et al., 2001). The buffer solutions used were 5% acetonitrile/0.1% formic acid (buffer A), 80%

acetonitrile/0.1% formic acid (buffer B), and 500 mM ammonium acetate/5% acetonitrile/0.1% formic acid (buffer C). Step 1 consisted of a 80 min gradient from 0-100% buffer B. Steps 2-4 had a similar profile except 5 min of 100% buffer A, 3 min of X% buffer C, a 10 min gradient from 0-15% buffer B, and a 108 min gradient from 15-100% buffer B. The 5 min buffer C percentages (X) were 40, 70, 100% respectively for the 4-step analysis. As peptides eluted from the microcapillary column, they were electrosprayed directly into an *LTQ Orbitrap* XL mass spectrometer (Thermo Finnigan, Palo Alto, CA) with the application of a distal 2.4 kV spray voltage. A cycle of one full-scan mass spectrum (400-1600 m/z) followed by 5 data dependent MS/MS spectra at a 35% normalized collision energy was repeated continuously throughout each step of the multidimensional separation. Application of mass spectrometer scan functions and HPLC solvent gradients were controlled by the Xcaliber data system.

Analysis of Tandem Mass Spectra

MS/MS spectra were analyzed using the following software analysis protocol. Poor quality spectra were removed from the dataset using an automated spectral quality assessment algorithm(Bern et al., 2004). MS/MS spectra remaining after filtering were searched with the ProLuCID algorithm against the **EBI-IPI_Human_3_30_06-28-2007** concatenated to a decoy database in which the sequence for each entry in the original database was reversed(Peng et al., 2003a). All searches were parallelized and performed on a Beowulf computer cluster consisting of 100 1.2GHz Athlon CPUs(Sadygov et al., 2002). Searches were performed with Cysteine carbamidomethylation as a fixed modification and Lysine acetylation was searched as a differential modification with an additional mass of 383.2281 and 114.0429 Da. ProLuCID(Eng, 1994) results were

assembled and filtered using the DTASelect (version 2.0) program(Tabb et al., 2002). DTASelect 2.0 uses a linear discriminate analysis to dynamically set XCorr and DeltaCN thresholds for the entire dataset to achieve a user-specified false positive rate (5% in this analysis). The false positive rates are estimated by the program from the number and quality of spectral matches to the decoy database. Confidence for modifications was estimated from overlapping modified peptides as described previously(MacCoss et al., 2002). Only peptides with at least 1 tryptic termini were considered. Confidence for modifications was estimated from overlapping modified peptides as described previously(MacCoss et al., 2002). The validity of peptide/spectrum matches was assessed using the SEQUEST-defined parameters, cross-correlation score (XCorr), and normalized difference in cross-correlation scores (DeltaCn).

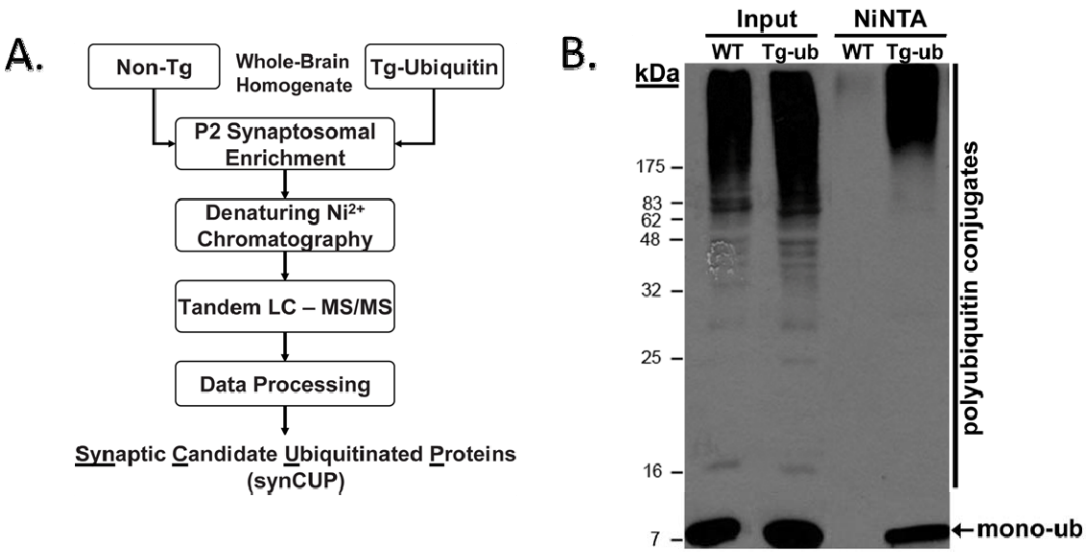

Figure 1. Isolation and identification of synaptic ubiquitinated proteins. (A) Schematized overview of proteomic screen for the isolation and identification of synaptic ubiquitinated proteins from mice expressing a hexahistidine-tagged ubiquitin GFP fusion transgene under the human UbC promoter (Tg-Ub mice). (B) Representative immunoblot depicting the ubiquitin immunoreactivity in Tg-Ub and WT (non-Tg) P2' synaptosomal membrane total lysates or following nickel-affinity purification. As shown, both Tg-Ub and WT samples have relative equal amounts of ubiquitinated proteins in total lysates but following nickel-affinity purification we only observed ubiquitin immunoreactivity in Tg-Ub samples.

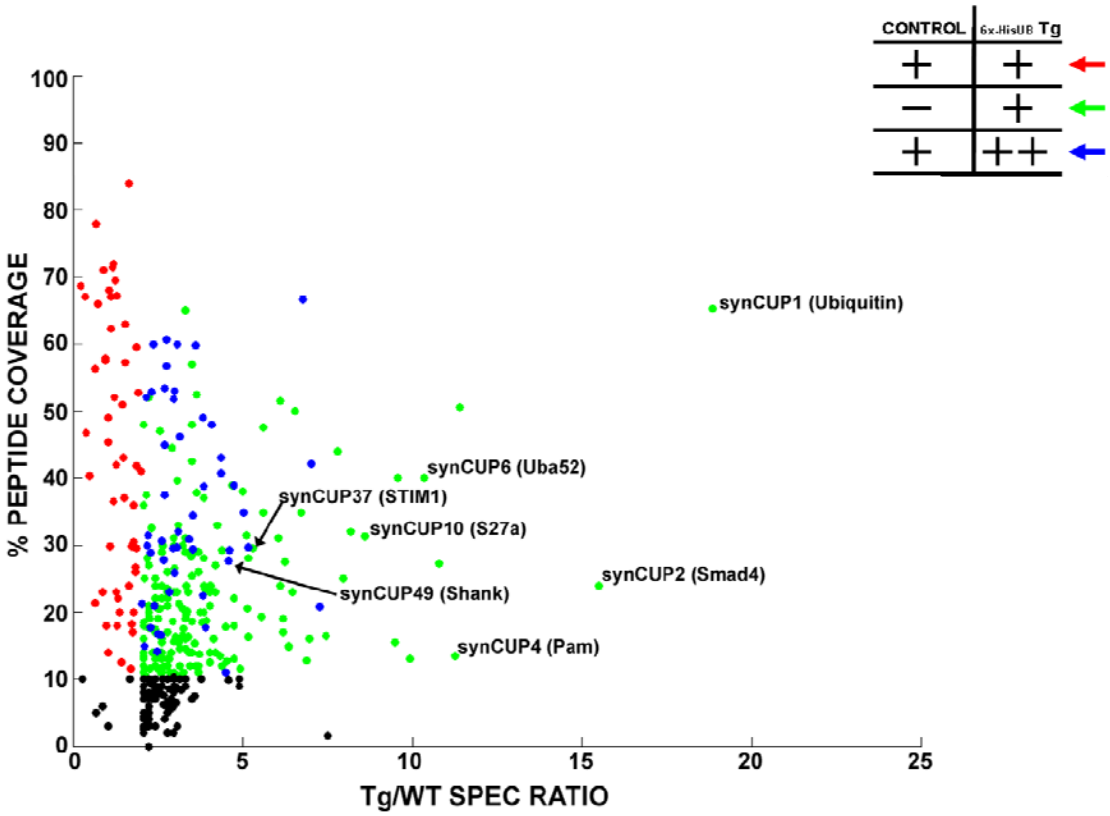

Figure 2. Identification of synaptic ubiquitinated proteins Scatter plot (% peptide coverage vs.Tg/WT spec ratio) of 385 distinct proteins identified via tandem LC-MS/MS. 279 proteins with greater than 10% peptide coverage and a Tg/non-Tg spec ratio greater than 2, were considered a synaptic candidate ubiquitinated protein (synCUP). Proteins with less than 10% peptide coverage plotted as black circles; proteins with a Tg/WT spec ratio of less than 2 plotted as red circles; low abundant proteins with Tg/WT spec ratio greater than 2 plotted as green circles; high abundant proteins with Tg/WT spec ratio greater than 2 plotted as blue circles. **Inset:** Three potential outcomes from Mass SPEC. Spectral hits identified by mass spec. Red arrow – equal amounts in both control and Tg - low ratio; Green arrow – very low to none observed in control with varying amounts in Tg – low to high ratios; Blue arrow – Larger amounts in Tg relative to control – low to high ratios.

Table 2. Top 40 synaptic ubiquitinated proteins by ratio. Table showing the 40 proteins by ratio that were identified by our NiNTA affinity purification and mass spec method from 6x-his-ubiquitin transgenic mice. Spectral score for both WT (non-transgenic) and Tg (transgenic), percent (%) coverage, Tg/WT ratio, and functional classification are shown. Note: Of a total of 279 proteins identified – the highest ratio is for ubiquitin.

Top 40 Synaptic Ubiquitnated Proteins (by Ratio)

	Protein ID	Classification	TG/WT Spec Ratio	Percent Coverage
1	Ubd	Other/UPS Transcription	18.85	65
2	Smad4	Other/Disease	15.49	24
3	Atn1	Metabolism	11.4	51
4	Pam	GTPases	11.27	14
5	RIM-BP2	Other/UPS	10.78	27
6	Uba52	Transcription	10.36	40
7	Hivep2	Kinases/Phosphatases	9.94	13
8	Cdkl5	Transcription	9.59	40
9	Tsc22d1	Translation	9.51	16
10	S27a	Unknown	8.61	31
11	Lrch1	Other	8.18	32
12	Ogt	Metabolism	7.98	25
13	Lta4h	Cytoskeleton/Other	7.8	44
14	Ptpn23	Kinases/Phosphatases	7.51	16
15	Dmxl	Unknown	7.46	21
16	Dlgap1	Cytoskeleton/Other	7.28	42
17	Dpp9	Other/Protease	7.03	16
18	Nbea	Membrane Trafficking	6.98	13
19	Abat	Kinases/Phosphatases	6.91	67
20	Syn	Other/Membrane Trafficking	6.78	35
21	Cycs	Metabolism	6.75	50
22	Hip1r	Membrane Trafficking	6.55	23
23	Hdac6	Transcription	6.46	15
24	Cbl	Other/UPS	6.37	15
25	Caskin1	Other/Scaffold	6.36	28
26	Cpeb	Translation	6.26	17
27	Dhx15	Translation	6.2	19
28	Gm879	Unknown	6.19	52
29	Irs	Other	6.11	24
30	Btbd11	Transcription	6.11	31
31	Nfix	Transcription	6.06	48
32	Actin	Cytoskeleton	5.61	35
33	Satb	Transcription	5.59	19
34	Tbrg4	Kinases/PHosphatases	5.54	30
35	Stim	Other/SOCE Regulator	5.3	28
36	L27a	Translation	5.18	30
37	Wdr7	Unknown	5.18	16
38	Gad1	Metabolsim	5.18	21
39	Rpl27a	Metabolism	5.15	32
40	Tubulin	Cytoskeleton	5.13	35

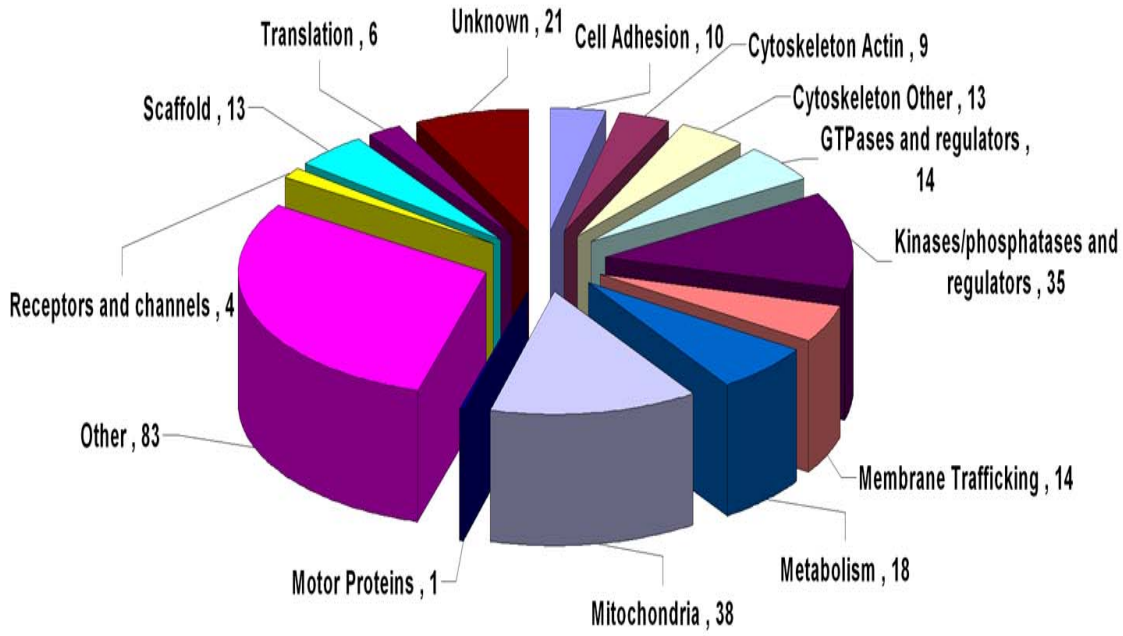

Figure 3. Pie chart showing function classification of synaptic candidate ubiquitinated proteins (synCUP's) purified by NiNTA affinity chromatography and then identified by mass spec. Cell adhesion (3.6%), cytoskeleton actin (3.2%), cytoskeletal other (4.7%), gtpases and regulators (5%), kinases/phosphatases and regulators (12.5%), membrane trafficking (5%), metabolism (6.5%), mitochondria (5%), motor proteins (0.4%), receptors and channels (1.4%), scaffold (4.7%), translation (2.2%), other (29.8%), unknown (7.5%) are shown. The number of proteins in each category is given. Classified using DAVID ontology analysis.

Table 3. Unfiltered, non-redundant list of proteins identified via proteomic screen for synaptic ubiquitinated proteins, CONTINUED. A total of 3,031 IPI proteins from the forward database were identified, while 102 proteins (3% protein FDR) from the reverse database were identified. Proteins with the same set or subsets of unique peptides were grouped into protein groups to minimize protein redundancy. There were 911 and 26 protein groups (3% FDR) identified from forward and reverse database, respectively. Spec# and Intensity are arbitrary units assigned based relative abundance of the detected proteins. See Supplementary Methods for more details

Number	Gene Symbol	Tg/WT Ratio-spec#	WT-spec#	WT-intensity	Tg-spec#	Tg-Intensity	accession_number	% Coverage	numPepsUnique
1	Bsn	15.68148451	44	16400000	690	3850000000	IPI00621373	63	159
2	LOC381358	16.72584311	11	2700000	184	604000000	IPI00665841	45	90
3	Spnb2	11.04124828	24	16000000	265	978000000	IPI00319830	46	86
4	Ank3	11.6329789	30	17400000	349	1950000000	IPI00475362	53	77
5	Shank1	25.59836011	15	24600000	384	2200000000	IPI00465999	54	72
6	D14Ertd171e	14.06312578	79	97500000	1111	7380000000	IPI00460558	63	74
7	Sorbs2	6.895710506	48	21100000	331	1840000000	IPI00672949	70	73
8	Dmxl2	47.99060188	5	790000	240	887000000	IPI00223517	33	71
9	Syngap1	13.74026888	27	31100000	371	3050000000	IPI00352783	58	65
10	BC026657	17.61410661	13	5770000	229	1240000000	IPI00222026	53	54
11	Grit	23.99616731	6	2940000	144	530000000	IPI00274140	49	53
12	Dlgap3	7.694258493	36	46900000	277	1980000000	IPI00134997	68	49
13	Rab11fip5	5.416543985	36	13500000	195	820000000	IPI00480432	50	43
14	Trio	14.79724055	5	1640000	74	204000000	IPI00668683	19	45
15	Camk2b	6.965875194	176	344000000	1226	24200000000	IPI00649778	74	38
16	Ogdh	26.8290285	6	1000000	161	627000000	IPI00626237	46	39
17	Ablim1	13.33281947	24	15100000	320	2860000000	IPI00463138	66	37
18	Stxbp1	7.053890435	37	20200000	261	2000000000	IPI00415402	70	37
19	Iqsec2	30.19416117	5	1440000	151	1020000000	IPI00468181	55	35
20	Atxn2l	29.49287678	4	773000	118	635000000	IPI00458001	40	39
21	Mecp2	5.970075074	67	35600000	400	3530000000	IPI00131063	68	35
22	Fbxo41	12.44380868	18	11100000	224	1020000000	IPI00415914	52	34
23	Rims1	23.49437641	4	3150000	94	274000000	IPI00118692	39	36
24	Farp1	24.74406398	4	2240000	99	467000000	IPI00356904	46	36
25	Top1	7.356688808	14	11900000	103	508000000	IPI00605629	44	33
26	Atp1a3	16.77602489	9	8770000	151	501000000	IPI00122048	37	32
27	Brsk1	12.22097545	9	8920000	110	560000000	IPI00515701	58	32
28	Wdr1	4.509027109	55	50800000	248	1490000000	IPI00314748	62	29
29	Atxn2	18.24784402	8	5110000	146	582000000	IPI00117229	29	31
30	Hnrpl	1.014353998	209	138000000	212	1290000000	IPI00653643	75	27
31	4930589M24Rik	46001	0	0	46	149000000	IPI00665988	31	30
32	Safb2	13.33127812	6	4260000	80	257000000	IPI00330878	38	28
33	Atn1	70001	0	0	70	404000000	IPI00387342	48	28
34	Pcx	29.48575712	2	473000	59	189000000	IPI00114710	37	30
35	Mtap2	17.3278907	3	4590000	52	104000000	IPI00118075	27	29
36	Slc25a12	20.33011165	6	5970000	122	351000000	IPI00308162	53	27
37	Nono	4.61531509	52	31200000	240	2530000000	IPI00320016	71	27
38	Cdkl5	48001	0	0	48	152000000	IPI00381416	40	30
39	Arhgef7	18.24568858	4	861000	73	254000000	IPI00460843	53	27
40	Abat	42.65278241	3	1400000	128	589000000	IPI00407499	70	25
41	E030025D05Rik	15.39712058	5	962000	77	376000000	IPI00464113	58	25
42	Apba1	10.49881265	8	5750000	84	230000000	IPI00223019	49	25
43	BC033915	49001	0	0	49	155000000	IPI00453673	35	27
44	Mapk8ip3	11.19796041	5	2700000	56	300000000	IPI00230501	28	24
45	Mtap6	38001	0	0	38	99500000	IPI00115833	40	25
46	Pafah1b1	25.82919513	6	6840000	155	816000000	IPI00309207	67	24
47	Cacnb2	62.93806194	1	194000	63	230000000	IPI00228423	55	26
48	A230072E10Rik	85.91508492	1	78900	86	315000000	IPI00416122	33	23
49	4933426L22Rik	43.95704296	1	745000	44	80300000	IPI00667973	22	26
50	Brd4	21.48975512	2	125000	43	148000000	IPI00652110	24	25
51	Ptpn23	41001	0	0	41	119000000	IPI00464166	20	22
52	Dpysl5	5.571102064	14	5770000	78	505000000	IPI00318578	62	22
53	IPI00604969_reve	42001	0	0	42	207000000	IPI00604969_reverse	2	30
54	Caskin1	32001	0	0	32	98500000	IPI00553267	26	23
55	Etfdh	11.87364079	8	1990000	95	452000000	IPI00121322	41	21
56	Nbea	36001	0	0	36	105000000	IPI00469204	13	24
57	Nlgn1	13.42679617	7	6020000	94	349000000	IPI00309113	35	20
58	Ddx42	13.66244585	3	3810000	41	117000000	IPI00329839	36	19
59	Btbd11	34001	0	0	34	129000000	IPI00556801	33	21
60	Cbl	41001	0	0	41	145000000	IPI00652341	33	20
61	Lta4h	38001	0	0	38	201000000	IPI00229527	44	20
62	Gm1052	46.95404595	1	270000	47	297000000	IPI00378764	39	18
63	Syn1	38001	0	0	38	109000000	IPI00649886	49	20
64	A930033C01Rik	57001	0	0	57	133000000	IPI00675641	30	19
65	Idh3b	22.49641726	6	5100000	135	725000000	IPI00126635	51	18
66	Tubb5	48001	0	0	48	194000000	IPI00117352	63	20
67	Sod2	1.866134912	127	150000000	237	7150000000	IPI00109109	81	16
68	9430020K01Rik	29001	0	0	29	77100000	IPI00129924	27	19
69	Lrch1	44001	0	0	44	114000000	IPI00420521	32	18
70	Lrpap1	16.49612597	4	1400000	66	341000000	IPI00469307	47	20
71	Ppp1r10	23.48875562	2	1260000	47	101000000	IPI00330483	34	18
72	Ogt	39001	0	0	39	163000000	IPI00420870	25	19
73	Mtap1a	24001	0	0	24	48300000	IPI00676243	12	22
74	Hivep2	50001	0	0	50	99900000	IPI00115900	13	21
75	1500005I02Rik	20.6601133	3	4510000	62	391000000	IPI00119130	48	17
76	Ubap2l	20.49025487	2	389000	41	88100000	IPI00407835	29	17
77	Nell2	41.95904096	1	92200	42	109000000	IPI00268444	32	17
78	Irs1	33001	0	0	33	98800000	IPI00605223	28	20
79	Adrbk1	25.48775612	2	1690000	51	232000000	IPI00320687	36	19
80	Car2	4.152105389	46	99800000	191	5840000000	IPI00121534	66	15
81	LOC640467	18.39826017	10	2230000	184	1310000000	IPI00379202	60	15
82	Gpi1	14.99650087	4	1040000	60	209000000	IPI00228633	40	18

Table 3. Unfiltered, non-redundant list of proteins identified via proteomic screen for synaptic ubiquitinated proteins, CONTINUED

Number	Gene Symbol	Tg/WT Ratio-spec#	WT-spec#	WT-intensity	Tg-spec#	Tg-Intensity	accession_number	% Coverage	numPepsUnique
83	D430041B17Rik	32.49212697	4	2460000	130	2150000000	IPI00225153	54	17
84	Rims2	29.97102897	1	427000	30	41400000	IPI00468810	18	18
85	Hip1r	31001	0	0	31	111000000	IPI00622564	24	18
86	Cherp	37.96303696	1	98500	38	98900000	IPI00229604	30	18
87	Acot9	38.96203796	1	52000	39	152000000	IPI00314069	37	17
88	Ttn	28001	0	0	28	124000000	IPI00604969	1	22
89	Phactr1	6.66572238	6	1460000	40	100000000	IPI00480534	38	17
90	Clasp1	24.97602398	1	313000	25	46900000	IPI00674669	16	18
91	Cpeb4	38001	0	0	38	92900000	IPI00454005	33	15
92	Csnk2a1	6.624296963	8	27600000	53	288000000	IPI00408176	51	15
93	Chd2	20001	0	0	20	45100000	IPI00661316	14	16
94	Hbb-b1	5.999928572	70	80300000	420	5160000000	IPI00553333	84	14
95	Mgll	13.99740052	5	1470000	70	359000000	IPI00132874	54	15
96	Wdr7	24001	0	0	24	57500000	IPI00653237	17	16
97	Pde4b	2.999750031	8	2210000	24	64600000	IPI00647997	29	17
98	Stim1	37001	0	0	37	87800000	IPI00108041	30	16
99	Cask	13.49375312	2	631000	27	106000000	IPI00119517	25	16
100	2410044A07Rik	38.96203796	1	2970000	39	117000000	IPI00227171	32	16
101	D10Jhu81e	1.884581362	26	12000000	49	1510000000	IPI00133284	67	13
102	Pam	63001	0	0	63	289000000	IPI00323974	22	15
103	Ndufa9	10.49762559	4	3710000	42	278000000	IPI00120212	50	15
104	Ckb	16.5692044	7	3270000	116	445000000	IPI00136703	55	13
105	Pfkm	7.664445185	3	597000	23	98200000	IPI00331541	23	15
106	Hba-a1	3.703082764	64	295000000	237	18200000000	IPI00110658	85	11
107	LOC434822	22001	0	0	22	64200000	IPI00463033	24	16
108	Ncor2	23001	0	0	23	34500000	IPI00123871	12	15
109	Atp2b2	28001	0	0	28	52900000	IPI00127713	20	15
110	Sf3a2	50.95004995	1	155000	51	213000000	IPI00380281	32	13
111	Smarcc2	5.498875281	4	1760000	22	50900000	IPI00459742	17	13
112	Tnks	21001	0	0	21	60700000	IPI00420879	13	15
113	Actg1	34001	0	0	34	127000000	IPI00110851	55	13
114	Nfix	27001	0	0	27	91200000	IPI00137503	50	13
115	Ctbp1	9.247938015	4	1850000	37	178000000	IPI00128155	37	11
116	Gm879	30001	0	0	30	150000000	IPI00380894	38	14
117	Dhx15	29001	0	0	29	69700000	IPI00128818	19	13
118	Sf1	21.48975512	2	640000	43	196000000	IPI00116284	30	13
119	Mtap1b	18001	0	0	18	28200000	IPI00130920	11	15
120	Arsb	33.96703297	1	190000	34	371000000	IPI00652358	29	13
121	Gad1	27001	0	0	27	60400000	IPI00318496	25	12
122	1700028K03Rik	18001	0	0	18	35200000	IPI00623761	18	13
123	Satb2	28001	0	0	28	39400000	IPI00128650	27	11
124	Sod1	2.903164414	31	15900000	90	1670000000	IPI00130589	50	11
125	Stim2	18001	0	0	18	35100000	IPI00662191	26	13
126	Slc39a10	9.997750562	4	3210000	40	180000000	IPI00273801	16	11
127	4931406C07Rik	3.333236115	24	8950000	80	258000000	IPI00126172	41	11
128	Irs2	21001	0	0	21	40400000	IPI00379844	18	12
129	Tbrg4	25001	0	0	25	99500000	IPI00623789	31	13
130	Hdac6	30001	0	0	30	65900000	IPI00323705	15	11
131	Hagh	4.428326548	14	5880000	62	492000000	IPI00115866	60	10
132	Ptk9	14.59728054	5	1750000	73	310000000	IPI00314844	43	11
133	Tsc22d1	49001	0	0	49	86900000	IPI00420803	16	12
134	Yy1	9.495752124	2	199000	19	49500000	IPI00311892	35	12
135	Aldoa	12.49425287	2	479000	25	97200000	IPI00221402	46	10
136	BC010304	16001	0	0	16	27400000	IPI00469237	13	13
137	Ampd2	16001	0	0	16	45900000	IPI00623834	20	12
138	Tnr	13001	0	0	13	35900000	IPI00227126	14	11
139	Dpp9	36001	0	0	36	58500000	IPI00462461	17	12
140	Ppm1f	20001	0	0	20	81300000	IPI00275512	34	10
141	Bphl	19001	0	0	19	123000000	IPI00320462	49	11
142	Tuba1	26.65811396	3	979000	80	191000000	IPI00652705	32	11
143	Mbp	2.714163274	14	4150000	38	955000000	IPI00223377	51	10
144	Nckipsd	16001	0	0	16	24400000	IPI00467223	24	11
145	Ctnnb1	18001	0	0	18	73900000	IPI00125899	21	10
146	Aco2	21001	0	0	21	52000000	IPI00116074	18	11
147	Atp6v1h	23.97702298	1	832000	24	455000000	IPI00311461	30	10
148	Mdh2	15001	0	0	15	76100000	IPI00331590	46	12
149	Tha1	25001	0	0	25	67700000	IPI00119576	34	9
150	Eif2c2	13001	0	0	13	43100000	IPI00475248	24	12
151	LOC546052	39.32055981	3	1670000	118	924000000	IPI00474407	41	9
152	Abcf2	31001	0	0	31	60500000	IPI00116825	22	12
153	Dlgh2	14001	0	0	14	39100000	IPI00649556	19	12
154	2610110G12Rik	23001	0	0	23	123000000	IPI00230368	33	11
155	Rasgrf2	14001	0	0	14	47300000	IPI00108372	14	10
156	Synj1	16001	0	0	16	32400000	IPI00229626	10	12
157	Elac2	14001	0	0	14	37000000	IPI00400401	18	10
158	Gls	18.98201798	1	244000	19	80600000	IPI00464317	22	11
159	Cntnap1	15001	0	0	15	35900000	IPI00338983	11	11
160	Aldh18a1	13.98701299	1	279000	14	39000000	IPI00129350	17	10
161	Smad4	81001	0	0	81	187000000	IPI00125567	24	9
162	Pak7	21001	0	0	21	61600000	IPI00225805	22	11
163	LOC381240	24.97602398	1	230000	25	67000000	IPI00622961	22	10
164	P140	11001	0	0	11	16600000	IPI00649708	17	10

Table 3. Unfiltered, non-redundant list of proteins identified via proteomic screen for synaptic ubiquitinated proteins, CONTINUED

Number	Gene Symbol	Tg/WT Ratio-spec#	WT-spec#	WT-intensity	Tg-spec#	Tg-Intensity	accession_number	% Coverage	numPepsUnique
165	Dync1i2	10.33022326	3	271000	31	56000000	IPI00653072	23	10
166	Pkm2	17001	0	0	17	48100000	IPI00407130	24	10
167	Gda	19001	0	0	19	101000000	IPI00469987	26	10
168	Dock3	12001	0	0	12	19500000	IPI00284521	7	9
169	Wdr42a	12.98801199	1	338000	13	46800000	IPI00229856	24	10
170	Pitrm1	13001	0	0	13	32600000	IPI00170126	16	10
171	1110001M19Rik	17001	0	0	17	59800000	IPI00330146	26	10
172	Ap2a1	15001	0	0	15	44500000	IPI00621985	14	10
173	Zfp187	15001	0	0	15	38100000	IPI00108738	28	10
174	Cat	11001	0	0	11	42500000	IPI00312058	23	10
175	Pafah1b3	14.49325337	2	620000	29	204000000	IPI00118819	58	10
176	Pak1ip1	15.98501499	1	1170000	16	33200000	IPI00120790	32	10
177	Centa1	18001	0	0	18	80500000	IPI00378768	31	8
178	Pde1a	16.98401598	1	251000	17	106000000	IPI00121336	21	9
179	Sos1	12001	0	0	12	21900000	IPI00311611	12	10
180	Plekha5	11001	0	0	11	35000000	IPI00460678	12	10
181	Zfp281	23001	0	0	23	73500000	IPI00116926	20	10
182	Frmd4a	15001	0	0	15	33200000	IPI00222107	12	9
183	Syt1	13001	0	0	13	24300000	IPI00129618	29	10
184	Krt2-17	21001	0	0	21	68700000	IPI00157501	30	10
185	Axin1	12001	0	0	12	16300000	IPI00132686	13	10
186	Dvl3	17001	0	0	17	78600000	IPI00117059	23	11
187	Slc25a5	15001	0	0	15	26200000	IPI00127841	34	10
188	Cspg2	11001	0	0	11	16500000	IPI00408445	5	10
189	Adam23	17001	0	0	17	67300000	IPI00458025	18	9
190	Alb1	15001	0	0	15	35900000	IPI00131695	26	9
191	Rapgef2	10001	0	0	10	20300000	IPI00275899	12	9
192	Vcpip1	14001	0	0	14	30500000	IPI00377609	10	9
193	Hspg2	11001	0	0	11	58300000	IPI00515360	5	9
194	1700012H17Rik	18001	0	0	18	46000000	IPI00226450	36	8
195	C030032C09Rik	13001	0	0	13	41100000	IPI00664176	8	8
196	Haghl	18001	0	0	18	61200000	IPI00119017	42	8
197	LOC545810	14001	0	0	14	45400000	IPI00659430	13	10
198	Vps11	19001	0	0	19	35500000	IPI00229777	12	9
199	Tcf20	15001	0	0	15	61900000	IPI00407458	8	10
200	Cp	12001	0	0	12	45800000	IPI00605187	12	10
201	Ctnnd2	13001	0	0	13	14800000	IPI00136135	9	9
202	Gap43	14001	0	0	14	6680000	IPI00128973	57	9
203	Sdf2	38.96203796	1	596000	39	295000000	IPI00123852	45	8
204	Cnot1	12001	0	0	12	16200000	IPI00673465	8	11
205	Xrn1	4.498250875	2	449000	9	12000000	IPI00129132	6	8
206	Ubap2	18001	0	0	18	35900000	IPI00457533	14	8
207	Sbf1	13001	0	0	13	17700000	IPI00457486	9	10
208	Nmnat3	14001	0	0	14	47000000	IPI00115459	48	9
209	Cryzl1	20.98001998	1	196000	21	77100000	IPI00122320	27	8
210	Phf3	10001	0	0	10	14200000	IPI00675015	8	9
211	Tssc1	13001	0	0	13	86900000	IPI00321310	31	8
212	Cntn1	17001	0	0	17	52500000	IPI00123058	14	9
213	Foxp1	2.666111296	3	1440000	8	25500000	IPI00323239	21	9
214	Arhgap21	11001	0	0	11	24000000	IPI00330139	9	10
215	3200001K10Rik	11001	0	0	11	17200000	IPI00658921	10	9
216	D030060M11Rik	14001	0	0	14	13500000	IPI00153284	25	10
217	Tcf4	20001	0	0	20	28700000	IPI00120128	29	8
218	Homer1	17.98301698	1	118000	18	36000000	IPI00395134	24	8
219	AI851076	9.991008991	1	51500	10	22000000	IPI00345960	20	8
220	Atp1b1	14001	0	0	14	95200000	IPI00622442	25	8
221	Hk1	11001	0	0	11	188000000	IPI00283611	14	10
222	Map4k4	14001	0	0	14	21900000	IPI00130014	11	9
223	Pib5pa	15001	0	0	15	28400000	IPI00173277	16	9
224	Ncam1	13001	0	0	13	22800000	IPI00122971	21	9
225	Ppp3cc	14001	0	0	14	40800000	IPI00468124	21	8
226	Ubd	115001	0	0	115	645000000	IPI00458995	70	7
227	Ptges2	11001	0	0	11	24400000	IPI00312174	30	7
228	Vps29	26.97402597	1	73600	27	265000000	IPI00230513	44	7
229	Cit	12001	0	0	12	21900000	IPI00655040	8	10
230	Fdxr	13001	0	0	13	31400000	IPI00453981	19	8
231	1110012J17Rik	8.992007992	1	338000	9	17100000	IPI00624581	7	9
232	Pitpnm2	11001	0	0	11	18300000	IPI00460698	9	9
233	App	11001	0	0	11	25500000	IPI00230494	14	7
234	Mrg1	14001	0	0	14	53000000	IPI00124199	23	7
235	Sdf2l1	5.33188937	3	2340000	16	90300000	IPI00227657	50	7
236	2310021P13Rik	13001	0	0	13	24300000	IPI00467933	8	8
237	Ndufs6	1.545438017	33	41500000	51	937000000	IPI00128345	62	7
238	Helz	14001	0	0	14	23500000	IPI00453654	7	8
239	Sf3b4	0.83871488	31	47600000	26	228000000	IPI00154082	25	6
240	Slc12a5	12001	0	0	12	27400000	IPI00465769	10	9
241	Fah	18001	0	0	18	33800000	IPI00653931	27	8
242	Sox8	8001	0	0	8	16200000	IPI00111141	28	8
243	Nef3	12001	0	0	12	28500000	IPI00323800	10	8
244	Sdfr1	20001	0	0	20	73000000	IPI00662285	31	8
245	Tjp1	11001	0	0	11	13900000	IPI00135971	9	9
246	Dock9	8001	0	0	8	6640000	IPI00337050	7	8

Table 3. Unfiltered, non-redundant list of proteins identified via proteomic screen for synaptic ubiquitinated proteins, CONTINUED

Number	Gene Symbol	Tg/WT Ratio-spec#	WT-spec#	WT-intensity	Tg-spec#	Tg-Intensity	accession_number	% Coverage	numPepsUnique
247	LOC637074	3.249437641	4	367000	13	36200000	IPI00661480	7	7
248	Krt1-10	9.495752124	2	218000	19	80100000	IPI00110670	10	7
249	Pou3f3	8.496251874	2	759000	17	65500000	IPI00133442	26	7
250	Cacna2d1	9001	0	0	9	18400000	IPI00319970	12	8
251	Prkcc	14.98601399	1	238000	15	21700000	IPI00122069	16	8
252	Pde2a	14001	0	0	14	28400000	IPI00380799	10	7
253	5730453I16Rik	6.997001499	2	476000	14	42100000	IPI00225249	21	7
254	Spen	12001	0	0	12	35300000	IPI00378158	3	9
255	Neb	11001	0	0	11	72200000	IPI00475078	2	9
256	Sardh	8001	0	0	8	30000000	IPI00136213	10	8
257	1110049F12Rik	22001	0	0	22	51000000	IPI00309077	41	7
258	Garnl1	13001	0	0	13	16800000	IPI00454161	7	8
259	Mapt	13001	0	0	13	21300000	IPI00648564	27	7
260	Hint1	6.998000666	3	9010000	21	229000000	IPI00108189	72	6
261	Coq6	17001	0	0	17	78500000	IPI00222526	21	7
262	Grin2b	8001	0	0	8	12400000	IPI00321320	7	7
263	E130014H08Rik	9001	0	0	9	13400000	IPI00672763	8	6
264	Bmp2k	9001	0	0	9	14800000	IPI00313513	13	8
265	Pik3r4	9001	0	0	9	19200000	IPI00406045	10	7
266	LOC624853	12001	0	0	12	37000000	IPI00480560	18	8
267	Man2c1	13001	0	0	13	32100000	IPI00127450	9	7
268	Plxna1	11001	0	0	11	24400000	IPI00137311	6	8
269	Gnn	8001	0	0	8	25100000	IPI00648312	17	7
270	Epb4.1l4b	10001	0	0	10	24900000	IPI00649652	14	7
271	Slc4a10	11001	0	0	11	25300000	IPI00227302	8	7
272	IPI00672741	10001	0	0	10	18200000	IPI00672741	15	7
273	Stk25	8001	0	0	8	16500000	IPI00421210	16	6
274	Sin3a	9001	0	0	9	20000000	IPI00276051	9	7
275	IPI00625588	14001	0	0	14	69000000	IPI00625588	19	6
276	Grlf1	11001	0	0	11	21200000	IPI00480321	6	6
277	Trp53bp1	11001	0	0	11	36800000	IPI00229801	5	6
278	Lrrc7	11001	0	0	11	61300000	IPI00658526	9	8
279	Wasf1	9001	0	0	9	31700000	IPI00471372	16	7
280	2410012H02Rik	32001	0	0	32	150000000	IPI00109395	44	6
281	Gria2	8001	0	0	8	388000000	IPI00608015	9	7
282	Nucb2	8001	0	0	8	11400000	IPI00309704	22	7
283	Cs	11001	0	0	11	24300000	IPI00113141	31	7
284	Letm1	10001	0	0	10	35400000	IPI00131177	12	6
285	E030041M21Rik	10001	0	0	10	17500000	IPI00621558	11	8
286	Bckdk	10001	0	0	10	49700000	IPI00115094	26	6
287	LOC640847	10001	0	0	10	34700000	IPI00475310	18	7
288	Dld	17001	0	0	17	78900000	IPI00115569	20	6
289	B230118G17Rik	18001	0	0	18	77900000	IPI00108479	19	7
290	IPI00268933_reve	12001	0	0	12	24900000	IPI00268933_reverse	3	8
291	D3Bwg0562e	23.97702298	1	133000	24	47300000	IPI00420590	10	6
292	2810421I24Rik	12001	0	0	12	24000000	IPI00267299	14	7
293	Basp1	13001	0	0	13	8010000	IPI00129519	65	7
294	Brcc3	16001	0	0	16	86800000	IPI00137103	28	6
295	Tbr1	8.992007992	1	201000	9	17800000	IPI00133372	18	7
296	Mllt4	7001	0	0	7	23300000	IPI00660193	6	7
297	Ncdn	8001	0	0	8	21400000	IPI00331299	10	6
298	9030409G11Rik	9001	0	0	9	20000000	IPI00222264	20	7
299	Tle4	9001	0	0	9	15900000	IPI00407702	13	7
300	9030217H17Rik	19001	0	0	19	45400000	IPI00662157	12	6
301	Slc39a6	5.665111629	3	3790000	17	114000000	IPI00469000	9	6
302	Purg	4.998001	2	2650000	10	35800000	IPI00153880	23	6
303	Phyhip	9001	0	0	9	52200000	IPI00169622	29	7
304	Usp9x	5.995004995	1	1050000	6	8220000	IPI00108388	3	6
305	Serac1	9001	0	0	9	15400000	IPI00134821	14	7
306	Stx1b2	8001	0	0	8	12600000	IPI00113149	26	6
307	Actn1	8001	0	0	8	21300000	IPI00380436	8	6
308	Cyfip2	7001	0	0	7	11000000	IPI00625090	7	7
309	Aass	10001	0	0	10	61700000	IPI00387491	13	7
310	Dgki	11001	0	0	11	19900000	IPI00402764	7	6
311	Cltc	6001	0	0	6	14500000	IPI00648173	4	6
312	Eif3s8	6001	0	0	6	14100000	IPI00321647	8	6
313	Arpc2	13001	0	0	13	34600000	IPI00658951	20	6
314	Zfp609	7001	0	0	7	10200000	IPI00227314	8	7
315	Gsr	9001	0	0	9	48100000	IPI00111359	22	7
316	2010300C02Rik	7001	0	0	7	5760000	IPI00454053	10	7
317	Nlk	6001	0	0	6	18500000	IPI00119899	12	6
318	Limk1	10001	0	0	10	15000000	IPI00133642	17	6
319	Mpst	11001	0	0	11	14400000	IPI00604945	24	5
320	Vps39	8001	0	0	8	11800000	IPI00460712	10	7
321	Gldc	5001	0	0	5	6830000	IPI00127267	10	5
322	Tmlhe	8001	0	0	8	25000000	IPI00129163	17	7
323	Gcat	18001	0	0	18	33200000	IPI00136655	23	6
324	H2afv	2.714040851	7	2490000	19	303000000	IPI00555055	53	5
325	Mcart1	15001	0	0	15	27400000	IPI00262198	26	6
326	Ppia	6001	0	0	6	22700000	IPI00554989	48	6
327	Ube1x	9001	0	0	9	6680000	IPI00123313	11	6
328	Clstn1	8001	0	0	8	16600000	IPI00620988	7	6

Table 3. Unfiltered, non-redundant list of proteins identified via proteomic screen for synaptic ubiquitinated proteins, CONTINUED

Number	Gene Symbol	Tg/WT Ratio-spec#	WT-spec#	WT-intensity	Tg-spec#	Tg-Intensity	accession_number	% Coverage	numPepsUnique
329	Mpp3	11001	0	0	11	30400000	IPI00351246	15	6
330	Rbm15b	5.995004995	1	302000	6	16200000	IPI00278942	14	5
331	LOC547176	7001	0	0	7	13800000	IPI00356000	11	7
332	BC021611	14001	0	0	14	46700000	IPI00121528	39	6
333	Mars2	6001	0	0	6	10100000	IPI00226952	13	5
334	Sts	6001	0	0	6	14600000	IPI00118038	11	5
335	Bcas3	9001	0	0	9	14400000	IPI00515222	15	6
336	1700037H04Rik	17001	0	0	17	44200000	IPI00230436	39	5
337	Tns1	5001	0	0	5	5110000	IPI00659967	4	5
338	Cox4i1	9001	0	0	9	23900000	IPI00117978	35	5
339	Epb4.1l1	8001	0	0	8	25700000	IPI00465812	10	6
340	IPI00265239	31001	0	0	31	134000000	IPI00265239	50	5
341	AU024582	8001	0	0	8	18100000	IPI00627000	9	6
342	Bcl11a	19001	0	0	19	54300000	IPI00272308	18	6
343	D430007A19Rik	8001	0	0	8	17600000	IPI00469437	8	6
344	A930017N06Rik	12001	0	0	12	24600000	IPI00227288	10	5
345	Dciad2	10.99000999	1	360000	11	57400000	IPI00112139	43	5
346	Foxj3	11001	0	0	11	40100000	IPI00225578	12	5
347	Map3k7ip2	6001	0	0	6	17900000	IPI00115639	13	6
348	Pde8b	9001	0	0	9	24200000	IPI00261641	9	5
349	Taz	7001	0	0	7	22600000	IPI00128095	27	5
350	Prkaa1	8001	0	0	8	15000000	IPI00556823	13	5
351	Add1	6001	0	0	6	26700000	IPI00136000	13	5
352	2810443J12Rik	8001	0	0	8	12700000	IPI00112046	15	6
353	Gpatc2	8001	0	0	8	14700000	IPI00416341	20	5
354	Cox6a1	3.499750025	10	8620000	35	1050000000	IPI00121443	60	4
355	Gnao1	6001	0	0	6	17800000	IPI00230192	16	5
356	Wdr33	8001	0	0	8	16000000	IPI00170242	7	5
357	Mcfd2	7.331222926	3	2980000	22	49700000	IPI00170316	52	4
358	IPI00126181_reve	11001	0	0	11	50100000	IPI00126181_reverse	4	6
359	Cnp1	8001	0	0	8	20300000	IPI00319602	17	5
360	Atpif1	14.98601399	1	105000	15	742000000	IPI00331463	26	5
361	Abcb7	7001	0	0	7	17000000	IPI00672663	11	5
362	Col18a1	5001	0	0	5	17000000	IPI00284816	3	5
363	Cacna1b	8001	0	0	8	18800000	IPI00466672	3	5
364	Wdr81	5001	0	0	5	11600000	IPI00663537	4	5
365	Ndufs5	17001	0	0	17	48800000	IPI00117300	40	4
366	4631403P03Rik	7001	0	0	7	8260000	IPI00224269	23	4
367	LOC634141	8001	0	0	8	33600000	IPI00122307	17	5
368	Cadps	6001	0	0	6	11700000	IPI00330163	5	5
369	Vps35	5001	0	0	5	18900000	IPI00111181	7	5
370	Sepp1	10001	0	0	10	38200000	IPI00137599	22	5
371	Tcf7l2	6001	0	0	6	26000000	IPI00129307	18	5
372	Ap2b1	6001	0	0	6	12100000	IPI00378063	8	5
373	Dyrk1a	6001	0	0	6	25000000	IPI00118849	11	5
374	Prpf4b	7001	0	0	7	11800000	IPI00320690	5	5
375	Plec1	5001	0	0	5	5920000	IPI00421270	1	5
376	Ube3b	5001	0	0	5	9850000	IPI00112716	9	5
377	IPI00674050_reve	8001	0	0	8	19200000	IPI00674050_reverse	4	6
378	Fubp1	5001	0	0	5	9130000	IPI00123292	9	5
379	Akr1a4	7001	0	0	7	19600000	IPI00466128	20	5
380	Zfx	5001	0	0	5	9610000	IPI00620170	8	4
381	Gm48	10001	0	0	10	32100000	IPI00345813	5	5
382	Arpc1a	6001	0	0	6	17800000	IPI00127987	19	5
383	Gclc	5001	0	0	5	16500000	IPI00125658	9	4
384	Amot	12001	0	0	12	61900000	IPI00623015	12	5
385	mt-Co2	10001	0	0	10	42500000	IPI00131176	23	4
386	Strn4	6001	0	0	6	16100000	IPI00119524	7	5
387	38970	5001	0	0	5	4580000	IPI00223838	15	4
388	Snap25	14001	0	0	14	23900000	IPI00125635	24	4
389	Trim35	6001	0	0	6	54500000	IPI00410787	18	5
390	Ppm2c	8001	0	0	8	14500000	IPI00378636	10	4
391	Dpysl3	6001	0	0	6	15500000	IPI00122349	11	4
392	Plp1	14001	0	0	14	51600000	IPI00263013	15	4
393	Slc25a3	8001	0	0	8	16100000	IPI00124771	12	5
394	Gopc	4001	0	0	4	5290000	IPI00221745	13	4
395	Epb4.1l3	6001	0	0	6	11300000	IPI00229294	8	4
396	Lace1	7001	0	0	7	18600000	IPI00169752	10	5
397	C230096C10Rik	4001	0	0	4	21100000	IPI00226932	5	4
398	Stox2	5001	0	0	5	16600000	IPI00467354	9	5
399	Zfp365	6001	0	0	6	12900000	IPI00399502	11	4
400	Ckmt1	3.997002997	1	181000	4	10400000	IPI00128296	16	4
401	Sdha	6001	0	0	6	7880000	IPI00230351	11	4
402	Ganab	5001	0	0	5	6830000	IPI00115679	6	4
403	Acy1	6001	0	0	6	19900000	IPI00132960	14	4
404	Gcap14	5001	0	0	5	24500000	IPI00606737	8	4
405	IPI00470025	4001	0	0	4	10100000	IPI00470025	19	4
406	Aaas	8001	0	0	8	11900000	IPI00311509	13	4
407	IPI00453810_reve	6001	0	0	6	16400000	IPI00453810_reverse	11	5
408	Skb1	9001	0	0	9	19800000	IPI00229845	9	3
409	Ankrd28	7001	0	0	7	10200000	IPI00405443	4	4
410	Rbmx2	5001	0	0	5	8060000	IPI00261255	13	4

Table 3. Unfiltered, non-redundant list of proteins identified via proteomic screen for synaptic ubiquitinated proteins, CONTINUED

Number	Gene Symbol	Tg/WT Ratio-spec#	WT-spec#	WT-intensity	Tg-spec#	Tg-Intensity	accession_number	% Coverage	numPepsUnique
411	Pik4ca	7001	0	0	7	8480000	IPI00115875	4	5
412	Usp20	5001	0	0	5	6660000	IPI00469997	12	5
413	Rtn4	4001	0	0	4	6100000	IPI00469392	8	4
414	Inpp5e	5001	0	0	5	9520000	IPI00120199	10	4
415	38965	10001	0	0	10	19700000	IPI00416280	23	4
416	Ethe1	5001	0	0	5	17200000	IPI00113386	23	4
417	Dnajb12	4001	0	0	4	12300000	IPI00331598	14	4
418	Ywhag	7001	0	0	7	7130000	IPI00230707	21	4
419	Zcchc11	6001	0	0	6	30700000	IPI00648042	4	5
420	Pdha1	6001	0	0	6	38200000	IPI00337893	12	5
421	D10Bwg1379e	6001	0	0	6	9370000	IPI00116462	2	4
422	Arid5b	8001	0	0	8	34500000	IPI00322729	6	5
423	Wdr47	5001	0	0	5	6120000	IPI00330193	8	4
424	IPI00625633	9001	0	0	9	46900000	IPI00625633	21	4
425	Bcas1	4001	0	0	4	5130000	IPI00330860	10	4
426	Ndufb3	64.93606394	1	499000	65	979000000	IPI00133403	34	4
427	Lmna	4001	0	0	4	6910000	IPI00314019	7	4
428	Kif5c	5001	0	0	5	4700000	IPI00421137	7	5
429	BC037112	5001	0	0	5	6740000	IPI00351047	6	4
430	Prss15	5001	0	0	5	5530000	IPI00319518	9	4
431	Rusc1	5001	0	0	5	7280000	IPI00453890	6	4
432	D5Bwg0834e	5001	0	0	5	13500000	IPI00123541	20	4
433	Odz2	10001	0	0	10	17300000	IPI00649917	2	4
434	Rsbn1	5001	0	0	5	4300000	IPI00377608	6	4
435	2310061C15Rik	11001	0	0	11	138000000	IPI00169713	60	4
436	Ube2n	7001	0	0	7	35500000	IPI00165854	36	4
437	Tceb3	11001	0	0	11	16500000	IPI00317167	10	4
438	Got1	6001	0	0	6	12300000	IPI00230204	18	4
439	Cntnap4	5001	0	0	5	10300000	IPI00120292	4	5
440	Uqcrh	7001	0	0	7	30100000	IPI00129516	52	4
441	Dpysl2	5001	0	0	5	15200000	IPI00420349	7	4
442	Osbp	6001	0	0	6	13600000	IPI00138343	8	4
443	LOC634779	4001	0	0	4	8760000	IPI00665534	10	4
444	Tanc1	6001	0	0	6	15800000	IPI00349296	3	4
445	Dync1i1	6001	0	0	6	14600000	IPI00131084	15	4
446	Atp6v0a1	4001	0	0	4	11100000	IPI00130187	4	4
447	Mccc1	5001	0	0	5	13400000	IPI00320850	7	4
448	Sox1	9001	0	0	9	13600000	IPI00134803	13	4
449	Cbx4	5001	0	0	5	8650000	IPI00116041	9	4
450	Gm1057	4001	0	0	4	5910000	IPI00221968	14	4
451	Smad1	4001	0	0	4	8750000	IPI00556839	10	4
452	Lrp1	4001	0	0	4	4260000	IPI00119063	1	3
453	Immt	5001	0	0	5	6130000	IPI00554845	9	4
454	Crtc2	4001	0	0	4	10500000	IPI00621741	9	3
455	Ppp1r1b	4001	0	0	4	5330000	IPI00121349	29	4
456	Pld3	6001	0	0	6	15800000	IPI00130624	11	4
457	Otub1	4001	0	0	4	11200000	IPI00154004	21	4
458	Prrt1	7001	0	0	7	56800000	IPI00130766	19	3
459	Dlx6	8001	0	0	8	40500000	IPI00378824	24	3
460	Uqcrc1	6001	0	0	6	8590000	IPI00653598	10	3
461	Amt	5001	0	0	5	13900000	IPI00229274	17	4
462	38971	4001	0	0	4	7840000	IPI00627026	11	3
463	Mbc2	5001	0	0	5	5450000	IPI00128450	5	4
464	IPI00348769_reve	6001	0	0	6	7660000	IPI00348769_reverse	12	4
465	Wdr24	4001	0	0	4	13200000	IPI00229321	9	4
466	Tgfbrap1	7001	0	0	7	22400000	IPI00222627	4	3
467	Rbbp7	6001	0	0	6	15700000	IPI00122698	9	4
468	Lrrc4b	6001	0	0	6	24000000	IPI00381059	7	4
469	Pura	4001	0	0	4	5010000	IPI00118447	10	3
470	Fath	4001	0	0	4	2990000	IPI00663242	2	4
471	Ntrk2	5001	0	0	5	8630000	IPI00128360	13	4
472	Prdx3	9001	0	0	9	48400000	IPI00116192	24	4
473	1810038L18Rik	4001	0	0	4	6020000	IPI00468101	13	4
474	Hspcb	7001	0	0	7	52700000	IPI00229080	8	4
475	D9Ertd402e	5001	0	0	5	8660000	IPI00381300	14	4
476	Ncam2	4001	0	0	4	5320000	IPI00127556	7	4
477	Suhw4	3001	0	0	3	2480000	IPI00222033	7	3
478	Zic2	4001	0	0	4	8930000	IPI00127145	10	4
479	LOC639541	4001	0	0	4	7650000	IPI00671049	14	4
480	Ankrd50	5001	0	0	5	8080000	IPI00468603	4	4
481	AL033314	4001	0	0	4	5580000	IPI00123129	8	4
482	Phlda1	8001	0	0	8	19300000	IPI00124832	12	4
483	IPI00555125_reve	7001	0	0	7	16900000	IPI00555125_reverse	9	4
484	IPI00649060	3001	0	0	3	5100000	IPI00649060	3	3
485	Fnbp3	4001	0	0	4	10400000	IPI00338887	5	4
486	Cspg3	3001	0	0	3	11400000	IPI00135563	3	3
487	Glul	3001	0	0	3	7080000	IPI00320163	9	3
488	2610511M17Rik	4001	0	0	4	2320000	IPI00221567	4	4
489	2410127E16Rik	4001	0	0	4	8780000	IPI00399905	8	4
490	Mtap4	8001	0	0	8	6180000	IPI00408119	5	4
491	Cbll1	6001	0	0	6	23000000	IPI00310594	8	3
492	Rabepk	8001	0	0	8	10300000	IPI00227529	10	3

Table 3. Unfiltered, non-redundant list of proteins identified via proteomic screen for synaptic ubiquitinated proteins, CONTINUED

Number	Gene Symbol	Tg/WT Ratio-spec#	WT-spec#	WT-intensity	Tg-spec#	Tg-Intensity	accession_number	% Coverage	numPepsUnique
493	Etv6	5001	0	0	5	13400000	IPI00124171	20	4
494	BC021611	5001	0	0	5	17300000	IPI00654091	8	3
495	Stx1a	6001	0	0	6	17000000	IPI00131618	12	3
496	Sec13l1	4001	0	0	4	7880000	IPI00133920	15	3
497	Rbm27	4001	0	0	4	22700000	IPI00224881	4	4
498	Enpp6	5001	0	0	5	11500000	IPI00308077	15	4
499	Apxl	4001	0	0	4	3330000	IPI00463074	6	4
500	Ranbp9	6001	0	0	6	9390000	IPI00116285	5	3
501	Oplah	4001	0	0	4	2960000	IPI00169473	4	3
502	Axin2	5001	0	0	5	6780000	IPI00420883	6	3
503	Pdzrn3	0.666777741	3	732000	2	4270000	IPI00135609	5	3
504	Usp22	4001	0	0	4	10900000	IPI00228479	7	4
505	Map4k2	8001	0	0	8	17700000	IPI00117889	5	3
506	Abhd3	3001	0	0	3	14600000	IPI00131173	12	3
507	Pisd	3001	0	0	3	9600000	IPI00310099	13	3
508	Prpf38a	6001	0	0	6	23000000	IPI00226155	16	4
509	Camkv	8001	0	0	8	16600000	IPI00122486	7	3
510	2410025L10Rik	3001	0	0	3	13700000	IPI00471199	13	3
511	Vdac1	6001	0	0	6	12100000	IPI00122549	18	4
512	Zfyve1	3001	0	0	3	14100000	IPI00329871	6	3
513	Centd1	5001	0	0	5	3410000	IPI00667244	3	4
514	Atp5a1	2.998001998	1	142000	3	9250000	IPI00130280	7	3
515	Nsf	4001	0	0	4	6570000	IPI00311934	4	3
516	Car7	4001	0	0	4	9860000	IPI00187296	10	3
517	R3hdm1	4001	0	0	4	5760000	IPI00461460	4	3
518	Cox5a	6001	0	0	6	28400000	IPI00120719	27	3
519	Zfp37	4001	0	0	4	9490000	IPI00135679	10	4
520	Ap3d1	4001	0	0	4	4210000	IPI00117811	5	3
521	Dock11	4001	0	0	4	3440000	IPI00462949	2	4
522	2010107E04Rik	5001	0	0	5	33000000	IPI00113143	32	3
523	Sfxn3	3001	0	0	3	6070000	IPI00126115	13	3
524	Igsf4b	4001	0	0	4	6780000	IPI00118020	11	3
525	Idh3g	6001	0	0	6	23300000	IPI00109169	18	3
526	Gcs1	5001	0	0	5	6130000	IPI00330323	4	3
527	Pcmt1	3001	0	0	3	8680000	IPI00329913	30	3
528	Mtch2	5001	0	0	5	7310000	IPI00132039	9	3
529	Pip5k2c	4001	0	0	4	78500000	IPI00129479	10	3
530	Vdac3	4001	0	0	4	11500000	IPI00122548	12	3
531	Hpca	3001	0	0	3	9550000	IPI00230310	17	3
532	Olig2	3001	0	0	3	4010000	IPI00226995	17	3
533	4933406E20Rik	7001	0	0	7	11600000	IPI00620061	9	3
534	Nckap1	3001	0	0	3	4340000	IPI00319320	4	3
535	Eef1a1	3001	0	0	3	2900000	IPI00307837	15	3
536	Zcchc14	3001	0	0	3	3120000	IPI00403334	4	3
537	Prickle2	3001	0	0	3	4320000	IPI00349970	5	3
538	Cpt2	3001	0	0	3	5050000	IPI00131424	9	3
539	Mtch1	3001	0	0	3	11000000	IPI00137173	7	3
540	Gpm6a	4001	0	0	4	17000000	IPI00122974	10	3
541	Car1	3001	0	0	3	31800000	IPI00230320	15	3
542	Bdh	4001	0	0	4	19200000	IPI00330754	15	3
543	Epb4.1l2	3001	0	0	3	1550000	IPI00330289	5	3
544	Abcd3	4001	0	0	4	9710000	IPI00135646	7	3
545	IPI00551215	3001	0	0	3	2850000	IPI00551215	10	3
546	Usp6nl	3001	0	0	3	9350000	IPI00461339	7	3
547	Scfd2	5001	0	0	5	11700000	IPI00225317	8	3
548	1700066M21Rik	3001	0	0	3	17900000	IPI00112709	8	3
549	Slit3	5001	0	0	5	3120000	IPI00515332	4	3
550	Suclg1	3001	0	0	3	14400000	IPI00406442	11	3
551	Prdx5	3001	0	0	3	6230000	IPI00621771	16	3
552	Ivd	3001	0	0	3	6370000	IPI00471246	11	3
553	Hint2	5001	0	0	5	54500000	IPI00133034	18	2
554	Mib1	2001	0	0	2	1630000	IPI00330112	3	2
555	BC017647	4001	0	0	4	23600000	IPI00122461	11	3
556	Ankrd17	3001	0	0	3	5310000	IPI00622352	2	3
557	Hisppd2a	3001	0	0	3	343000000	IPI00222662	7	3
558	Osbpl10	4001	0	0	4	26800000	IPI00271388	9	3
559	Slc4a3	6001	0	0	6	10000000	IPI00470963	5	3
560	Tox	2001	0	0	2	2630000	IPI00471452	6	2
561	Hist1h2bp	12001	0	0	12	20500000	IPI00453744	23	3
562	2810485I05Rik	4001	0	0	4	8110000	IPI00330763	7	2
563	Lin7c	4001	0	0	4	9990000	IPI00136498	15	3
564	Gabra1	3001	0	0	3	8420000	IPI00113772	6	3
565	Baz1b	4001	0	0	4	9880000	IPI00130597	3	3
566	Zfp143	3001	0	0	3	5250000	IPI00221558	8	3
567	Hecw2	4001	0	0	4	7060000	IPI00453742	5	3
568	Stambp	3001	0	0	3	23700000	IPI00131905	10	3
569	2310030N02Rik	4001	0	0	4	6610000	IPI00341302	12	3
570	Dcps	4001	0	0	4	2420000	IPI00459280	7	2
571	A630047E20Rik	3001	0	0	3	5060000	IPI00222950	5	3
572	Tsc1	3001	0	0	3	2560000	IPI00109178	4	3
573	AI450948	3001	0	0	3	1420000	IPI00381608	4	3
574	Gata2	3001	0	0	3	2670000	IPI00114226	12	3

Table 3. Unfiltered, non-redundant list of proteins identified via proteomic screen for synaptic ubiquitinated proteins, CONTINUED

Number	Gene Symbol	Tg/WT Ratio-spec#	WT-spec#	WT-intensity	Tg-spec#	Tg-Intensity	accession_number	% Coverage	numPepsUnique
575	Fuk	3001	0	0	3	5880000	IPI00329962	5	3
576	Hdac4	2001	0	0	2	2030000	IPI00622324	5	2
577	Cttn	4001	0	0	4	4780000	IPI00118143	10	3
578	LOC633764	4001	0	0	4	8560000	IPI00406465	5	3
579	Mast1	3001	0	0	3	1980000	IPI00408233	4	3
580	Cox5b	6001	0	0	6	65800000	IPI00116154	24	3
581	Lancl1	5001	0	0	5	7730000	IPI00131535	7	3
582	Hnrpa2b1	3001	0	0	3	3590000	IPI00622847	13	3
583	Nelf	3001	0	0	3	14200000	IPI00272207	7	3
584	Coq7	3001	0	0	3	4660000	IPI00653062	10	2
585	Zfp319	5001	0	0	5	9200000	IPI00112643	4	3
586	Kctd16	5001	0	0	5	18200000	IPI00377344	7	3
587	IPI00625154_reve	3001	0	0	3	4450000	IPI00625154_reverse	1	3
588	IPI00263333_reve	4001	0	0	4	4820000	IPI00263333_reverse	6	3
589	Hapln1	3001	0	0	3	5970000	IPI00131995	8	3
590	Dbh	3001	0	0	3	4270000	IPI00132202	4	2
591	4932417H02Rik	4001	0	0	4	4070000	IPI00170249	3	3
592	Ube4b	3001	0	0	3	4380000	IPI00623239	6	3
593	Rutbc2	3001	0	0	3	5160000	IPI00654219	2	2
594	Vars2l	5001	0	0	5	4960000	IPI00222180	3	2
595	Limd1	3001	0	0	3	3210000	IPI00134881	7	3
596	IPI00649644	3001	0	0	3	9540000	IPI00649644	11	3
597	Mnt	4001	0	0	4	11300000	IPI00115664	5	2
598	Hspa4l	3001	0	0	3	72000000	IPI00317710	5	3
599	Nrxn2	4001	0	0	4	9680000	IPI00653859	2	3
600	Cdc14a	3001	0	0	3	7490000	IPI00345371	5	3
601	Fars2	3001	0	0	3	3360000	IPI00387505	7	3
602	Atp5j2	4001	0	0	4	11500000	IPI00271986	26	2
603	Chchd6	2001	0	0	2	3790000	IPI00313390	10	2
604	Hnt	3001	0	0	3	6110000	IPI00417005	11	2
605	Cox6b1	4001	0	0	4	7530000	IPI00225390	29	2
606	Eif2b2	6001	0	0	6	7580000	IPI00116804	14	2
607	0910001A06Rik	3001	0	0	3	6190000	IPI00122015	12	3
608	Vamp2	3001	0	0	3	7250000	IPI00621210	28	2
609	IPI00396779_reve	3001	0	0	3	2380000	IPI00396779_reverse	2	3
610	Neurod2	3001	0	0	3	3340000	IPI00312748	12	2
611	Atp5o	3001	0	0	3	3660000	IPI00118986	15	2
612	Idh2	2001	0	0	2	3090000	IPI00318614	6	2
613	Inpp5a	3001	0	0	3	3800000	IPI00653599	7	3
614	Mog	3001	0	0	3	7280000	IPI00126405	13	3
615	Slc1a2	2001	0	0	2	5620000	IPI00470184	4	2
616	Oxa1l	3001	0	0	3	4670000	IPI00308001	4	2
617	Dcamkl1	2001	0	0	2	2140000	IPI00468380	4	2
618	Pcnt	3001	0	0	3	7350000	IPI00457623	0	3
619	2310040A13Rik	3001	0	0	3	3530000	IPI00153206	5	3
620	9530033F24Rik	3001	0	0	3	6900000	IPI00648985	7	3
621	Manba	3001	0	0	3	6550000	IPI00118011	3	2
622	Cpsf3	2001	0	0	2	1120000	IPI00135099	3	2
623	2900024O10Rik	3001	0	0	3	3430000	IPI00222749	10	2
624	2610207I05Rik	3001	0	0	3	7840000	IPI00403352	0	3
625	Rps7	4001	0	0	4	9570000	IPI00136984	26	2
626	Apc	3001	0	0	3	7460000	IPI00119913	1	3
627	LOC637613	3001	0	0	3	26600000	IPI00670399	29	2
628	Rusc2	2001	0	0	2	2300000	IPI00153354	3	2
629	B230113M03Rik	2001	0	0	2	2540000	IPI00453803	3	2
630	Dos	2001	0	0	2	7300000	IPI00471473	5	2
631	Gbe1	1.999000999	1	73600	2	6670000	IPI00109823	3	2
632	Fxyd6	2001	0	0	2	3750000	IPI00133224	26	2
633	Gdap1	2001	0	0	2	5840000	IPI00134137	7	2
634	Rab3a	3001	0	0	3	9420000	IPI00122965	11	2
635	Clu	2001	0	0	2	1880000	IPI00320420	6	2
636	Nfasc	3001	0	0	3	4490000	IPI00329927	2	2
637	Cntnap3	2001	0	0	2	5900000	IPI00341569	2	2
638	Erbb2ip	2001	0	0	2	3260000	IPI00457485	2	2
639	Dctn1	3001	0	0	3	3520000	IPI00115663	3	2
640	Pde4d	2001	0	0	2	1610000	IPI00228346	17	2
641	Bcdin3	3001	0	0	3	3050000	IPI00322456	6	2
642	2310061I04Rik	2001	0	0	2	5100000	IPI00665637	6	2
643	D130029J02Rik	2001	0	0	2	1800000	IPI00659752	2	2
644	Trf	2001	0	0	2	3740000	IPI00139788	4	2
645	Ace	3001	0	0	3	9100000	IPI00272690	2	3
646	Ccnt1	3001	0	0	3	9420000	IPI00653975	8	2
647	BC019943	2001	0	0	2	2710000	IPI00223204	5	2
648	Lamb2	3001	0	0	3	3990000	IPI00109612	2	3
649	Wac	2001	0	0	2	5530000	IPI00471431	5	2
650	Qtrt1	2001	0	0	2	3930000	IPI00125326	7	2
651	Sccpdh	2001	0	0	2	3390000	IPI00153266	9	2
652	Cyc1	4001	0	0	4	7120000	IPI00132728	12	2
653	Slitrk3	7001	0	0	7	8260000	IPI00329845	4	2
654	LOC620592	2001	0	0	2	2880000	IPI00676321	7	2
655	IPI00458913_reve	19001	0	0	19	251000000	IPI00458913_reverse	9	2
656	Usp53	4001	0	0	4	19500000	IPI00228192	3	2

Table 3. Unfiltered, non-redundant list of proteins identified via proteomic screen for synaptic ubiquitinated proteins, CONTINUED

Number	Gene Symbol	Tg/WT Ratio-spec#	WT-spec#	WT-intensity	Tg-spec#	Tg-Intensity	accession_number	% Coverage	numPepsUnique
657	Adprh	4001	0	0	4	6630000	IPI00111149	9	2
658	Vps52	2001	0	0	2	3080000	IPI00623259	3	2
659	2610529H08Rik	2001	0	0	2	3270000	IPI00113099	8	2
660	Gnb2	3001	0	0	3	4940000	IPI00162780	8	2
661	Lphn3	4001	0	0	4	24800000	IPI00411157	2	2
662	4930539P14Rik	2001	0	0	2	2010000	IPI00124568	4	2
663	Nfx1	2001	0	0	2	3230000	IPI00123537	3	2
664	Rac3	3001	0	0	3	2900000	IPI00157462	9	2
665	Opcml	2001	0	0	2	6650000	IPI00463489	9	2
666	Magi3	2001	0	0	2	2950000	IPI00111234	3	2
667	2410003P15Rik	2001	0	0	2	2470000	IPI00109603	6	2
668	Nid2	2001	0	0	2	3620000	IPI00129903	3	2
669	Ppp2r5b	2001	0	0	2	2670000	IPI00356872	5	2
670	Nuak1	2001	0	0	2	3340000	IPI00465504	3	2
671	Peg3	3001	0	0	3	6910000	IPI00462561	2	2
672	Atxn1	2001	0	0	2	4530000	IPI00323787	6	2
673	Tarsl1	2001	0	0	2	2790000	IPI00132419	3	2
674	G630014P10Rik	2001	0	0	2	5130000	IPI00668797	4	2
675	D330017J20Rik	3001	0	0	3	2180000	IPI00465770	4	2
676	S100a9	4001	0	0	4	31000000	IPI00222556	18	2
677	6430598A04Rik	4001	0	0	4	7400000	IPI00341975	4	2
678	Gata3	2001	0	0	2	1700000	IPI00135883	7	2
679	Tmem30a	2001	0	0	2	1620000	IPI00387318	9	2
680	Rtn4r	2001	0	0	2	3280000	IPI00121067	7	2
681	Atp5f1	4001	0	0	4	4910000	IPI00341282	8	2
682	Zfp655	2001	0	0	2	3230000	IPI00112984	7	2
683	Atp6v0d1	2001	0	0	2	3390000	IPI00313841	5	2
684	1700052N19Rik	2001	0	0	2	4990000	IPI00117106	10	2
685	Acat1	2001	0	0	2	2630000	IPI00154054	9	2
686	Ddef2	2001	0	0	2	2010000	IPI00355808	2	2
687	Foxo1	2001	0	0	2	2210000	IPI00311101	4	2
688	4632415K11Rik	3001	0	0	3	5150000	IPI00157480	5	2
689	Syp	3001	0	0	3	10100000	IPI00123505	7	2
690	Arf2	2001	0	0	2	3050000	IPI00135730	10	2
691	Glud1	2001	0	0	2	3010000	IPI00114209	2	2
692	C030018G13Rik	3001	0	0	3	2450000	IPI00222432	5	2
693	Vamp1	3001	0	0	3	9640000	IPI00407347	14	2
694	Pitpnm1	4001	0	0	4	10600000	IPI00136246	3	2
695	Usp7	2001	0	0	2	2250000	IPI00463367	2	2
696	G630024C07Rik	2001	0	0	2	8440000	IPI00222330	6	2
697	Dlat	2001	0	0	2	3640000	IPI00153660	4	2
698	Snap91	2001	0	0	2	3930000	IPI00122409	2	2
699	Slitrk5	2001	0	0	2	2870000	IPI00329844	3	2
700	Exoc4	2001	0	0	2	6520000	IPI00129959	2	2
701	Ptk9l	6001	0	0	6	8110000	IPI00129299	9	2
702	Dnm1	2001	0	0	2	2610000	IPI00620377	4	2
703	Csnk2b	3001	0	0	3	3890000	IPI00126762	15	2
704	Prr7	3001	0	0	3	5650000	IPI00132812	17	2
705	38967	3001	0	0	3	5610000	IPI00224626	8	2
706	IPI00663002	2001	0	0	2	5220000	IPI00663002	1	2
707	Marcks	2001	0	0	2	1020000	IPI00229534	15	2
708	Dars	4001	0	0	4	4460000	IPI00222457	7	2
709	Fbxo11	2001	0	0	2	3110000	IPI00330330	2	2
710	Hdac5	3001	0	0	3	6230000	IPI00283913	2	2
711	Syt10	2001	0	0	2	4810000	IPI00127866	3	2
712	Calm2	4001	0	0	4	3480000	IPI00467841	10	2
713	Vdac2	2001	0	0	2	3530000	IPI00122547	7	2
714	Atp2a2	2001	0	0	2	3840000	IPI00338964	3	2
715	Ppa2	2001	0	0	2	3170000	IPI00127050	8	2
716	Hs3st1	3001	0	0	3	4480000	IPI00129676	7	2
717	Igsf8	2001	0	0	2	5380000	IPI00321348	5	2
718	Igsf4d	2001	0	0	2	4340000	IPI00453537	13	2
719	Tiam2	3001	0	0	3	1270000	IPI00453791	2	2
720	Ampd3	2001	0	0	2	9640000	IPI00275398	3	2
721	Hspd1	2001	0	0	2	1090000	IPI00308885	8	2
722	Pard6g	2001	0	0	2	8710000	IPI00122398	4	2
723	IPI00223045_reve	3001	0	0	3	3540000	IPI00223045_reverse	6	2
724	LOC629059	3001	0	0	3	3690000	IPI00277852	6	2
725	A730042J05Rik	4001	0	0	4	5440000	IPI00128991	7	2
726	Sfxn5	2001	0	0	2	3780000	IPI00221602	9	2
727	Agxt2l1	2001	0	0	2	3970000	IPI00625940	4	2
728	Harsl	2001	0	0	2	4400000	IPI00116138	4	2
729	Cct2	1001	0	0	1	1040000	IPI00320217	2	1
730	Gpr158	2001	0	0	2	1970000	IPI00465871	2	2
731	4933402J24Rik	2001	0	0	2	3190000	IPI00137094	7	2
732	Tmem33	2001	0	0	2	4990000	IPI00133234	4	1
733	Sv2a	2001	0	0	2	4110000	IPI00465810	4	2
734	Dock4	3001	0	0	3	4090000	IPI00223070	1	2
735	BC006662	2001	0	0	2	3840000	IPI00124027	9	1
736	Clstn3	2001	0	0	2	2030000	IPI00115312	3	2
737	1500001H12Rik	2001	0	0	2	778000	IPI00122826	14	2
738	Alad	2001	0	0	2	1570000	IPI00112719	5	1

Table 3. Unfiltered, non-redundant list of proteins identified via proteomic screen for synaptic ubiquitinated proteins, CONTINUED

Number	Gene Symbol	Tg/WT Ratio-spec#	WT-spec#	WT-intensity	Tg-spec#	Tg-Intensity	accession_number	% Coverage	numPepsUnique
739	Ndufa8	3001	0	0	3	13800000	IPI00120984	13	2
740	IPI00515622_reve	0.00049975	2	350000	0	0	IPI00515622_reverse	1	2
741	Negr1	2001	0	0	2	5400000	IPI00330887	10	2
742	Car14	3001	0	0	3	5290000	IPI00126501	5	2
743	IPI00354300_reve	2001	0	0	2	1400000	IPI00354300_reverse	0	2
744	G430041M01Rik	3001	0	0	3	30100000	IPI00377298	12	2
745	Ncln	2001	0	0	2	2690000	IPI00226958	4	2
746	IPI00308658_reve	4001	0	0	4	22500000	IPI00308658_reverse	6	2
747	IPI00170013_reve	2001	0	0	2	5980000	IPI00170013_reverse	4	2
748	IPI00651964	2001	0	0	2	2940000	IPI00651964	11	2
749	Tex15	3001	0	0	3	7040000	IPI00118096	1	2
750	AW125753	1001	0	0	1	1970000	IPI00320004	4	1
751	Acot11	2001	0	0	2	1880000	IPI00623737	3	2
752	Grip1	2001	0	0	2	2710000	IPI00127232	3	2
753	IPI00623553	1001	0	0	1	1370000	IPI00623553	7	1
754	IPI00229601_reve	2001	0	0	2	10000000	IPI00229601_reverse	3	2
755	Hnrpu	2001	0	0	2	2280000	IPI00458583	1	1
756	2900002H16Rik	2001	0	0	2	1580000	IPI00121674	8	2
757	4921505C17Rik	2001	0	0	2	5860000	IPI00399440	1	2
758	Galc	2001	0	0	2	7190000	IPI00109904	6	2
759	Dynll1	2001	0	0	2	3870000	IPI00121623	24	1
760	Ndufs8	2001	0	0	2	6110000	IPI00170093	8	1
761	Ccnt2	3001	0	0	3	6740000	IPI00654257	4	2
762	5830411G16Rik	2001	0	0	2	2390000	IPI00330249	2	2
763	Fip1l1	2001	0	0	2	1730000	IPI00110716	5	2
764	2810405J04Rik	1001	0	0	1	4600000	IPI00457756	2	1
765	Enpp5	2001	0	0	2	5460000	IPI00111163	6	2
766	1810060J02Rik	2001	0	0	2	4020000	IPI00187274	4	2
767	Gpd2	2001	0	0	2	1680000	IPI00387307	4	2
768	Dynll2	3001	0	0	3	6550000	IPI00132734	24	1
769	Gbas	3001	0	0	3	14800000	IPI00115827	4	1
770	Uqcrfs1	1001	0	0	1	824000	IPI00133240	9	1
771	LOC636066	1001	0	0	1	1220000	IPI00662977	4	1
772	Zfp316	1001	0	0	1	1330000	IPI00420907	2	1
773	Gad2	1001	0	0	1	2810000	IPI00318522	3	1
774	Pip5k2a	1001	0	0	1	1480000	IPI00115708	3	1
775	Tbl3	1001	0	0	1	288000	IPI00124057	1	1
776	Ndufa12	2001	0	0	2	4800000	IPI00344004	11	1
777	Trappc2	10001	0	0	10	17700000	IPI00153838	10	1
778	Gtf2a1	5001	0	0	5	40200000	IPI00121198	2	1
779	Rpl8	1001	0	0	1	1360000	IPI00137787	4	1
780	Cox7a2l	2001	0	0	2	1810000	IPI00115949	28	1
781	Ppp1r9a	2001	0	0	2	1170000	IPI00336313	1	1
782	D12Ertd553e	1001	0	0	1	2020000	IPI00222044	4	1
783	Ephb2	1001	0	0	1	773000	IPI00648802	1	1
784	Foxp1	1001	0	0	1	2390000	IPI00654217	25	1
785	Dnajb9	1001	0	0	1	2520000	IPI00136218	6	1
786	Slc6a1	2001	0	0	2	3380000	IPI00227928	3	1
787	Timp4	1001	0	0	1	3570000	IPI00119215	8	1
788	AI326876	1001	0	0	1	480000	IPI00379159	5	1
789	Mrps2	1001	0	0	1	466000	IPI00126011	7	1
790	LOC634664	1001	0	0	1	2040000	IPI00670819	17	1
791	IPI00653798	3001	0	0	3	7320000	IPI00653798	7	1
792	Tbc1d10b	1001	0	0	1	1090000	IPI00469012	1	1
793	Atp5l	4001	0	0	4	11800000	IPI00133342	14	1
794	Scamp5	1001	0	0	1	1190000	IPI00122865	4	1
795	IPI00662904	1001	0	0	1	1120000	IPI00662904	7	1
796	Kng1	2001	0	0	2	5450000	IPI00114958	2	1
797	Cdh2	1001	0	0	1	3050000	IPI00404670	3	1
798	Sema6b	1001	0	0	1	564000	IPI00119931	3	1
799	Canx	1001	0	0	1	709000	IPI00119618	3	1
800	1200009B18Rik	2001	0	0	2	6230000	IPI00133365	5	1
801	BC039093	2001	0	0	2	1900000	IPI00342747	5	1
802	Fasn	1001	0	0	1	3710000	IPI00113223	0	1
803	Ndufv2	1001	0	0	1	1660000	IPI00109167	7	1
804	Cirh1a	1001	0	0	1	1070000	IPI00331601	2	1
805	Thy1	1001	0	0	1	11800000	IPI00109727	8	1
806	IPI00620636	1001	0	0	1	1250000	IPI00620636	4	1
807	Ndufb11	3001	0	0	3	3900000	IPI00114246	11	1
808	Mat2b	1001	0	0	1	2130000	IPI00468802	3	1
809	Aprin	1001	0	0	1	405000	IPI00317401	1	1
810	Aptx	1001	0	0	1	2750000	IPI00624837	5	1
811	Gm1673	1001	0	0	1	2960000	IPI00377774	8	1
812	Slc2a1	1001	0	0	1	1650000	IPI00308691	2	1
813	IPI00626163	1001	0	0	1	2800000	IPI00626163	4	1
814	Kcnd2	1001	0	0	1	784000	IPI00129491	3	1
815	IPI00116718	1001	0	0	1	3920000	IPI00116718	14	1
816	Rpl19	1001	0	0	1	1070000	IPI00122426	8	1
817	Metapl1	1001	0	0	1	1640000	IPI00132105	4	1
818	C630007B19Rik	1001	0	0	1	1790000	IPI00380407	11	1
819	Cryab	1001	0	0	1	804000	IPI00138274	7	1
820	Gnaq	1001	0	0	1	965000	IPI00228618	3	1

Table 3. Unfiltered, non-redundant list of proteins identified via proteomic screen for synaptic ubiquitinated proteins, CONTINUED

Number	Gene Symbol	Tg/WT Ratio-spec#	WT-spec#	WT-intensity	Tg-spec#	Tg-Intensity	accession_number	% Coverage	numPepsUnique
821	Neo1	2001	0	0	2	2030000	IPI00129159	1	1
822	Akap5	1001	0	0	1	1000000	IPI00667326	6	1
823	1200007B05Rik	1001	0	0	1	1450000	IPI00387392	9	1
824	Arbp	1001	0	0	1	992000	IPI00314950	9	1
825	1810035L17Rik	1001	0	0	1	747000	IPI00318935	10	1
826	4933407N01Rik	2001	0	0	2	13000000	IPI00338270	4	1
827	IPI00621661	1001	0	0	1	639000	IPI00621661	8	1
828	Rutbc1	1001	0	0	1	787000	IPI00515672	1	1
829	Gm1494	2001	0	0	2	2200000	IPI00381805	8	1
830	Ptprz1	1001	0	0	1	632000	IPI00627008	0	1
831	Ndufs2	1001	0	0	1	1750000	IPI00128023	4	1
832	IPI00668982	2001	0	0	2	3040000	IPI00668982	5	1
833	Wdr6	1001	0	0	1	1950000	IPI00117632	1	1
834	6330583M11Rik	2001	0	0	2	653000	IPI00165731	4	1
835	Prdx6-rs1	2001	0	0	2	1850000	IPI00221454	4	1
836	IPI00229906_reve	1001	0	0	1	568000	IPI00229906_reverse	1	1
837	6330403A02Rik	1001	0	0	1	4060000	IPI00462375	12	1
838	Mpped1	1001	0	0	1	1360000	IPI00131155	3	1
839	LOC634597	7001	0	0	7	8610000	IPI00668716	10	1
840	Lrrc4c	1001	0	0	1	1550000	IPI00309419	1	1
841	Wdr22	1001	0	0	1	140000	IPI00340504	1	1
842	LOC639819	1001	0	0	1	885000	IPI00668082	4	1
843	1110004F10Rik	1001	0	0	1	969000	IPI00127941	8	1
844	Suhw3	1001	0	0	1	1440000	IPI00622268	6	1
845	Mkl2	1001	0	0	1	1640000	IPI00172027	2	1
846	A430105I05Rik	1001	0	0	1	1190000	IPI00670075	0	1
847	5430405G24Rik	2001	0	0	2	3000000	IPI00341196	1	1
848	Suox	1001	0	0	1	933000	IPI00153144	3	1
849	Abhd11	1001	0	0	1	1630000	IPI00170213	12	1
850	Cited2	1001	0	0	1	3410000	IPI00133949	9	1
851	Gphn	2001	0	0	2	4820000	IPI00225670	2	1
852	LOC633821	2001	0	0	2	3050000	IPI00108740	7	1
853	S100a8	2001	0	0	2	2810000	IPI00230768	22	1
854	Syngr3	1001	0	0	1	3030000	IPI00331579	5	1
855	Nup43	1001	0	0	1	1410000	IPI00177202	2	1
856	Cdh1	1001	0	0	1	524000	IPI00318626	2	1
857	IPI00230018_reve	1001	0	0	1	1020000	IPI00230018_reverse	0	1
858	E430028B21Rik	1001	0	0	1	1670000	IPI00420284	1	1
859	LOC545854	1001	0	0	1	2990000	IPI00661705	14	1
860	Cpne5	1001	0	0	1	750000	IPI00170387	1	1
861	Pgrmc1	2001	0	0	2	1900000	IPI00319973	10	1
862	2900006B13Rik	2001	0	0	2	2890000	IPI00283339	2	1
863	Syngr1	2001	0	0	2	2400000	IPI00115763	5	1
864	Paqr4	1001	0	0	1	1670000	IPI00121743	6	1
865	Slc27a1	1001	0	0	1	1120000	IPI00120097	4	1
866	C030011J08Rik	3001	0	0	3	12600000	IPI00222792	1	1
867	IPI00338053_reve	1001	0	0	1	1320000	IPI00338053_reverse	2	1
868	Znhit4	1001	0	0	1	1110000	IPI00110781	4	1
869	Tbc1d10a	1001	0	0	1	1160000	IPI00139383	2	1
870	Exoc1	1001	0	0	1	1000000	IPI00153813	1	1
871	38781	1001	0	0	1	1050000	IPI00131895	5	1
872	IPI00309958_reve	1001	0	0	1	2030000	IPI00309958_reverse	1	1
873	Heca	1001	0	0	1	6140000	IPI00380838	2	1
874	Copa	1001	0	0	1	627000	IPI00229834	1	1
875	Grm3	1001	0	0	1	688000	IPI00136716	1	1
876	LOC638010	1001	0	0	1	710000	IPI00675804	5	1
877	Esd	2001	0	0	2	3330000	IPI00624892	5	1
878	Akap3	1001	0	0	1	1670000	IPI00136657	1	1
879	Aak1	1001	0	0	1	1510000	IPI00458612	2	1
880	Atp2b4	1001	0	0	1	1700000	IPI00463589	13	1
881	Zfp444	1001	0	0	1	102000	IPI00278424	3	1
882	Palm	1001	0	0	1	984000	IPI00129298	5	1
883	Rpusd4	1001	0	0	1	3820000	IPI00109744	3	1
884	Gnpda2	1001	0	0	1	3450000	IPI00133593	4	1
885	LOC638592	1001	0	0	1	1210000	IPI00673922	32	1
886	Ppp2r1a	1001	0	0	1	1170000	IPI00310091	3	1
887	Slc25a22	1001	0	0	1	10900000	IPI00109275	2	1
888	Klf12	1001	0	0	1	838000	IPI00133918	4	1
889	Sin3b	1001	0	0	1	587000	IPI00608092	1	1
890	Ilf3	1001	0	0	1	581000	IPI00130591	2	1
891	4631427C17Rik	1001	0	0	1	478000	IPI00308446	2	1
892	Itpka	1001	0	0	1	838000	IPI00153136	2	1
893	Slc8a2	1001	0	0	1	1010000	IPI00170310	1	1
894	Fth1	1001	0	0	1	2030000	IPI00230145	8	1
895	IPI00673003_reve	1001	0	0	1	1720000	IPI00673003_reverse	5	1
896	Mrpl9	1001	0	0	1	1510000	IPI00654010	5	1
897	IPI00109806_reve	1001	0	0	1	6760000	IPI00109806_reverse	3	1
898	Brp44	1001	0	0	1	1790000	IPI00131896	6	1
899	Slc4a4	1001	0	0	1	1180000	IPI00314749	2	1
900	Rab3gap2	1001	0	0	1	1080000	IPI00404477	0	1
901	Rhot1	1001	0	0	1	1160000	IPI00515349	1	1
902	Msl31	1001	0	0	1	2200000	IPI00331512	2	1

Table 3. Unfiltered, non-redundant list of proteins identified via proteomic screen for synaptic ubiquitinated proteins, CONTINUED

Number	Gene Symbol	Tg/WT Ratio-spec#	WT-spec#	WT-intensity	Tg-spec#	Tg-Intensity	accession_number	% Coverage	numPepsUnique
903	IPI00453842_reve	1001	0	0	1	48500	IPI00453842_reverse	0	1
904	C130038G02Rik	1001	0	0	1	3340000	IPI00380426	0	1
905	Nrgn	1001	0	0	1	2050000	IPI00380227	19	1
906	Strn	1001	0	0	1	2260000	IPI00352986	2	1
907	IPI00622396	1001	0	0	1	966000	IPI00622396	15	1
908	BC019806	1001	0	0	1	1250000	IPI00123765	5	1
909	IPI00136734_reve	1001	0	0	1	1930000	IPI00136734_reverse	2	1
910	Slit1	1001	0	0	1	2630000	IPI00330211	0	1
911	IPI00330900_reve	1001	0	0	1	3690000	IPI00330900_reverse	2	1

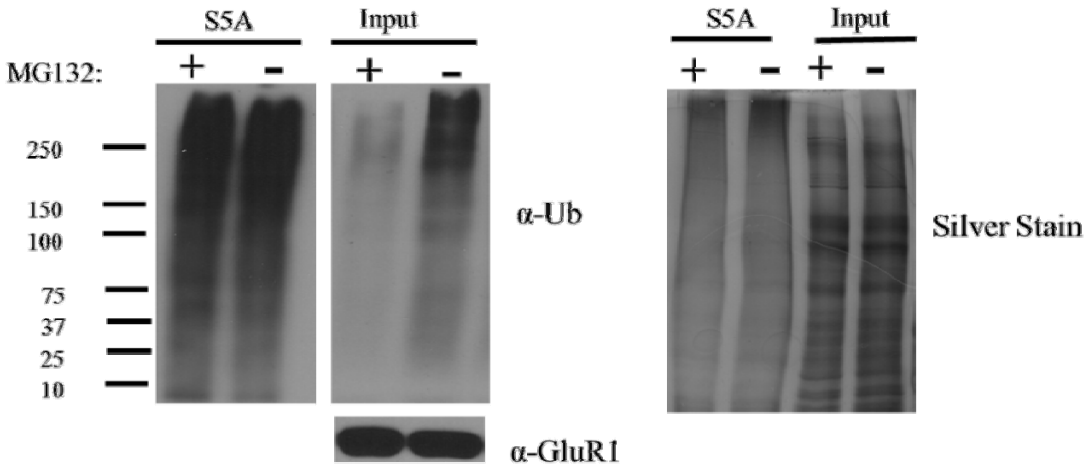

Figure 4. S5A enrichment of rat P2 lysates for mass spectrometry. Rat P2 lysates purified using GST-S5A conjugated beads, then analyzed via Mudpit-LC-MS/MS. Rat cortical neurons (DIV 18) were treated with MG-132 (5 μM) or DMSO for 8 hours prior to lysis and differential and density gradient fractionation. S5A-purified ubiquitin conjugates (left panel) and input lysates (middle panel) were subjected to SDS-PAGE and examined via western blot or silver stain (right panel).

Table 4. Top 50 hits from S5A directed screen for synaptic poly-ubiquitinated proteins. Rat P2 lysates purified using GST-S5A conjugated beads, then analyzed via Mudpit-LC-MS/MS. Rat hippocampal neurons (DIV 18) were treated with MG-132 (5 μM) or DMSO for 8 hours prior to lysis and differential and density gradient fractionation. Top 50 proteins identified by MS are listed based on spectrum count (highest to lowest) for DMSO or MG-132 treated samples

DMSO					MG-132			
Number	Descriptive Name	Sequence Count	Spectrum Count	Sequence Coverage	Number2	Descriptive Name3	Sequence Count4	Spectrum Count5	Sequence Coverage6
1	Psmd4 Antisecretory factor	25	90	0.503	1	Ubc Polyubiquitin	18	154	0.081
2	Ubc Polyubiquitin	15	89	0.079	2	(ligand binding domain rainbow trout)	26	142	0.228
3	Ubc similar to ubiquitin C isoform 1	15	74	0.23	3	Ubb Ubc protein	18	126	0.153
4	Ubb Ubc protein	15	74	0.149	4	Psmd4 Antisecretory factor	33	117	0.626
5	Rps27a Ribosomal protein S27a	15	73	0.41	5	Ubc similar to ubiquitin C isoform 1	18	117	0.237
6	no description	15	73	0.842	6	Rps27a Ubiquitin	18	117	0.868
7	Rps27a Ubiquitin	15	73	0.842	7	Rps27a Ribosomal protein S27a	18	116	0.423
8	Uba52 Ubiquitin A-52 residue ribosomal protein fusion product 1	15	73	0.5	8	no description	18	116	0.868
9	Tubb3 Tubulin beta-3 chain	20	68	0.498	9	Uba52 Ubiquitin A-52 residue ribosomal protein fusion product 1	18	116	0.516
10	LOC498736 Tubulin beta-2A chain	25	64	0.557	10	LOC498736 Tubulin beta-2A chain	21	74	0.589
11	Tubb2b Tubulin beta-2B chain	25	63	0.557	11	Tubb2b Tubulin beta-2B chain	21	73	0.589
12	Cfl1 Cofilin-1	17	57	0.488	12	Tubb3 Tubulin beta-3 chain	18	67	0.471
13	Tubb5 Isoform 1 of Tubulin beta-5 chain	17	56	0.486	13	Cfl1 Cofilin-1	15	64	0.5
14	Eno1 Alpha-enolase	21	48	0.482	14	Tuba1 Tubulin alpha-1A chain	19	60	0.486
15	LOC688509 similar to Alpha-enolase	21	48	0.422	15	Tuba1;RGD1565476_predicted Tubulin alpha-1B chain	19	58	0.486
16	Tubb2c Tubulin beta-2C chain	19	47	0.524	16	Tubb2c Tubulin beta-2C chain	18	57	0.53
17	Dpysl5 Dihydropyrimidinase-related protein 5	24	47	0.408	17	Tubb5 Isoform 1 of Tubulin beta-5 chain	16	54	0.459
18	no description	26	44	0.408	18	Heat shock 70 kDa protein 1A/1B	24	47	0.452
19	Tubb4 similar to tubulin, beta 4	16	42	0.475	19	Tubb4 similar to tubulin, beta 4	14	47	0.444
20	Tuba1;RGD1565476_predicted Tubulin alpha-1B chain	17	42	0.461	20	Eef1a1 Elongation factor 1-alpha 1	17	47	0.292
21	Tuba1 Tubulin alpha-1A chain	17	42	0.461	21	- 50 kDa protein	17	47	0.292
22	Gsta2;Gsta3;Yc2 Glutathione S-transferase alpha (Fragment)	15	40	0.602	22	Dpysl5 Dihydropyrimidinase-related protein 5	27	44	0.436
23	no description	20	36	0.367	23	Gsta2;Gsta3;Yc2 Glutathione S-transferase alpha (Fragment)	16	43	0.588
24	Pkm2 Isoform M2 of Pyruvate kinase isozymes M1/M2	18	35	0.366	24	Tuba4 Tubulin alpha-4A chain	16	43	0.362
25	RGD1561179_predicted similar to pyruvate kinase 3	18	35	0.367	25	Eno1 Alpha-enolase	15	41	0.491
26	Pkm2 Isoform M1 of Pyruvate kinase isozymes M1/M2	18	34	0.366	26	LOC688509 similar to Alpha-enolase	15	41	0.43
27	BSA	12	32	0.188	27	Psmc5 26S protease regulatory subunit 8	17	39	0.404
28	Gfap Isoform 1 of Glial fibrillary acidic protein	16	31	0.349	28	Tubb6 Tubulin, beta 6	11	39	0.289
29	Gfap Isoform 2 of Glial fibrillary acidic protein	16	31	0.35	29	Gfap Isoform 1 of Glial fibrillary acidic protein	21	38	0.463
30	Hspa8 Heat shock cognate 71 kDa protein	21	31	0.313	30	Gfap Isoform 2 of Glial fibrillary acidic protein	21	38	0.465
31	Rps3 40S ribosomal protein S3	10	29	0.395	31	Psmc4 26S protease regulatory subunit 6B	16	38	0.416
32	Serbp1	16	28	0.474	32	Psmb5 similar to proteasome subunit, beta type 5	12	36	0.449
33	Eef1a1 Elongation factor 1-alpha 1	14	28	0.29	33	Psmc3 Proteasome (Prosome, macropain) 26S subunit, ATPase 3	19	36	0.443
34	- 50 kDa protein	14	28	0.29	34	Psmc1 26S protease regulatory subunit 4	17	36	0.414
35	Hnrpk 48 kDa protein	15	27	0.388	35	RGD1561179_predicted similar to pyruvate kinase 3	20	34	0.421
36	Stxbp1 Isoform 1 of Syntaxin-binding protein 1	17	27	0.301	36	Pkm2 Isoform M1 of Pyruvate kinase isozymes M1/M2	20	34	0.388
37	Stxbp1 Isoform 2 of Syntaxin-binding protein 1	17	27	0.297	37	Prss1 Anionic trypsin-1 precursor	3	33	0.081
38	Tubb6 Tubulin, beta 6	12	27	0.255	38	Crmp1 Dihydropyrimidinase-related protein 1	23	32	0.434
39	LOC680312;LOC682665 similar to H2B histone family, member T	6	26	0.421	39	Hspa8 Heat shock cognate 71 kDa protein	20	31	0.372
40	RGD1561543_predicted similar to Histone H2B 291B isoform 2	6	26	0.421	40	- 67 kDa protein	20	31	0.393
41	Hist1h2bn_predicted similar to Histone H2B 291B	6	26	0.356	41	Actb Actin, cytoplasmic 1	14	31	0.317
42	Hist1h2bm_predicted;LOC682355 similar to Histone H2B 291B	6	26	0.384	42	Actg1 similar to Actin, cytoplasmic 2	14	31	0.317
43	Histone H2B 291B	6	26	0.421	43	LOC295810 similar to Actin, cytoplasmic 2	14	31	0.222
44	Hist1h2bp_predicted 15 kDa protein	6	26	0.396	44	Actg1 similar to Actin, cytoplasmic 2	14	31	0.17
45	- 15 kDa protein	6	26	0.396	45	Stxbp1 Isoform 1 of Syntaxin-binding protein 1	25	30	0.5
46	- 14 kDa protein	6	26	0.421	46	Stxbp1 Isoform 2 of Syntaxin-binding protein 1	25	30	0.493
47	Hist1h2bl Histone H2B type 1	6	26	0.424	47	Serbp1	18	29	0.435
48	LOC684647;LOC679910 similar to Histone H2B 291B	6	26	0.421	48	no description	17	28	0.32
49	Arf3 ADP-ribosylation factor 3	8	26	0.354	49	Arf3 ADP-ribosylation factor 3	11	26	0.547
50	Arf1 ADP-ribosylation factor 1	8	26	0.354	50	Arf1 ADP-ribosylation factor 1	11	26	0.547

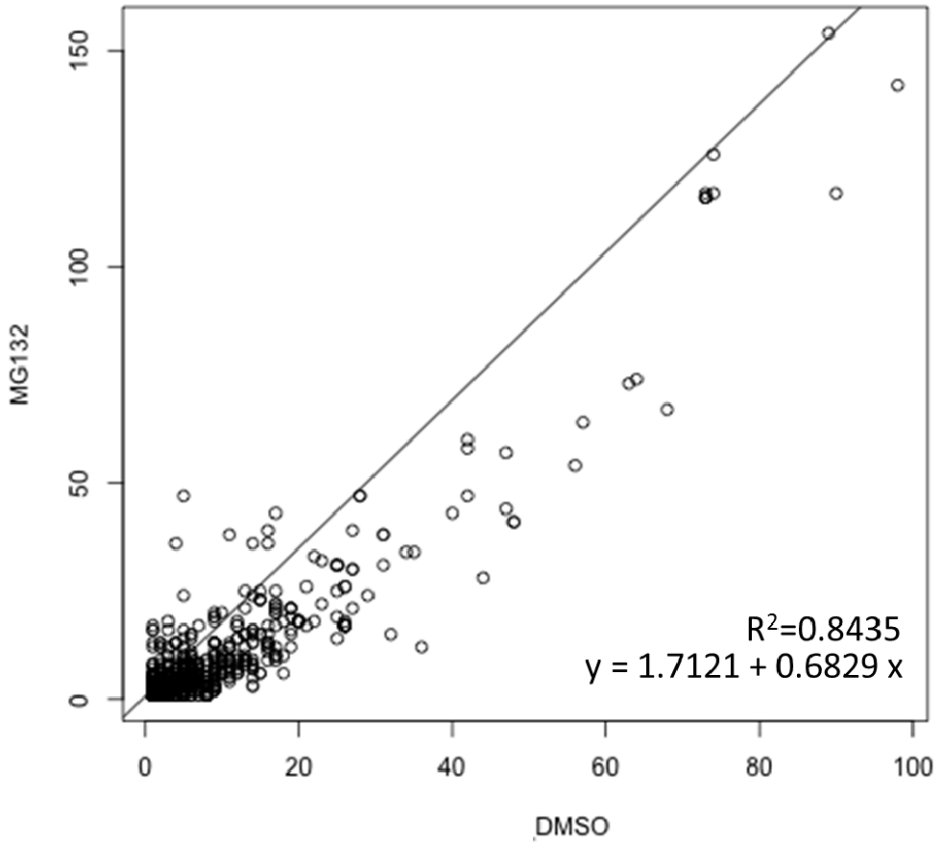

Figure 5. Scatterplot of top 150 overlapping targets between DMSO and MG-132 treated samples. The top 150 hits of the DMSO (x-axis) and MG-132 (y-axis) samples from S5A-directed screen for synaptic, poly-ubiquitinated proteins were plotted. A linear model was fit and tested for significance of correlation. The best fit line is plotted, and the P-value testing the null hypothesis that the slope of the line is equal to zero was $P<10^{-16}$.

Chapter II

Characterization of Stromal Interaction Molecule I (STIM1)

INTRODUCTION

Protein modification via the covalent attachment of ubiquitin is one of the most common regulatory processes in mammalian cells (See Review by (Pickart, 2004)). Classically, ubiquitination is a process whereby target proteins can be marked for degradation by the proteasome. It is a multi-step enzymatic process, using three classes of enzymes (E1s, E2s, and E3s), and it involves the sequential transfer of ubiquitin from these enzymes to a lysine residue on the target protein. Both degradative and non-degradative forms of ubiquitination have been implicated in a myriad of cellular processes. Depending on the topology of the ubiquitin chain, changes in protein stability, interaction, and localization can be effected (Hochstrasser, 2006). Specificity of the ubiquitination reaction depends on the later steps of the ubiquitination process. There are a significant but limited number of ubiquitin-carrier enzymes (E2s), and a much larger number of ubiquitin ligases (E3s). Thus, the ubiquitination enzymes form a hierarchical cascade, where the substrate specificity of the overall ubiquitination reaction depends on the specific E2s and E3s that pair up to ubiquitinate the substrate.

In a sense, calcium is similar to ubiquitin in both its abundance and widespread role in cellular signaling (Berridge et al., 2000). Accordingly, mechanisms regulating ubiquitination and calcium levels will have great effects on cellular signaling and function. One of the more intriguing targets to appear in the aforementioned synaptic screen for ubiquitinated proteins was just such regulator - Stromal Interaction Molecule I (STIM1). In brief, STIM1 is a type-I membrane, endoplasmic reticulum

(ER)-resident protein and probable sensor of store-operated calcium entry (SOCE) (Liou et al., 2005; Roos et al., 2005; Spassova et al., 2006). In both excitable and non-excitable cells, SOCE is generally characterized by the process in which depletion of internal Ca^{2+} stores leads to an activation of plasma membrane Ca^{2+} channels, and subsequent refilling of internal stores (Lewis, 2007; Putney, 2007). In addition to refilling stores, SOCE has been implicated in a myriad of diverse processes, including gene expression, apoptosis, and exocytosis (See Review by Parekh and Putney, 2005) (Parekh and Putney, 2005). In the last ten years, a great deal of research has been conducted on the cellular function of STIM1. STIM1 was originally discovered in concurrent, yet independent set of RNAi screens for effectors of SOCE (Liou et al., 2005; Roos et al., 2005; Zhang et al., 2005). STIM1 has been shown to be both necessary and sufficient for SOCE activation. In addition to STIM1, another STIM isoform, STIM2 was also found to regulate SOCE and basal calcium levels, albeit at lower calcium thresholds (Brandman et al., 2007).

STIM1 is found distributed diffusely throughout the ER when Ca^{2+}-stores are replete; but once stores are emptied, it oligomerizes and redistributes into discrete, punctate clusters within the ER, at or near the plasma membrane (Hewavitharana et al., 2008; Liou et al., 2007; Zhang et al., 2005). This process is rapidly reversibly, but by mechanisms not yet understood (Smyth et al., 2008; Tamarina et al., 2008). The oligomerization and redistribution precedes and is correlated with subsequent activation of SOCE (Calloway et al., 2009; Luik et al., 2008; Stathopulos et al., 2006; Wu et al., 2006). STIM1 also undergoes numerous post-translational modifications,

each effecting a change in localization and function. STIM1 is phosphorylated at Serine-486 and Serine-668 during mitosis, resulting in an inhibition of SOCE through the prevention of STIM1 redistribution (Smyth et al., 2009). Moreover, glycosylation of the SAM (sterile-alpha motif) domain positively regulates the insertion of STIM1 into the plasma membrane, as well as promoting the interaction of various binding-partners(Csutora et al., 2008; Williams et al., 2002).

It is also inversely related to the calcium-bound state of the EF-hand domain (Liou et al., 2005; Zhang et al., 2005). Populations of STIM1 have been found both within and near the plasma membrane (Lewis, 2007; Zhang et al., 2005). Biotinylation studies have shown a significant population (20 – 30%) of total STIM1 residing at the surface (Manji et al., 2000). Whether STIM1 is inserted into the plasma membrane as a functional response to activated SOCE is still contested (Lewis, 2007; Liou et al., 2007; Zhang et al., 2005). It has been demonstrated that translocation to the plasma without STIM1 insertion is sufficient to activate SOCE (Baba et al., 2006). This begs the question, what is the role of surface STIM1? Moreover, it also suggests trafficking mechanisms, whether active or passive, are integral to STIM1 functionality.

The identity of putative SOC channels remains a bit nebulous (see review by(Cahalan, 2009). STIM1 has been shown to interact with the recently identified Ca^{2+}-release activated Ca^{2+} channel (CRAC) components, Orai, providing a link between store-depletion and plasma membrane CRAC channel activation (Yeromin et al., 2006). STIM1 couples and activates Orai1-3 through its C-terminus, in calcium-

store dependent manner, although truncation analyses of STIM1 show that interaction and activation of OraiI does not require prior redistribution (Muik et al., 2009; Park et al., 2009). STIM1 also interacts with and activates and TRPC1-6 channels (Alicia et al., 2008). The likely conclusion is that STIM1 is promiscuous with regard to channel coupling and activation, with no single channel typifying SOCE.

With regards to the central nervous system, SOCE has been implicated in such neuronal phenomena as synaptic plasticity and neurite outgrowth, but very little is known about STIM1 in neurons (Baba et al., 2003; Tang and Kalil, 2005). Recent studies examining STIM1 and STIM2 knockout mice demonstrate suggest a reversal of roles in terms of regulation of internal calcium stores (Berna-Erro et al., 2009). In neurons, STIM2 appears to be the essential regulator of SOCE, with a yet unidentified role for STIM1. As a known regulator of SOCE and putative target of the UPS, we sought to characterize STIM1 in neurons and to examine the role of ubiquitination in STIM1 function. We report that STIM1 is distributed in a punctate, peri-synaptic fashion in hippocampal neurons. STIM1 is also detected at the surface of both mature and developing neurons including growth cones. STIM1 is ubiquitinated in heterologous cells and in neuronal tissues; however, we have found no direct evidence for its degradation by the proteasome. Thapsigargin-induced calcium store depletion, which promotes STIM1 redistribution to or near the plasma membrane and induces SOCE, modulates STIM1 ubiquitination. This suggests ubiquitination may be involved in STIM1 localization and function in cells. In line with this hypothesis, we find that co-expression of STIM1 with POSH, a RING finger E3 ligase implicated in

SOCE function, negatively regulates STIM1 surface population in HEK293T cells. Taken together, our findings suggest ubiquitination to be a novel mechanism for regulating STIM1 distribution and function in both excitable and non-excitable cells.

RESULTS

Validation of STIM1 Ubiquitination

Following the sorting and filtering of the targets obtained from the mass spectrometry screen, the first protein to examine more thoroughly was STIM1. The nature of the screen, as well as the stringency of the subsequent data filtering, greatly lowered the chance for non-specific hits. Since the screen was carried out under denaturing conditions, proteins that bound to the nickel-affinity beads did so because of covalently attached His-6X-ubiquitin, or internal stretches of amino acids able to coordinate nickel. However, further validation was necessary to determine the accuracy of the screen, but also to determine the type of ubiquitination. There are a variety of ways to validate ubiquitination and home –in on the specific ubiquitination type. The first method involved a sequential IP, using antibodies specific for ubiquitin (DAKO) itself, followed by those specific for STIM1. Starting with P2 synaptosomal rat lysates, similar to those used in the screen, a ubiquitinated population was isolated, with an approximately 105 kDa (Fig. 6A, top panel). Unmodified STIM1 usually runs around 97 – 100 kDa, so this shift is consistent a single (8 kDa) ubiquitin addition, or monoubiquitination (Hershko and Ciechanover, 1998). Moreover, the ubiquitin blot for the sequential IP shows a similar band migrating around this distance (Fig. 6A, bottom panel). Another method to identify ubiquitinated proteins is through the use of ubiquitin-binding beads. One such bead, p62-agarose, contains the ubiquitin associated domain (UBA), and binds to both mono- and poly-ubiquitin (Ciani et al., 2003; Long et al., 2008).

STIM1 was again isolated from endogenous, rat P2 preparations as in Figure 6A, albeit at a lesser extent (Fig. 6B). This may be due to the fact that p62 affinity for poly-ubiquitin conjugated proteins is reported to be 4-fold higher than that of mono-ubiquitinated conjugates (Long et al., 2008).

Another immuno-based approached produced similar results. This time, using an antibody that recognizes conjugated mono- and poly-ubiquitin, modified STIM1 was identified from rat P2 synaptosomal lysates (Fig. 6C). An 8-10 kDa shift was again observed, suggesting a mono-ubiquitin modification. The final initial examination of STIM1 ubiquitination employed an overexpression approach. Much of the research done up to the time these experiments were conducted had been carried out in non-neuronal cells. Since HeLa and HEK-293 cells were the common used, we decided to examine whether this mono-ubiquitination observed in mouse and rat brain was also conserved in the other cell types. As expected, STIM1 appears to be mono-ubiquitinated in HEK-293T cells as well (Fig. 6D). There may also be multi-mono or poly ubiquitin conjugates, as shown by the HA-immunoreactive smears above the STIM1-GFP arrow. Initial observations clearly indicate that STIM1 is mono-ubiquitinated in neuronal and non-neuronal tissues. Unfortunately, the screen was only directed against ubiquitin modifications, with no secondary phenotype examined that may provide insight into cause or effect of this ubiquitination. This, along with basic characterization of STIM1 in neuronal tissues, was the impetus behind the remainder of the experiments.

Characterization of STIM1 in neurons

Basic understanding of STIM1 function in neurons will begin with an examination of temporal and spatial expression patterns. With no difference reported in the literature concerning the structure of STIM1 in neurons versus non-excitable cell types, it would reason that STIM1 localization and function in neurons would be similar. In non-excitable cell types, STIM1 is ubiquitously expressed throughout all stages of development and cell cycle and it is primarily localized to the endoplasmic reticulum (ER), with a smaller, yet significant population migrating at or near the plasma membrane (Lewis, 2007; Liou et al., 2007; Zhang et al., 2005). In terms of neuronal and synaptic expression, there are additional developmental timeframes and subcellular compartments to explore (Cline, 2005; Gibson and Ma, 2011; Harris, 1999). Whether a protein is pre- or post-synaptic, or where within the postsynaptic side it resides greatly underlies its function (Kim and Huganir, 1999). We first determined the temporal protein expression profile of STIM1 from cultured, dissociated cortical neurons. As shown in Figure 7A, STIM1 proteins levels are low in young developing cultures (DIV 3; days in vitro) and increase to a steady-state level in mature cultures (DIV 21 and 25). This suggests STIM1 functions in both developing and mature neurons. To determine the subcellular distribution of STIM1, we fractionated rat brain by differential and density gradient fractionation methods as previously described (Carlin et al., 1980; Cho et al., 1992). We found STIM1 to be present in both soluble and pellet fractions (Fig. 6B). Moreover, STIM1 was present

in fractions enriched for postsynaptic densities, suggesting that it may function at or near synapses (Fig. 7B).

To further characterize STIM1 in neurons, we immunostained dissociated hippocampal neurons with anti-STIM1 antibodies. We found endogenous STIM1 immunoreactivity to be present in a membranous and punctate fashion in both somatic and dendritic compartments of mature hippocampal neurons (Fig. 8). Interestingly, several STIM1 punctate clusters co-localized and co-distributed with postsynaptic density (PSD) protein marker Shank, further indicating STIM1 to be present near the PSD. In addition, we expressed STIM1-GFP in neurons by Sindbis virus transduction methods. Hippocampal cultures were infected with STIM1-GFP virion for approximately 12 hours, at which time the cultures were fixed and stained with either anti-STIM1, PSD-95, synapsin or calreticulin antibodies. As shown in Figure 9A, STIM1-GFP is recognized by anti-STIM1 antibodies. Similar to endogenous STIM1, STIM1-GFP is distributed in a membranous and punctate fashion (Fig. 9A-D). STIM1-GFP partially co-localized and co-distributed with presynaptic and postsynaptic protein markers, synapsin and PSD-95, respectively. As expected, STIM1-GFP protein is abundantly found in the ER as indicated by the high degree of co-localization with the ER associated protein, calreticulin (Fig. 9D). This indicates STIM1-GFP is distributed in a similar manner as endogenous STIM1 in neurons.

Surface expression of STIM1 is known to occur in non-excitable cells, although strong debate lingers regarding the role of this surface population (Lewis, 2007; Liou et al., 2007; Zhang et al., 2005). In search for a similar surface population

in neurons, rat cortical lysates were biotinylated and the neutravidin precipitates were analyzed via western blot. Surface populations of endogenous STIM1 were identified in cortical neurons (Fig. 10A). Surface population were also seen following live-labeling of STIM1-GFP infected neurons (Fig. 10B and C). Interestingly, this surface population is present in both immature (DIV4) and mature (DIV 21) rat hippocampal neurons (Fig 10B and C). The surface signal identified in the immature neurons was also present at the tips of developing growth cones (Fig. 10C). This localization strongly suggests a role in axon has been shown to be localized to the plasma membrane (Hauser and Tsien, 2007). To do this, we expressed STIM1-GFP in hippocampal neurons, and then live-labeled the cultures with anti-GFP antibodies. If STIM1-GFP was integrated into the plasma membrane, the GFP epitope-tag should be displayed on the surface and thus accessible to the anti-GFP antibodies. Indeed, we observed a punctate, surface signal for STIM1-GFP in both somatic and dendritic compartments of hippocampal neurons (Figure 10B). Interestingly, the majority of these puncta in dendrites were juxtaposed to PSD-95 clusters indicating that STIM1-GFP is primarily integrated into the plasma membrane at or near synapses. Live-labeled STIM1-GFP expressing immature cultures (DIV 4) with anti-GFP antibodies. revealed punctate clusters on the surface of growth cones, many of which were at the tips growth cone extensions (Figure 10C). These data suggest STIM1 may function at the surface of neurons at or near synapses and in growth cones. Furthermore, STIM1 function may be important for growth cone dynamics to facilitate outgrowth and guidance.

Although the physiological relevance of SOCE has been shown in neurons, very little is known about its role in neuronal development. Cytoplasmic calcium has been shown to play a critical role in growth cone dynamics, neurite outgrowth, and the development of synapses (Henley et al., 2004). Since STIM1 is expressed in immature neurons and localized to growth cones, we wondered what the functional consequences of blocking SOCE would be on neurite outgrowth. Treating cultured hippocampal neurons (DIV1) with the IP3 receptor antagonist and SOCE inhibitor 2-aminoethoxydiphenyl borate (*2-APB*) for various periods of time, and then comparing neurite length between control and treated groups revealed a striking connection between SOCE and neurite outgrowth. Within 36 hours of exposure to 2-APB, we found MAP2 positive neurites to be significantly shorter than control treated neurons. Neurite length in the 2-APB treated samples are roughly 40% shorter through the 60 hour mark, and begin to recover slightly, with only a 30% deficit at the end of 96 hours (Fig. 10C). Together, with the fact that STIM1-GFP is localized to growth cones and the tips of growth cone processes, this indicates STIM1 and SOCE function are important for neurite outgrowth of developing neurons (Fig. 11 A-C).

During depletion of internal calcium stores, STIM1 rapidly redistributes into membranous puncta within the ER and near the plasma membrane (Liou et al., 2007; Wu et al., 2006; Zhang et al., 2005). This redistribution correlates with and is necessary for activation of SOCE (Baba et al., 2006). To determine if this trait held true for STIM1 in neurons, we treated STIM1-GFP expressing neurons with the SERCA (Sarco/Endoplasmic Reticulum Ca^{2+} ATPase) pump antagonist thapsigargin

(TG) and monitored STIM1-GFP redistribution in living neurons (Fig. 12). As previously shown in Figure 7 and 8, STIM1-GFP is distributed in a membranous and punctate fashion in the absence of store-depletion (Fig. 12A – left panel). However, STIM1-GFP rapidly redistributes into large, punctate clusters within minutes of adding TG to the bath solution (Fig. 12A – right panel, Fig. 12B). Therefore, the mechanism of STIM1 activation and TG-induced redistribution is very similar to that found in non-excitable cells.

The role of proteasome in SOCE function and STIM1 localization

Since STIM1 was identified in a screen for novel synaptic ubiquitinated proteins, an possibility was that proteasome inhibition may affect SOCE function. This was before it appeared that STIM1 is mono-ubiquitinated, and thus not destined for degradation of the proteasome(Kirkpatrick et al., 2005b). However, the results obtained were quite interesting, albeit difficult to model given the current understanding of STIM1 function. Utilizing HEK293T cells loaded with calcium indicator Fluor4-AM, we examined thapsigargin-induced calcium influx in the presence of proteasome inhibitor MG-132. Compared to control treated cells, proteasome inhibitors significantly increased peak TG-induced SOCE in HEK293T (TG, 1.54 ±0.08; MG-132+TG, 2.16 ±0.23; MG-132, 1.08±0.04 fold change of control; $p<0.05$ compared to STIM1-GFP alone, unpaired Student t-test) (Fig. 13A and B). Previous studies have shown STIM1 functionality is dependent on both STIM1 levels as well as localization (Liou et al., 2005; Spassova et al., 2006). Overexpression of STIM1 results in an increase in the amplitude of SOCE (Liou et al.,

2005), whereas application of STIM1 antibodies specific to extracellular domains leads to an inhibition of CRAC channel current (Spassova et al., 2006). Thus, we next wanted to examine if this proteasome-dependent increase in peak SOCE correlated with a change in either STIM1 localization or stability. Under identical experimental parameters, we first examined the STIM1 surface population. HEK293T cells expressing STIM1-GFP were treated as in Figure 13 A, B with proteasome inhibitor MG-132 (10 μM) one hour prior to store-depletion with TG (1 μM) (Figure 10C). We found that STIM1-GFP surface levels were significantly increased in cells pretreated with MG132 (Figure 13D; TG + MG132, 1.54±0.07 fold change relative to control; $p<0.05$ compared to STIM1-GFP alone, unpaired Student t test). This was in contrast to surface STIM1-GFP levels in cells treated with MG132 or TG alone (MG-132, .95±0.06; TG, 1.02±0.05 fold change relative to control). This would suggest the component of SOCE that is potentiated by proteasome inhibition is coupled to the TG-induced depletion of internal stores.

Since proteasome inhibitors cause both an increase in SOCE and STIM1 surface levels, we next examined whether STIM1 was degraded by the proteasome. Steady-state levels of endogenous STIM1 protein in HEK293T cells treated with TG (1μM) in the presence of proteasome inhibitor, MG132 (10 μM), and in the presence or absence of protein synthesis inhibitors (cycloheximide, 50 μg/mL). As seen in Figure 13E, we found no difference in STIM1 protein levels between vehicle-treated, TG-treated, or TG plus MG132-treated cells in the presence or absence of protein synthesis inhibitors after 8 hours. This suggests that STIM1 is not degraded by the

proteasome under these conditions. Furthermore, it suggests that store-depletion does not cause a change in the turnover-rate of STIM1 in cells. Total STIM1 levels do not appear to be changing following activation of SOCE, with or without proteasome inhibition. When the ubiquitinated population of STIM1 is examined, however, these conditions do result in an observable change. Using p62-agarose beads to isolate ubiquitinated or ubiquitin-associated STIM1, the amount of STIM1 immunoreactive precipitates increase with concomitant proteasome inhibition (MG) and store-depletion (TG) (Fig. 14 A and B). The total levels, however, do not appear to change (Fig. 14A). This would suggest that STIM1 ubiquitination is not leading to degradation via the proteasome, but in fact, a proteasome sensitive factor promotes STIM1 ubiquitination in SOCE-dependent manner. Induction of SOCE via application of thapsigargin occurs in less than a minute(Parekh and Putney, 2005). Perhaps the 30 minute or 2 hour drug-treatments were resulting in a non-physiological modifications of STIM1. Short applications of TG revealed that STIM1 ubiquitination is rapid, but transient (Fig. 14C). There are a number of possible reasons for this transient ubiquitination – there are likely a host of other (proteasome-dependent) factors that are required for modification of STIM1.

UPS mediated perturbations of STIM1 function and localization

Since we did not observe any proteasome-dependent change in STIM1 stability, we wondered if ubiquitination might regulate STIM1 distribution in cells. Recently, the RING-finger ubiquitin ligase POSH (plenty of SH3's) was found to be involved in calcium homeostasis. POSH, which is associated with the trans-golgi

network and was originally identified as a factor required for the targeting of HIV-1 to the plasma membrane (Alroy et al., 2005), was shown to regulate calcium homeostasis by promoting the redistribution of Herp (homocysteine-inducible ER protein) to the ER (Tuvia et al., 2007). Upon TG-induced ER calcium store depletion, POSH promotes Herp lys-63-linked poly-ubiquitination, which in turn promotes the redistribution of Herp to the ER (Tuvia et al., 2007). Interestingly, POSH overexpression attenuates TG-induced calcium burst. Conversely, the inhibition of POSH by the expression of a RING-finger mutant, $POSH^{V14A}$, or by RNAi, enhances this phenomenon. Since POSH function is required for the maintenance of calcium homeostasis, presumably by controlling the distribution of regulatory molecules, we wondered if POSH might be involved in the regulation of STIM1 distribution. To examine this, we co-expressed WT myc-tagged POSH or $POSH^{V14A}$ (a catalytically inactive variant) together with STIM1-GFP in HEK293T cells. The cells were then live-labeled HEK293T with anti-GFP antibodies to detect surface STIM1-GFP. Overexpression of WT POSH dramatically reduced surface STIM1-GFP levels (STIM1-GFP alone, 1.0±0.16; STIM1-GFP plus POSH WT, 0.43±0.12 $p<0.01$ compared to STIM1-GFP alone, unpaired Student t test; STIM1-GFP plus POSH V14A, 1.17±0.19) (Figure 15A and B). This was dependent on POSH ligase activity, as the RING finger mutant, $POSH^{V14A}$, had no effect on STIM1-GFP surface levels (Figure 15A and B). As expected, POSH overexpression had no effect on the stability of STIM1 (Fig. 15 C). Unfortunately, overexpression of POSH (either WT or V14A) has not observable effect on STIM1 ubiquitination (data not shown).

Immunoprecipitation of STIM1, however, does reveal that STIM1 and POSH are able to interact (Fig. 15D – Top Panel). Interestingly, the V14A is able to co-precipitate with STIM1 at a much higher level than the WT (Fig. 15D – Top Panel). The RING finger mutant affects binding of the E2-E3 complex, thus the reaction may be halted at the STIM1-POSH complex step (Alroy et al., 2005; Deshaies and Joazeiro, 2009).

It has been confirmed that STIM1 is ubiquitinated, and that the E3 ligase, POSH, interacts with and down regulates STIM1 from the surface in a RING-finger dependent manner. What is not known is if there are any preferred sites of ubiquitination, and if those sites are critical for localization and function of STIM1. Typically, mass spectrometric analysis of purified lysates provides the best avenue for identifying modified lysine residues. Even with ample amounts of modified target, the promiscuous nature of ubiquitination can make finding a single, specific site impossible (Danielsen et al., 2010; Peng, 2008). In lieu of this mass spectrometry, ubiquitin site prediction algorithms were used {Radivojac, 2010 #378, with the top five candidates from mouse STIM1. Targets were examined using site-directed mutagenesis and immunoprecipitation using ubiquitin antibodies (Fig. 16). The sites with the highest predicted score were K536R, K570R, K580R, K650R, and K651R. Lysine to arginine mutants were created to maintain the charge, but prevent covalent attachment of ubiquitin at that particular residue. The five candidates were all tested using the methodology presented in Figure 6C. Only one of the five tested, K650R, showed a change in ubiquitination (data not shown). STIM1 K650R showed enhanced *poly*-ubiquitination, and was destabilized in a proteasome dependent manner (Fig. 17

C). We had inadvertently created a proteasome-sensitive mutant of STIM1. As an ER-resident protein, it is likely that this mutant, although it contains a conserved positive charge, was improperly folded and became a substrate of the ERAD pathway. This mutant is mentioned, despite its apparent aberrant expression, because it showed some interesting localization patterns and effects on SOCE. Although it was degraded, the K650R mutant showed pronounced surface expression relative to wild-type STIM1 (Fig. 17A). This suggests that STIM1-K650R is stable long enough to transit to the plasma membrane prior to becoming shuttled to aggresomes. What is a bit counter-intuitive is the fact that this increase in surface STIM1 does not, as has been shown earlier, correlate with increased SOCE. In fact, the K650R mutant leads to a pronounced down-regulation of TG-induced SOCE (Fig. 17B).

Physiological occurrences of STIM1 ubiquitination

In addition to ubiquitination, it has been established that STIM1 is glycosylated and phosphorylated {Williams, 2002 #26}(Smyth et al., 2009). Glycosylation of STIM1 at N131 and N171 are necessary for surface expression of STIM1(Williams et al., 2002). Generally, STIM1 is found as a doublet in straight lysates, corresponding to unmodified STIM1 and N-glycosylated STIM1 (Fig. 18, Lane 1). This shift usually corresponds to 2-3 kDa increase in size. During mitosis, STIM1 is also phosphorylated at Ser-486 and Ser-668, which prevents STIM1 from redistributing and activating SOCE(Smyth et al., 2009). This phosphorylation leads to an additional shift, often seen as three bands (Fig. 18, Lane 5). Treatment with nocodazole, an inhibitor of microtubule polymerization, synchronizes cells in mitosis

after approximately 12 hours. Examination of STIM1 from these mitotic lysates reveals a multi-banded shift compared to unsynchronized lysates (Fig 18, Lanes 1 and 5). In-vitro DUB reactions using the synchronized lysates revealed that the change in STIM1 mobility was sensitive to de-ubiquitinating enzymes (Fig. 18, Lanes 5 and 6). Moreover, this shift was approximately 10-12 kDa, which would account for a combination of mono-ubiquitination and multiple phosphorylation events. These results would suggest that in addition to phosphorylation, STIM1 is mono-ubiquitinated during mitosis. Unfortunately, it is unclear at this time what role ubiquitination is playing in this process.

DISCUSSION

For some time it was thought that SOCE was absent in excitable cells. However, several reports in the last few years have shown that SOCE occurs in numerous types of excitable cells, including neurons (Emptage et al., 2001). Furthermore, SOCE has been shown to be involved in neuronal processes such as long-term potentiation (LTP) (Ris et al., 2003), neurite initiation and elongation (Mattson et al., 2000), and neurodegenerative disease (Mattson et al., 2000; Smith et al., 2002; Waldron et al., 1997; Yoo et al., 2000). It therefore seems plausible that SOCE may be an important regulator of calcium homeostasis in neurons.

In this study, we characterized the ER calcium sensor and essential regulator of SOCE, STIM1, in neurons. STIM1 is expressed in immature neurons and its levels increase throughout development and remain relatively high in mature neurons (Fig. 2A). Upon biochemical fractionation of rat hippocampal tissues, we found STIM1 to be present in most subcellular fractions, including postsynaptic densities (Fig. 2B). Furthermore, using immunohistochemistry we found that both endogenous STIM1 and ectopically expressed STIM1-GFP partially co-localize with synaptic proteins (Fig. 4A-D). These expression and localization patterns suggest a role for STIM1 both in developing neurons and mature neurons, at or near synapses. In neurons, endogenous STIM1 and ectopically expressed STIM1-GFP were found to be distributed in a membranous and punctate fashion. Using time-lapse confocal microscopy, we monitored STIM1-GFP redistribution in hippocampal neurons in response to TG-induced store depletion (Fig. 7). STIM1-GFP rapidly mobilizes into large punctate

clusters in both somatic and dendritic compartments. This is similar to what has been observed for STIM1 redistribution in non-excitable cells (Liou et al., 2005; Wu et al., 2006). One difference is that there is a large population of clustered STIM1 puncta present even prior to the addition of TG. In some cases, we also observed multiple STIM1 puncta combine into even larger puncta. In non-excitable cells such as HEK293T cells, endogenous or ectopically expressed STIM1 is distributed in a more diffuse, membranous pattern, and only upon store-depletion does it rapidly redistribute into large, punctate clusters. In neurons, it is plausible that the dynamic clustering and movement of STIM1 is not only promoted by store-depletion, but also by other effectors of calcium entry and ER calcium release.

Although the physiological relevance of SOCE has been shown in neurons, very little is known about its role in neuronal development. Cytoplasmic calcium has been shown to play a critical role in growth cone dynamics, neurite outgrowth, and the development of synapses (Henley et al., 2004). Interestingly, we also observed punctate STIM1-GFP clusters in dendritic growth cones when expressed in immature hippocampal neurons (Fig. 5C). Moreover, a distinct population of STIM1-GFP was localized to the surface of dendrites and growth cones and at the tips growth cone extensions. Using surface biotinylation methods and stringent lysis buffer conditions, we detected endogenous STIM1 on the surface of mature neurons (Fig. 5A). Together, these data suggest that STIM1 physically inserts into the plasma membrane of neurons. However, we do not know if this population of STIM1 is functionally involved in SOCE. Indeed, there is heavy debate over whether STIM1 activation of

SOCE channels occurs by translocating to the PM or by clustering in the ER beneath the PM (Liou et al., 2007; Liou et al., 2005; Roos et al., 2005; Spassova et al., 2006; Wu et al., 2006). It is plausible, however, that STIM1 is distributed differently in neurons. As such, there could be a direct role for the physical insertion of STIM1 into the surface of neurons. Furthermore, it is intriguing to postulate a role for STIM1 and presumably SOCE function in growth dynamics and neurite outgrowth. Chronic inhibition of SOCE results in marked decrease in neurite outgrowth (Fig. 6). Combined with the observation that STIM1 is also present at the tip of these developing neurites, it would stand to reason that STIM1 plays some role in neuronal development. With the recent studies uncovering the STIM2 isoform as the indispensible regulator of neuronal SOCE (Berna-Erro et al., 2009), the possible roles of STIM1 in neuronal function are still left largely unexplored. STIM2 is thought to serve a calcium sensor at lower calcium thresholds(Bird et al., 2009), and the two STIM1 isoforms are highly homologous, except within their C-terminal domains(Stathopulos et al., 2006). It might be interesting to explore the role of the two STIM1 isoforms, and specifically, there cytoplasmic domains, on different forms of plasticity and calcium entry within neurons.

In this study, we have also uncovered a novel connection between the UPS and SOCE function. Foremost, in a proteomic screen for novel, synaptic ubiquitinated proteins, we identified STIM1. Poly-ubiquitinated proteins can be recognized and targeted for degradation by the 26S proteasome. However, ubiquitination is also a widely utilized cellular mechanism for controlling the interaction, function and the

cellular distribution of many protein (Hicke and Dunn, 2003). Notably, the covalent attachment of single ubiquitin molecules (monoubiquitination) or short ubiquitin chains have been shown to promote the down-regulation of integral membrane proteins. We confirmed the ubiquitination of endogenous STIM1 in the brain (Fig. 1A - C). However, ubiquitinated STIM1 migrated on SDS-PAGE primarily as a single, molecular weight species, running approximately 8-10 kDa higher than STIM1. This would indicate STIM1is modified by a single ubiquitin moiety. Furthermore, it suggests that ubiquitinated STIM1 may not be targeted to the 26S proteasome for degradation. Indeed, we found no evidence for STIM1 degradation by the proteasome (Fig. 8E). We then asked if proteasome inhibition affected SOCE. Surprisingly, brief exposure of proteasome inhibitors to HEK293 cells significantly increased SOCE (Fig. 8A and 8B). This suggests that proteasome activity is involved SOCE function. This increase in peak SOCE was only observed in cells treated with both TG and proteasome inhibitors, whereas treating cells with proteasome inhibitors alone had no effect. This indicates that one or more regulators of SOCE may be targeted for degradation by the proteasome under conditions of store-depletion and SOCE activation. The fact that surface STIM1-GFP levels are increased under similar conditions (Fig. 8 C and D) was surprising, as other data suggests STIM1 is not a direct target of the proteasome (Fig. 8E). This result suggests that STIM1 surface stability is regulated by an unidentified UPS target. Previous studies have already drawn a functional link between surface STIM1 and SOCE, wherein the blockade of surface STIM1 using N-terminal specific antibodies leads to a deficit in SOCE in

HEK293 cells (Hewavitharana et al., 2008), (Spassova et al., 2006) . Accordingly, our data would suggest that there are likely multiple levels at which the UPS regulates STIM1 and SOCE function. One scenario would involve the ubiquitination and proteasomal-independent regulation of STIM1. The second involves the ubiquitin-dependent proteasomal degradation of other regulators of SOCE function that likely converge to affect the distribution of STIM1. Although STIM1 levels are not affected by proteasome inhibition, p62 associated populations increase following concomitant activation of SOCE and inhibition of the proteasome (Fig. 9 A and B). This ubiquitination is also quite transient, disappearing by 15 minutes of application (Fig. 9C). The most parsimonious conclusion that can be drawn is that a SOCE-sensitive, proteasome-dependent co-factor is affecting the monoubiquitination of STIM1. All that is certain is that there is a yet unidentified activity dependent regulator of SOCE that is also a target of the proteasome.

In our search for a connection between STIM1 ubiquitination and SOCE function, we turned to the recently discovered RING-finger containing E3 ligase, POSH. This E3 ligase has been implicated in the regulation of calcium homeostasis (Tuvia et al., 2007). What made POSH an interesting candidate, aside from the fact that it was a negative regulator of SOCE, was that it ubiquitinated substrates in a non-degradative fashion. Overexpression of POSH was shown to decrease thapsigargin-induced calcium influx in HEK293 cells, whereas RNAi-mediated knockdown leads to a prolonged influx (Tuvia et al., 2007). We therefore hypothesized that POSH may act as negative regulator of STIM1. We examined whether POSH had any role in STIM1

stability or localization. While we found no effect of POSH overexpression on STIM1 stability (data not shown), co-expression of POSH dramatically reduces surface STIM1-GFP levels (Fig. 10A and 10B). This was dependent on POSH ligase activity, as the RING finger mutant, $POSH^{V14A}$, had no effect on STIM1-GFP surface levels. Taken together, this suggests POSH may regulate SOCE through direct or indirect regulation of STIM1 trafficking in cells. On a side note, Xu et al. published that POSH autoubiquitinates and degrades itself in a proteasome dependent manner(Xu et al., 2003). At no time, did we observe any change in total POSH stability, either overexpressed or endogenous (Fig. 10C). If this was the case, we would hypothesize that proteasome inhibition would lead to increased STIM1 surface levels and enhanced SOCE. It is also intriguing to postulate a role for POSH-mediated regulation of STIM1 trafficking in immature neurons since a recent study has implicated POSH as a negative regulator of axon outgrowth. In the study by Taylor et al., they found that RNAi-mediated inhibition of POSH significantly increased axon outgrowth in differentiating mouse primary cortical neurons and in neurons derived from mouse P19 cells (Taylor et al., 2008).

To date, there has not been any substantial connection between the UPS and SOCE function in both excitable and non-excitable cells. Furthermore, the components of SOCE have not been extensively studied in neurons. Our characterization of STIM1 in neurons indicates STIM1 as an important regulator of calcium homeostasis in the developing and mature brain. Furthermore, we show that there is a relationship between UPS activity and STIM1 distribution and SOCE

function. STIM1 is ubiquitinated in the brain; however, there is no evidence for STIM1 degradation by the proteasome. It is likely that an intact proteasome pathway is required for a normal TG-induced SOCE response, as we have found that TG-induced SOCE is significantly increased in cells that were pre-treated with proteasome inhibitors. At one level this indicates that one or more proteins involved in SOCE are degraded by the proteasome in response to store-depletion. Therefore, both STIM1 ubiquitination and the degradation of other functionally related proteins are likely involved in the regulation of SOCE and will be important to study. We predict that there is a larger functional relationship between the UPS and SOCE function that will be important to study further, which likely affects calcium homeostasis in both normal neuronal physiology and neurodegenerative disease.

Chapter II, in part, contains material previously published in Keil, JM, Shen Z, Briggs SP, Patrick GP**.** (2010). Regulation of STIM1 and SOCE by the ubiquitin proteasome system (UPS). *PloS One*. 5(10):e13465.,

MATERIALS AND METHODS

DNA and Sindbis constructs. STIM1-GFP was created by positioning EGFP (enhanced GFP; Clontech, Palo Alto, CA) at amino acid 23, immediately after the signal peptide sequence of mouse STIM1 (Accession: BC021644) purchased from Open Biosystems (Birmingham, AL). STIM1 signal peptide (amino acid 1 -22) was PCR amplified and ligated into a unique NheI site in EGFP-C1. STIM1 (amino acid 23 – 685) was then amplified and mobilized via Bgl2-ApaI into the signal peptide-EGFP-C1. STIM1-GFP was further subcloned into the XbaI site of SinRep5 (Invitrogen). For production of recombinant Sindbis virions, RNA was transcribed using the SP6 mMessage mMachine (Ambion, Austin, TX), and electroporated into BHK cells using a BTX ECM 600 at 220V, 129 Ω, and 1050 μF. Virion were collected after 24-32 hours and stored at -80°C until use. For Sindbis infection of hippocampal cultures STIM1-GFP virion were added directly to the culture media, with expression carried out for 12 – 18 hours prior to treatment and/or fixation. Wild-type myc-tagged POSH (Accession: AF030131; Tapon et al. 1998) was provided by Dr. Alan Hall through Addgene. $POSH^{V14A}$ RING-finger mutant was mutagenized by a Quickchange (Stratagene, La Jolla, CA) protocol changing codon 14 from GTG to GCG. The following Quickchange primers were used: Forward, TGTCCGGCGTGTCTCGAG CGCCTTGATGCTTCTGCGA. Reverse, GAACAACCTAGAAAACCTC ACAGGCCGCACAGAGCTC

Western blot analysis and PSD-fractionation.

For western blot analysis, all lysates were electrophoresed on SDS-polyacrylamide gels, transferred onto nitrocellulose membranes (Biorad, Hercules, CA), blocked with 5% fat-free milk in TBS/0.1% Tween20 (TBST), and incubated with primary antibodies in TBST +2%BSA overnight at 4^{o}C. Membranes were then washed in TBST, and incubated with the appropriate HRP-conjugated secondary antibody in TBST +2%BSA, and developed with HyGlo ECL (Denville Scientific Inc, South Plainfield, NJ). PSD fractionation was performed as previously described (Carlin et al., 1980; Cho et al., 1992). Briefly, adult female Sprague-Dawley rats (Harlan, Indianapolis, IN) were anesthetized with halothane (Baxter) and euthanized by rapid decapitation. Whole-brains were dounce homogenized (Teflon-glass) in 0.32 M Sucrose, 4 mM Hepes pH 7.4 plus Complete protease inhibitor cocktail (Roche, Indianapolis, IN). Synaptosomes were purified from crude membrane fraction (P2) by discontinuous sucrose density gradient centrifugation. PSD fractions were derived from synaptosomes by single (PSD-I) or double (PSD-II) extraction with 0.5% Triton X-100.

Immunoprecipitations.

For all immunoprecipitations, cells were scraped and lysed in PB buffer plus 1% TritonX-100, 0.1% SDS, Complete protease inhibitors, 25 μM MG132, 100 μM NEM. Lysates were cleared at 18,000 X g for 30', and the resulting supernatant was incubated with 2 μg of antibody overnight. Immune complexes were precipitated

using Protein A/G agarose beads (Pierce). Beads were washed 3 X in PB buffer and resuspended in 2X Laemelli sample buffer prior to western blotting.

Surface biotinylation and live-labeling.

For surface biotinylation, mature (> 21 DIV) rat cortical cultures were washed once in PBS-MC (10 mM phosphate buffer, 2.7 mM KCl, 137 mM NaCl, 1 mM $CaCl_2$, 0.5 mM $MgCl_2$, pH 7.4) and incubated with 1 mg/ml NHS-LC-biotin (Pierce, Rockford, IL) in PBS-MC for 2 h at 4^{o}C. Cells were then washed 2X in PBS-MC and lysed in precipitation (PB) buffer (10 mM $NaPO_4$, pH 7.4, 5 mM EDTA, 5 mM EGTA, 100 mM NaCl) with 0.1% SDS, 1% Triton X-100, and complete protease inhibitors; rotated at 4^{o}C for 30 min, and spun at 18,000 x g. Cleared lysates were incubated with 30 µl of a 50% neutravidin bead slurry (Pierce, Rockford, IL) rotating for 2 h at 4^{o}C. Beads were washed 4X in PB buffer and resuspended in 2X Laemelli sample buffer. Samples were resolved by SDS-PAGE and analyzed via western blot.

Measurement of intracellular calcium.

Fluo-4AM (Invitrogen, λex 495 nm; λem 516 nm) loaded HEK293 cells were prepared as previously described (Roos et al., 2005). Briefly, HEK293 cells plated in 96-well plates were treated with 1 hour with 10 µM MG132 or vehicle (DMSO) and loaded with 5 µM fluo-4AM in culture medium for 30 min at 25°C. Cells were washed twice in calcium-free HBSS (115 mM NaCl, 1 mM KCl, 1 mM $CaCl_2$, 1 mM $MgCl_2$, 10 mM glucose, 10 mM HEPES pH 7.4) and placed in a FlexstationII^{96} fluorimeter (Molecular Devices). At T=0s, the cells were treated with either 1 µM TG or vehicle (DMSO) for 5 min followed by re-addition of $CaCl_2$ to a final concentration of 1.8

mM. Fluorescence at 515nm was measured every 3 s after Ca^{2+} addition. Softmax Pro (Molecular Devices, Wokingham, UK) was used for data analysis. Traces of Relative Fluorescence Units (RFU) were normalized to control baseline and plotted from the point of calcium addition.

Immunostaining and confocal microscopy.

For all imaging purposes, we used a Leica (Wetzlar, Germany) DMI6000 inverted microscope outfitted with a Yokogawa (Tokyo, Japan) Spinning disk confocal head, a Orca ER High Resolution B&W Cooled CCD camera (6.45 μm/pixel at 1X) (Hamamatsu, Sewickley, PA), Plan Apochromat 40X/1.25 na and 63X/1.4 na objective, and a Melles Griot (Carlsbad, CA) Argon/Krypton 100 mW air-cooled laser for 488/568/647 nm excitations. Confocal z-stacks were acquired in all experiments. For fixed cell imaging following treatments, hippocampal cultures (4 – 21 DIV) were fixed in 4% paraformaldehyde/4% sucrose (PFA) for 10 minutes at room temperature, and blocked and permeabilized in PBS-MC (phosphate buffered saline with 1 mM MgCl2 and 0.1 M CaCl2) with Triton X-100 (0.2%) and BSA (2%) for 15 minutes. Cells were incubated overnight at 4^{o}C with primary antibody in PBS-MC and 2%BSA. Primary antibodies were visualized with appropriate secondary antibodies (1:1000): Cy3 goat anti-chicken IgG (Jackson Immuno Research, West Grove, PA); goat anti-mouse Alexa 488, goat anti-rabbit Alexa 568, goat anti-mouse Alexa 568, and goat anti-mouse Alexa 647 (Invitrogen, Carlsbad, CA). Cells were then washed and coverslips were mounted in Aqua Poly/Mount (Polysciences, Warrington, PA). For live-labeling of surface STIM1-GFP, HEK293 cells were plated on poly-D-lysine

(1 mg/ml) coated 35 mm glass coverslips and transfected with 1 μg of STIM1-GFP with Lipofectamine2000 (Invitrogen, Carlsbad, CA) according to the manufacturer's instructions. Prior to fixation and permeabilization, rabbit anti-GFP AlexaFluor 594 conjugated antibody (0.02 μg/μl final) was added directly to the cells in culture media and incubated 20 min at 37^{o}C. Cells were washed 3X in PBS-MC, fixed in 4%PFA/4%Sucrose at room temp for 10 min, washed 3X in PBS-MC and mounted in Aqua/Poly mount.

Antibodies, Reagents, and Drugs.

FK2, α-ubiquitin conjugate (mAb, 1:1000) antibody was purchased from Biomol (Plymouth Meeting, PA); α-ubiquitin (pAb, 1:2000) antibody was purchased from Dakocytomation (Kyoto, Japan); α-synapsin antibody (pAb, 1:1000) was purchased from Chemicon (Temecula, CA); α-PSD-95 antibody (mAb, 1:1000) was purchased from Calbiochem (La Jolla, CA); α-GluR1 (pAb, 1:1000 immunoblot) was purchased from Upstate Biotechnologies (Lake Placid, NY); α-STIM1 (mAb, 1:1000 immunoblot; 1:200 immunofluorescence) was purchased from BD Biosciences (Franklin Lakes, NJ); α-Calreticulin (pAb, 1:1000) was purchased from StressGen (Victoria, BC, Canada); MAP2 (pAb, 1:5000) was purchased from Abcam (Cambridge, UK). The following pharmacological reagents were used: MG132 from Peptide Institute (Osaka, Japan); Thapsigargin (TG) from Tocris-Cookson (Ellisville, MO) ; 2-Aminoethoxydiphenylborane (2-APB) Tocris Bioscience (Bristol, UK); and cycloheximide from Sigma-Aldrich (St. Louis, MO).

Image Analysis.

All imaging was acquired in the dynamic range of 8 bit (0-255) with Simple PCI (Hamamatsu) imaging software. For quantitation of surface STIM1 immunofluorescence, max projected confocal z-stacks were analyzed with NIH ImageJ (Bethesda, MD). Surface STIM1 images were thresholded to a level 2X background and normalized to a total STIM1-GFP signal thresholded at 1.5X background. Surface fluorescence intensities were normalized to control groups and plotted as mean intensity ± SEM. Pooled, average values within each experiment were normalized to control and plotted as mean length ± SEM. Statistical significance was determined by unpaired Student's t-test or ANOVA with *post hoc* Bonferroni's multiple-comparison test as indicated.

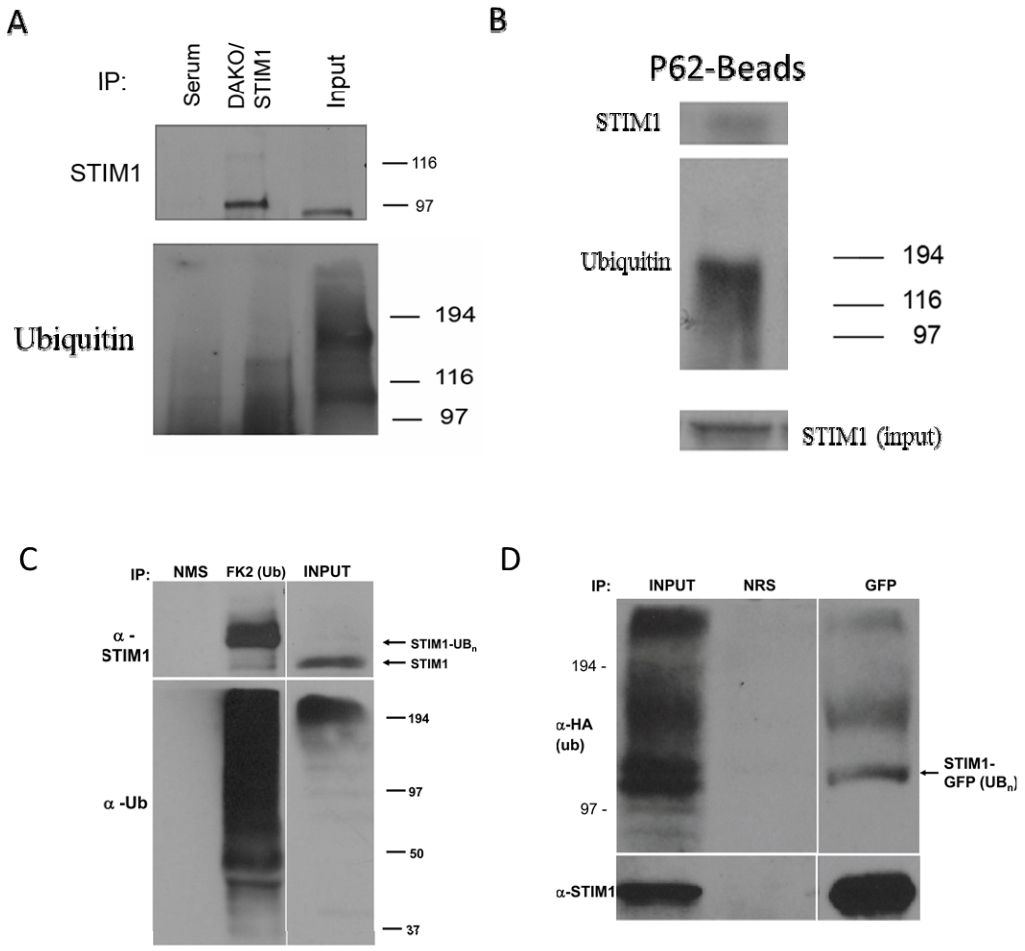

Figure 6. STIM1 is ubiquitinated in the rat brain and HEK-293T cells. (A) Adult rat brain P2' synaptosomal membranes were solubilized and then sequentially immunoprecipitated with α-DAKO, then or α-STIM1. Immune complexes were resolved by SDS-PAGE and subjected to western blot analysis with α-STIM1 (top) or α-ubiquitin (bottom) antibodies (B) Adult rat brain P2' synaptosomal membranes were solubilized and then sequentially precipitated with p62-agarose beads. Precipitates were resolved by SDS-PAGE and subjected to western blot analysis with α-STIM1 (top) or α-ubiquitin (bottom) antibodies. (C) Adult rat brain P2' synaptosomal membranes were solubilized and then immunoprecipitated with either α-STIM1 or α-ubiquitin (FK2). Immune complexes were resolved by SDS-PAGE and subjected to western blot analysis with α-STIM1 (top) or α-ubiquitin (bottom) antibodies Arrow indicates the relative mobility of unmodified STIM1. (D) HA-ubiquitin and STIM1-GFP were co-expressed in HEK293 cells. The resulting lysates were subjected to immunoprecipitation with either α-GFP or control serum (normal rabbit serum, NRS). Arrow indicates the relative mobility of monoubiquitinated-STIM1GFP. Representative blots depicted from 2 to 3 independent experiments for C and D.

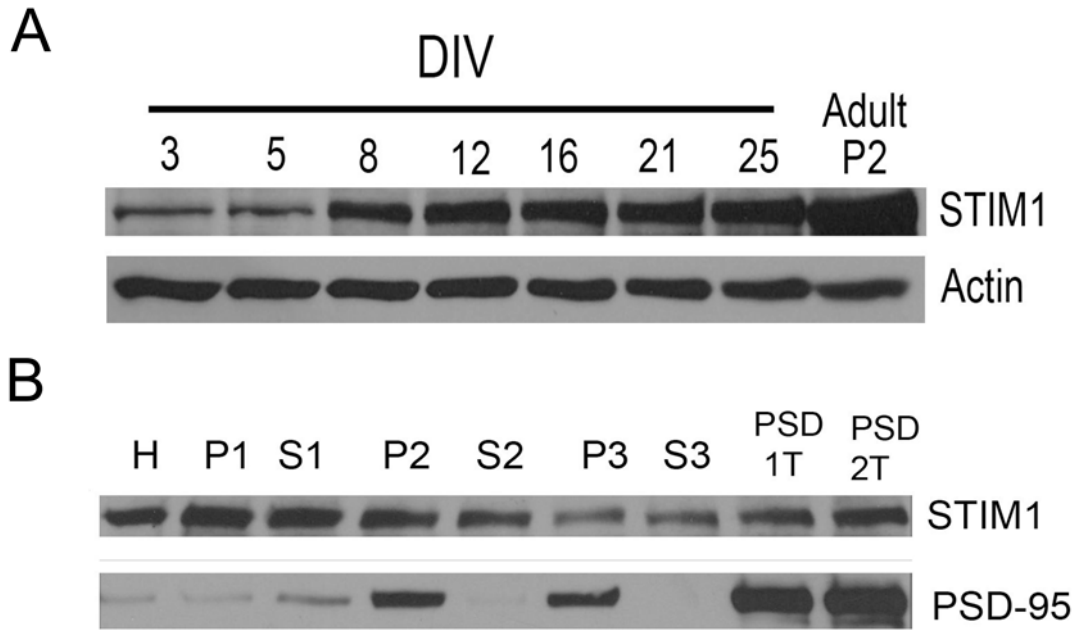

Figure 7. Biochemical examination of spatial and temporal expression patterns of STIM1 in the rat brain. (A). Lysates from cultured rat cortical neurons between days in vitro (DIV) 3 and DIV 25 were subjected to western blot analysis with α-STIM1 antibodies. Representative blots depicted from 3 independent experiments. (B) Western blot of adult rat brain fractions isolated by differential and density gradient fractionation probed with α-STIM1 antibodies (top panel) and α-PSD-95 (middle panel). Fractions are as follows: rat brain homogenate (*H*), crude synaptosome(*P2),* crude synaptosome supernatant (*S2),* lysed synaptosomal membrane fraction (*P3),* crude synaptic vesicle fraction (*S3*), single Triton X-100 extracted PSD (*PSD-1T*), and a double triton X-100 extracted PSD (*PSD-2T*). Representative blots depicted from 2 independent experiments

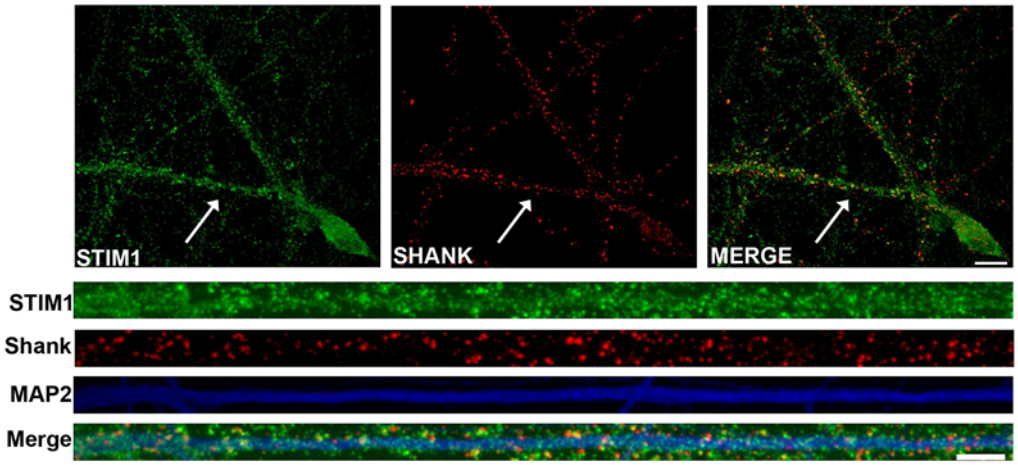

Figure 8. **Immunohistochemical examination of spatial and temporal expression patterns of endogenous STIM1 in the rat brain.** Immunostaining of endogenous STIM1 protein in cultured rat hippocampal neurons (DIV 21). Neurons were immunolabeled with α-STIM1 (green), α-Shank (red), and α-MAP2 (blue) antibodies. Whole scale bars, 20 μm; dendrite scale bar, 10 μm.

Figure 9. Immunohistochemical examination of spatial and temporal expression patterns of exogenous STIM1 in the rat brain Cultured rat hippocampal neurons (DIV 21 and 4; A thru D) were infected with Sindbis STIM1-GFP virion. Expression was allowed to continue for 12 hours prior to fixation, permeabilization, and immunolabeling with α- STIM1 (A), α- PSD-95 (B), α-synapsin (C, α-calreticulin (D) antibodies. Representative images depicted from > 30 images acquired per co-stain. Scale bar = 5 μm.

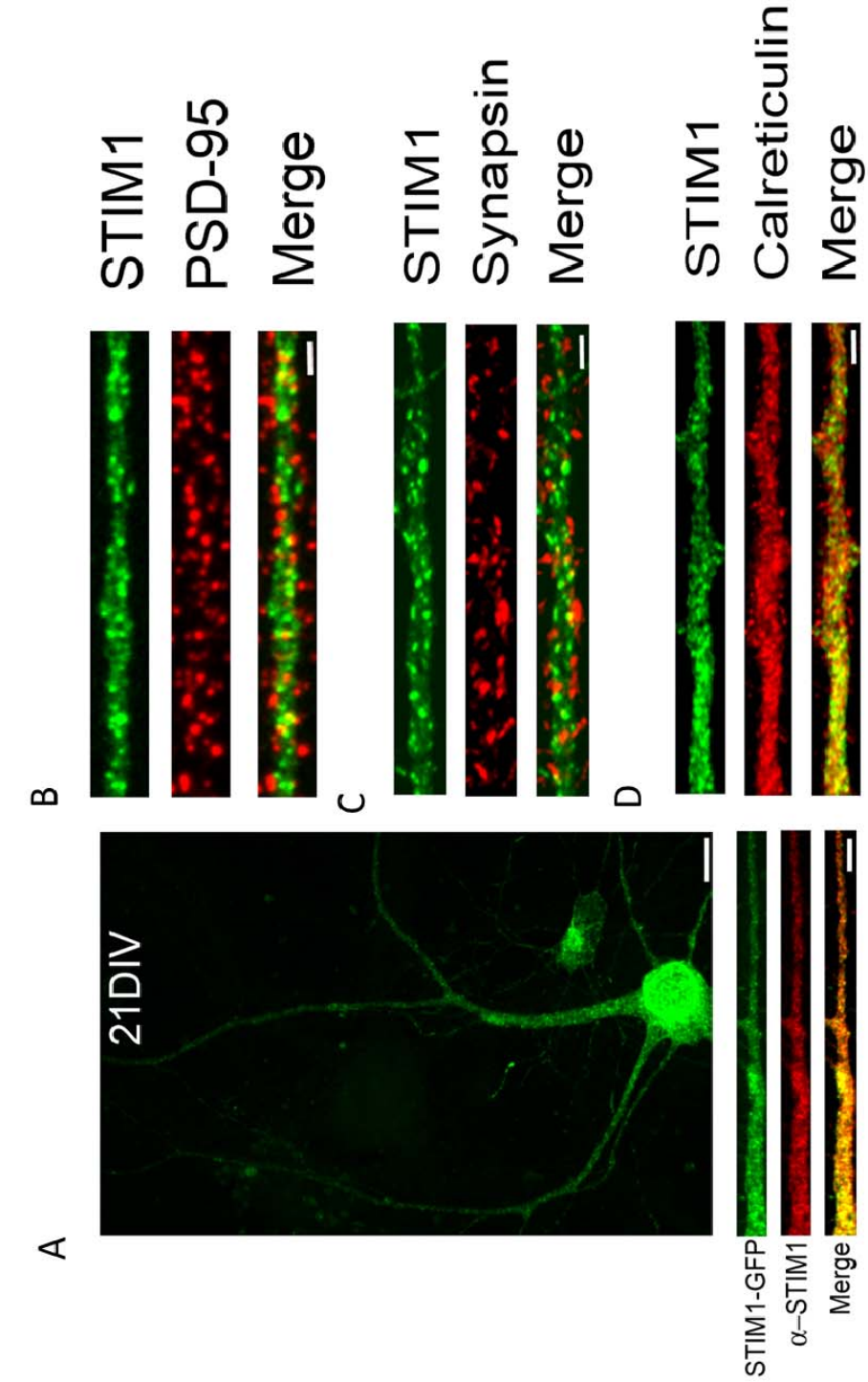
A
21DIV
STIM1-GFP
α–STIM1
Merge
B
STIM1
PSD-95
Merge
C
STIM1
Synapsin
Merge
D
STIM1
Calreticulin
Merge

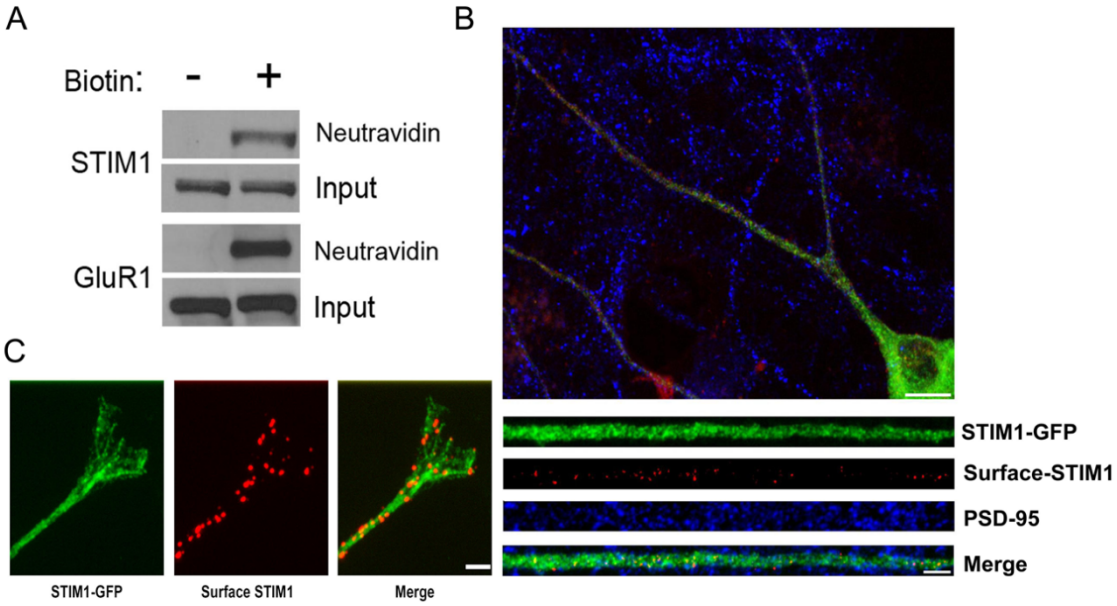

Figure 10. STIM1 is present at the surface of mature and developing hippocampal neurons. (A) Cell surface STIM1 protein populations were examined biochemically by labeling cortical neurons (DIV >21) with NHS-LC-biotin followed by precipitation of the resulting lysates with neutravadin biotin binding beads. Precipitates were resolved by SDS-PAGE and analyzed via western blot with α-STIM1 (top) or α-GluR1 (bottom) antibodies. Representative blots depicted from 3 independent experiments. (B) Rat hippocampal neurons (DIV 21 and 4) were infected with Sindbis STIM1-GFP virion. Expression was allowed to continue for 12 hours. The cells were then live-labeled with α-GFP-Alexa 594 conjugated antibodies (red) prior to fixation, permeabilization, and immunolabeling with α-PSD-95 antibodies (blue). As depicted in (B-C), STIM1-GFP is present on the surface of dendrites and growth cones. Representative images depicted from > 40 images acquired. Whole cell scale bar = 20 μm; dendrite scale bar = 10 μm; Growth cone scale bar = 5 μm.

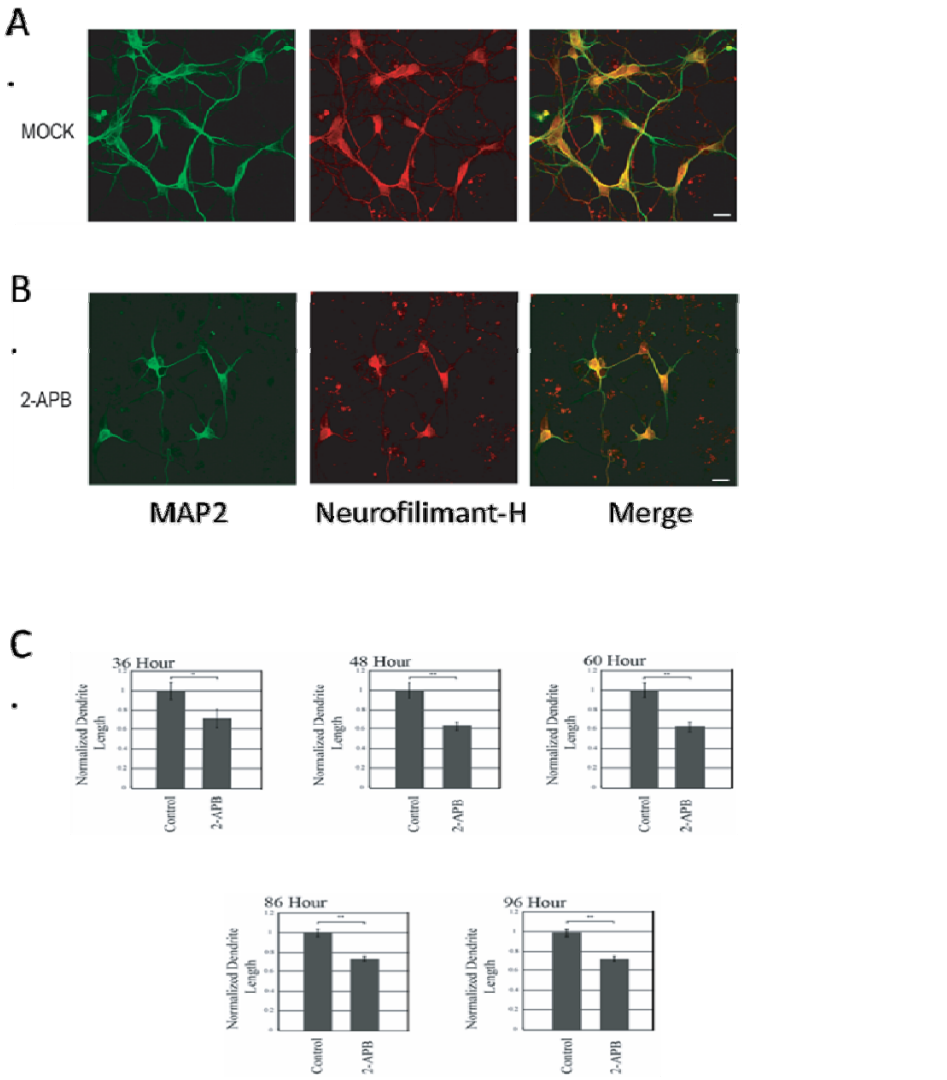

Figure 11. Inhibition of SOCE causes decreased neurite outgrowth in developing hippocampal neurons. Rat primary dissociated hippocampal neurons were treated with either (A) DMSO or (B) 20 μM 2-APB. At varying intervals between 36 and 96 hours in-vitro, neurons were fixed, permeabilized, and immunostained with α-MAP2 (green) and α-Neurofilament-H (red). As depicted, inhibition of SOCE inhibits neurite outgrowth. Representative max z-projected confocal images are shown. Scale bar = 10 μm. (C) For analysis, MAP2 positive neurites were straightened from the soma to the ends of each process, after which the lengths were measured using NIH ImageJ. Bar graphs represent averaged length of neurites between control and treated groups at each time-period. Average of 3 independent experiments ± SEM. $*p < 0.001$, $**p < 0.01$

Figure 12. Store-depletion induced rapid redistribution of STIM1-GFP in hippocampal neurons. Rat hippocampal neurons (DIV 18) were infected with Sindbis STIM1-GFP virion. Expression was allowed to continue for 12 hours prior to live-imaging in the presence of either vehicle or thapsigargin (TG; 2μM final). Confocal images were taken at 2 min. intervals before (A) and after the addition of drugs (B). Representative max z-projected confocal whole cell images (A and B) and corresponding straightened dendrites (C) at indicated time points are shown. As shown, TG-induced ER calcium store-depletion rapidly promotes the redistribution of STIM1-GFP into large punctate clusters in both somatic and dendritic compartments. Whole-cell scale bars = 20 μm; dendrite scale bar = 10 μm

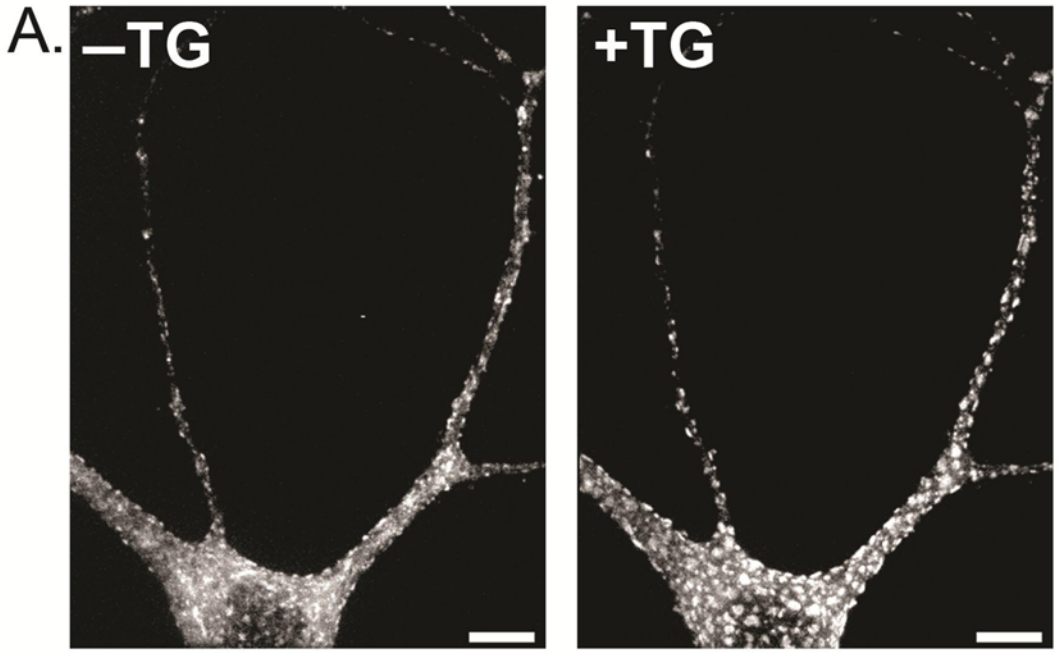
A.
–TG
+TG

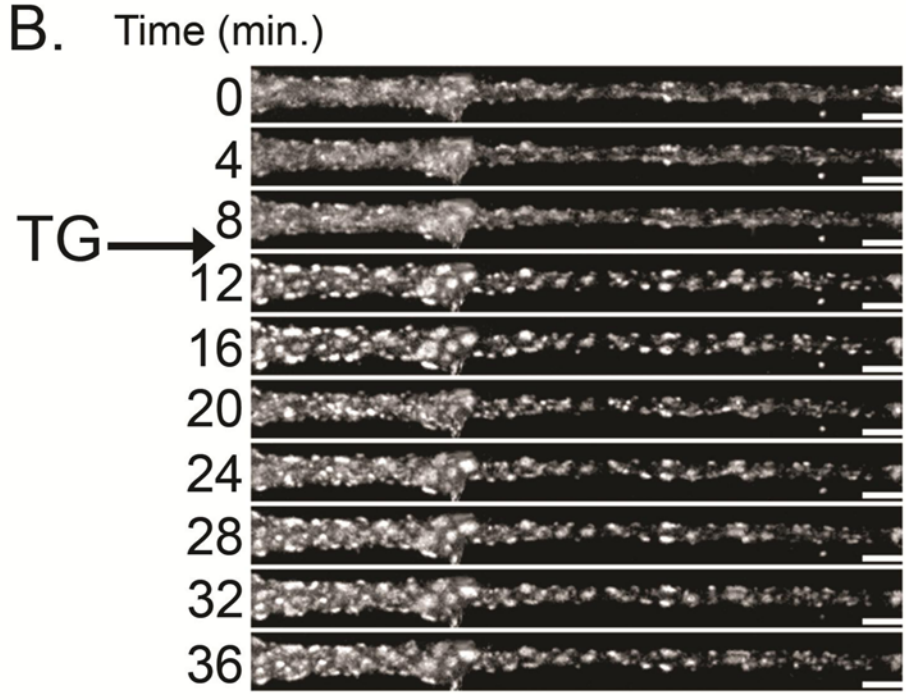
B.
Time (min.)
0
4
TG
8
12
16
20
24
28
32
36

Figure 13. Effects of proteasome inhibition on store-operated calcium (SOC) influx, STIM1 subcellular localization and STIM1 stability. Potentiation of TG-induced calcium influx in HEK293T cells following pretreatment with the proteasome inhibitor MG-132 (10μM). HEK293T cells plated in 96-well plates were loaded with the calcium indicator Fluo-4AM. Prior to loading the cells were pretreated with either vehicle (DMSO) or MG-132 (10 μM) for 1 h. The cells were then treated with 1 μM TG or vehicle (DMSO) for 30 min. Fluorescence was monitored by a FlexstationII 96-well fluorimeter, with Ca^{2+}-re-addition (1.8mM final) 5 minutes following baseline measurements. (A) Traces represent Ca^{2+}-influx normalized to baseline, averaged over 12 wells per treatment. (B) Bar graph depicts averaged peak Ca^{2+} influx ± SEM. For statistical analysis, one-way ANOVA with *post hoc* Bonferroni's multiple-comparison test was used. *$p < 0.05$; **$p < 0.01$; ***$p < 0.001$. (C) HEK293T cells expressing STIM1-GFP were treated as in (A), then live-labeled with α-GFP-Alexa 594 conjugated antibodies (red) prior to fixation. Scale bars, 10 μm. (D) Bar graph depicting the quantification of the STIM1-GFP surface levels from (D). Values were normalized to control. Mean values ± SEM are shown. * $p < 0.05$, unpaired Student t-test. Represents the average of three independent experiments; 40 to 60 fields of cells per condition (15-25 cells per field). (E) HEK293 cells were treated in the absence (-) or presence (+) of cycloheximide (50 μg/mL) with either (1) DMSO, (2) 2 μM thapsigargin, or (3) 2 μM thapsigargin plus 10 μM MG-132 for the indicated times. Following treatments, protein levels were examined by western blot analysis with α-STIM1 or α-actin antibodies. Represent blots from 3 independent experiments.

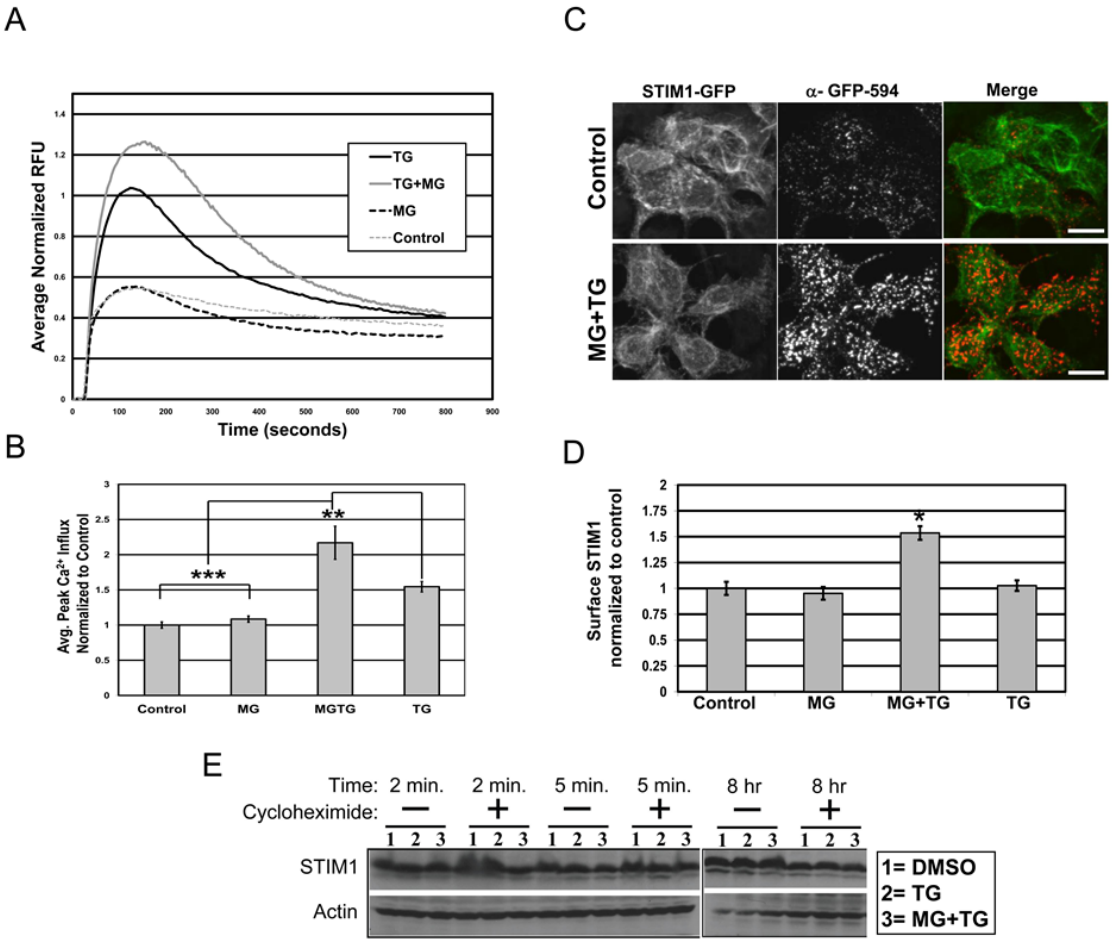
A
Average Normalized RFU
Time (seconds)
TG
TG+MG
MG
Control
C
STIM1-GFP
α- GFP-594
Merge
Control
MG+TG
B
Avg. Peak Ca2+ Influx Normalized to Control
***
**
Control
MG
MGTG
TG
D
Surface STIM1 normalized to control
*
Control
MG
MG+TG
TG
E
Time: 2 min. 2 min. 5 min. 5 min. 8 hr 8 hr
Cycloheximide: — + — + — +
1 2 3 1 2 3 1 2 3 1 2 3 1 2 3 1 2 3
STIM1
Actin
1= DMSO
2= TG
3= MG+TG

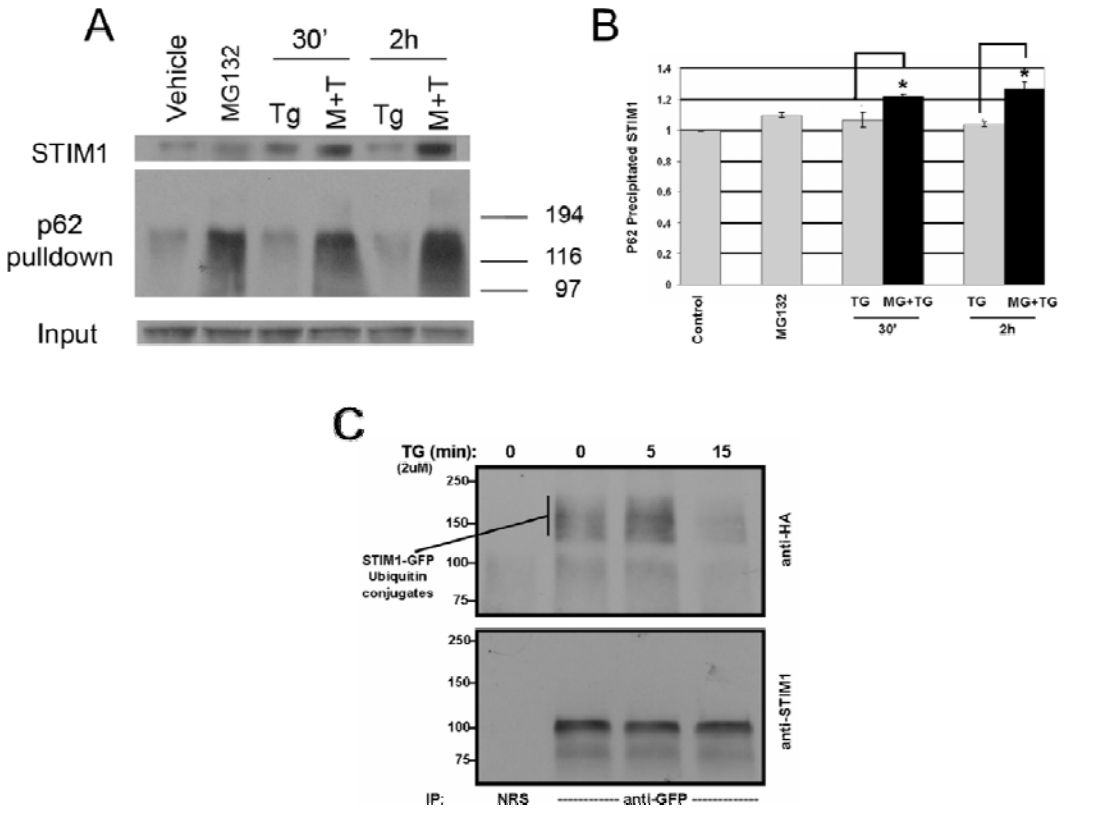

Figure 14. Store-depletion increases population of proteasome-dependent STIM1 ubiquitination. (A) HEK293T cells were pretreated with vehicle (DMSO) or MG132 (10 μM) for 1 h, then TG (2 μM) 30 min or 2 h. Lysates were precipitated with multi-ubiquitin binding p62-conjugated beads and analyzed by immunoblot with α-STIM1 (top;bottom) or α-ubiquitin (middle). (B) Densometry analysis shows significant increase in ubiquitinated STIM1 with proteasome inhibition prior to store depletion (N=3, *P<0.05). Error bars represent ±SEM. (C) HEK293T cells expressing STIM1-GFP and HA-Ubiquitin were treated with TG (2 μM) for 0, 5, or 15 min. Lysates were precipitated with α-GFP antibodies and analyzed by immunoblot with α-HA and α-STIM1 antibodies.

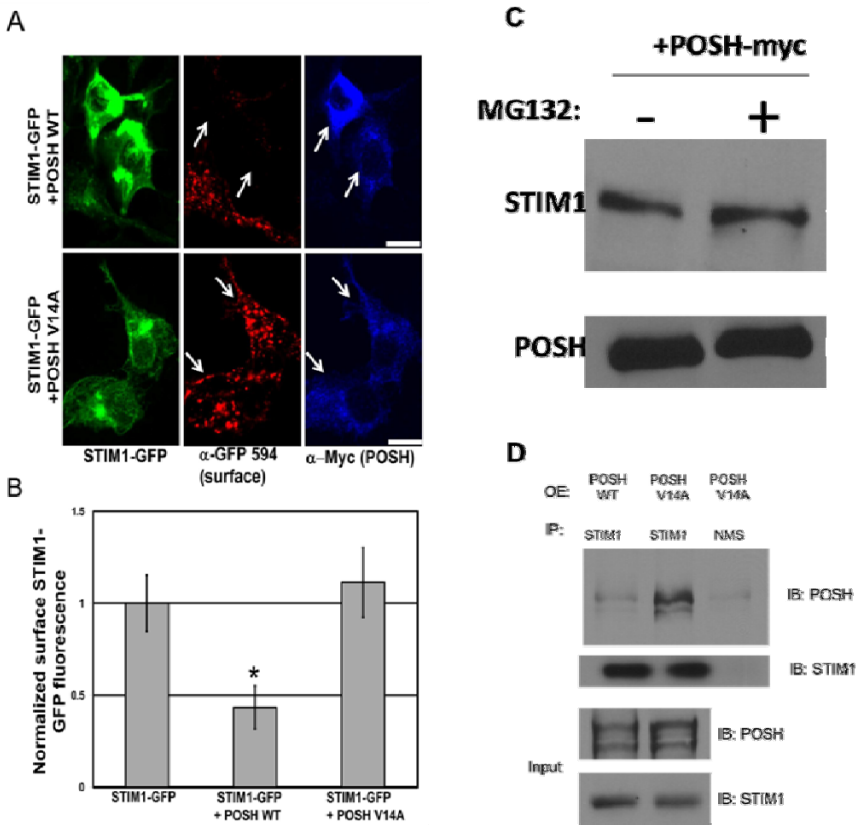

Figure 15. Overexpression of the E3 ligase POSH decreases surface STIM1-GFP levels. (A) HEK293T cells co-expressing STIM1-GFP (green), and WT or the RING-finger mutant (V14A) myc-tagged POSH constructs were live-labeled with α-GFP-Alexa 594 conjugated antibodies (red) prior to fixation, permeabilization and immunolabeling with α-Myc antibodies (blue). Co-expression of WT POSH dramatically reduced surface STIM1-GFP levels while the RING-finger mutant $POSH^{V14A}$ had no effect on STIM1-GFP surface levels. Representative max z-projected confocal images are depicted. Scale bars, 10 μm. (B) Bar graph depicting the quantification of the STIM1-GFP surface levels in STIM1-GFP alone, or STIM1-GFP plus WT or catalytically inactive POSH expressing cells. Values were normalized to STIM1-GFP alone. Mean values ± SEM are shown. * $p < 0.05$, unpaired Student t-test. Represents the average of three independent experiments; 40 to 60 fields of cells per condition (15-25 cells per field). (C) HEK293T cells were transfected with either myc-tagged POSH WT or $POSH^{V2A}$ for 24 hours. The resulting lysates were resolved on SDS-PAGE and analyzed via western blot with α-STIM1 (top) or α-myc (bottom) antibodies. Representative blot from 3 independent experiments.(D) HEK293T cells co-expressing STIM1-GFP (green), and WT or the RING-finger mutant (V14A) myc-tagged POSH were precipitated with α-STIM1, and analyzed via immunoblot with α-STIM1 (bottom) or α-POSH (top) antibodies.

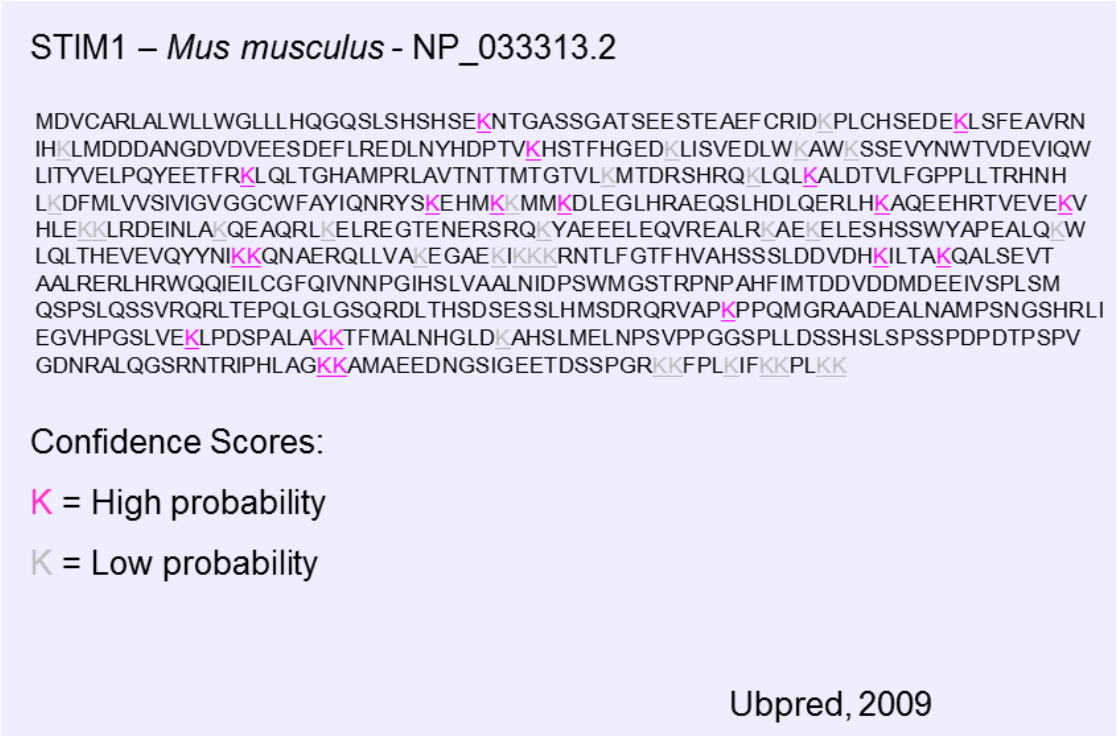

Figure 16. Predicted ubiquitination sites on mouse STIM1. Mouse STIM1, NCBI peptide accession number NP_033313.2 was analyzed via the algorithm developed by (Radivojac et al., 2010) through the website http://www.ubpred.org. Putative lysine residues were assigned a confidence score that has been summarized above as either having a High (magenta) or Low (gray) probability of supporting ubiquitination.

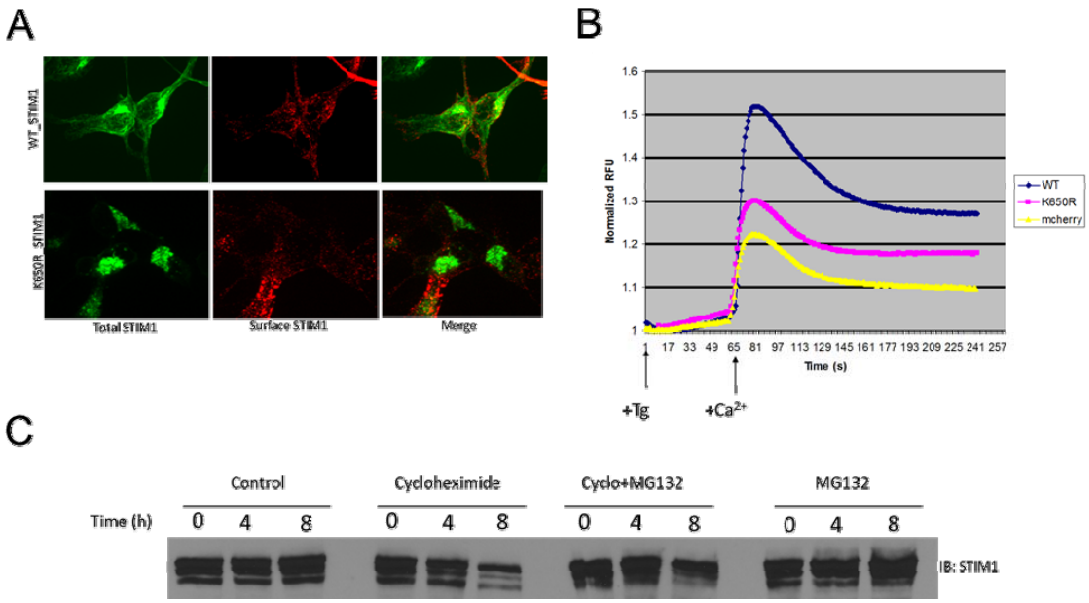

Figure 17. Lysine mutant of STIM1 shows defects in SOCE, with concomitant loss in stability and surface down-regulation. (A) HEK293T cells co-expressing WT STIM1-GFP (green), orK650R STIM GFP were live-labeled with α-GFP-Alexa 594 conjugated antibodies (red) prior to fixation. (B) HEK293T cells plated on Matteks were loaded with the calcium indicator Fluo-4AM. . The cells were then treated with 1 μM TG or vehicle (DMSO) for 30 min. Fluorescence was monitored by confocal microscopy (488 nm emission) every 15s, with Ca^{2+}-re-addition (1.8mM final) 5 minutes following baseline measurements. (A) Traces represent Ca^{2+}-influx normalized to baseline, averaged over 12 wells per treatment.

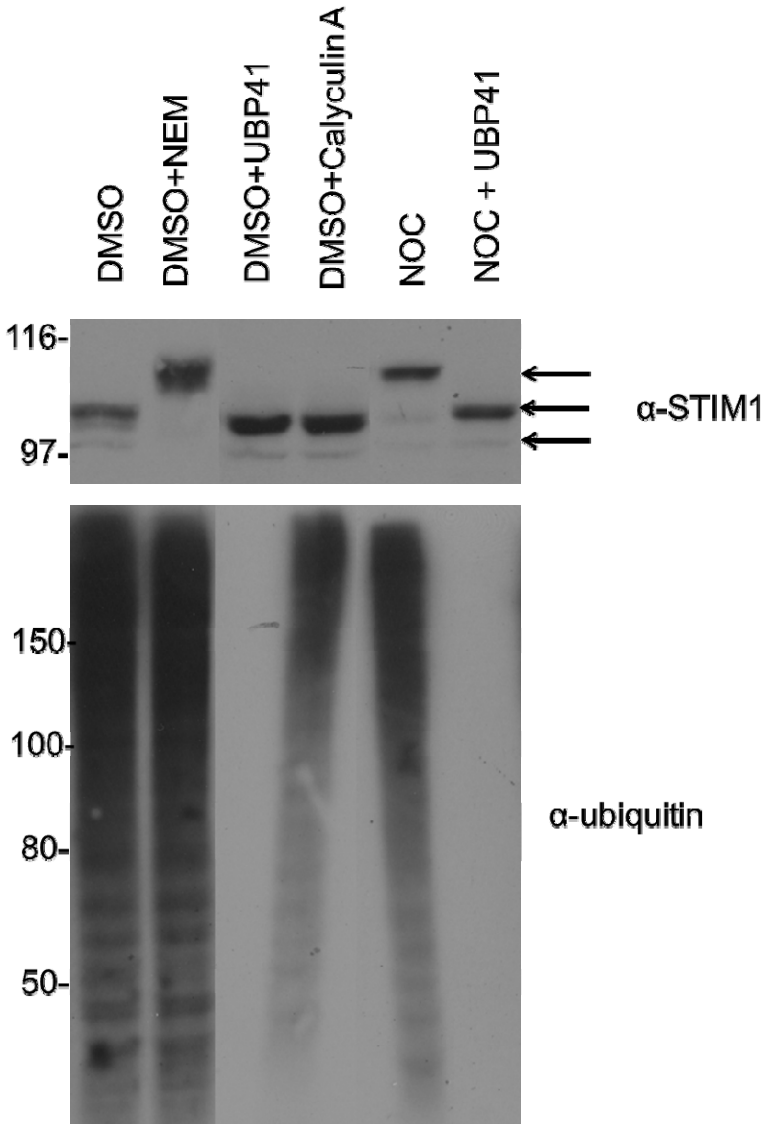

Figure 18. Mitosis-dependent posttranslational modifications of STIM1. HEK-293T cells were mitotically arrested with 1.67 μM nocodazole (NOC) for 12-16 h or treated with DMSO control prior to lysis. Lysates were treated with different inhibitors or purified enzymes (; NEM= N-ethylmaleimide; UBP-41; Crude reactions were carried out for 2 h at 37^{o}C. Lysates were resolved and analyzed via SDS-PAGE using α-STIM1 and α-Ubiquitin antibodies. Arrows mark unmodified STIM1 (bottom), glycosylated (middle) and ubiquitinated/phosphorylated (top).

Chapter III

Ubiquitin-mediated Regulation of Actin Dynamics

Introduction

Actin cytoskeletal dynamics are of great importance in neurobiology because they underlie the structural determinants for synaptic function and plasticity (Cingolani and Goda, 2008; Dent et al., 2010; Dillon and Goda, 2005). Synaptic plasticity, a hallmark neuronal function, and the underling basis of learning and memory, is defined as the ability of synapses to change the strength of their connection in response to stimuli (Holtmaat and Svoboda, 2009). Within the mammalian brain, the majority of excitatory synapses are located at dendritic protusions, or spines (Carlisle and Kennedy, 2005). Spine shape underlies many properties that feed directly into synaptic plasticity, including synapse stability, receptor populations, and calcium dynamics (Alvarez and Sabatini, 2007; Bourne and Harris, 2007; Okamoto et al., 2004). Actin has long been known to be a major cytoskeletal component of dendritic spines, with both structural and functional roles (Landis and Reese, 1983) (Cingolani and Goda, 2008; Dillon and Goda, 2005; Halpain, 2000; Tada and Sheng, 2006). Structurally, actin provides the basic skeleton of dendritic spines; functionally, actin serves as a scaffold crucial for organizing the post-synaptic density and receptors (Renner et al., 2008; Sheng and Hoogenraad, 2007). Moreover, actin-based changes in spine shape and size strongly correlate with changes in the strength of synaptic connections (Holtmaat and Svoboda, 2009; Yuste and Bonhoeffer, 2001).

Actin dynamically cycles between two forms, monomeric (G-actin) and filamentous (F-actin)(Matus, 2000). Induction of long-term potential (LTP) results in a shift in the F-actin/G-actin ratio towards F-actin, which correlates with increase in spine size(Okamoto et al., 2004). Conversely, a shift towards monomeric G-actin and

reduction in spine size, results from long-term depression (LTD) protocols (Okamoto et al., 2004). This bidirectional equilibrium is mediated by a family of actin-binding proteins (ABPs). ABPs can promote polymerization, de-polymerization, and formation of actin-chain superstructures (Blanchard et al., 1989; Stossel et al., 2001). Manipulation of ABP's, in terms of levels or functionality, has profound effects on spine size and density (Ethell and Pasquale, 2005; Okamoto et al., 2007; Schubert and Dotti, 2007). A large body of research has shown that numerous pathways connecting synaptic activity to spine structure affect local actin dynamics. Activation of NMDA and AMPA receptors leads to an inhibition of actin-based spine-motility and rounding of dendritic spines (Fischer et al., 2000). Downstream of this activation are myriad effectors of actin dynamics. Ca^{2+}/Calmodulin-dependent kinase II (CamkII), α-actinin, ephrins, Rho GTPases, and RhoGEFs are but a few of the signaling molecules that link synaptic activity with actin regulation (Kennedy et al., 2005; Lisman et al., 2002; Newey et al., 2005; Schubert and Dotti, 2007; Tada and Sheng, 2006; Wyszynski et al., 1997).

The Rho GTPases and their activators, RhoGEF's, have become noteworthy signaling molecules due to their important roles as regulators of the actin cytoskeleton(Heasman and Ridley, 2008; Jaffe and Hall, 2005). Rho GTPases are part of the Ras superfamily of small GTPases, and like other regulatory GTPases, Rho GTPases serve as a molecular switch, cycling between an active, GTP-bound state and an inactive GDP-bound state (Aspenstrom et al., 2004). This cycling is regulated by a set of three classes of enzymes. Guanine nucleotide exchange factors (GEFs) activate GTPases by exchanging GDP for GTP(Schmidt and Hall, 2002). GTPases-activating proteins (GAPs) promote the reverse reaction, inactivating the Rho GTPases (Bishop and Hall, 2000).

The last group, guanine nucleotide dissociation inhibitors (GDIs), prevent GDP to GTP exchange, thus locking the GTPases in an inactive state (Olofsson, 1999). Activation of Rho-GTPases translates into actin cytoskeletal rearrangements through activation of two major actin polymerizing factors. The Rho-GTPase Rac1 activates WAVE family of proteins, which in turn activates Apr2/3-complex, a major acting polymerizing factor (Soderling and Scott, 2006). Similarly, the Formin family of proteins induce actin polymerization following activation by a number of Rho GTPases(Chesarone et al., 2010; Zigmond, 2004).

In the brain, the study of Rho GTPases regulators, Rho-GEFs and Rho-GAPs, has revealed that these molecules play a crucial role in dendritic spine morphogenesis (Penzes and Jones, 2008). One particular regulator of Rac1, Kalirin-7, has been shown to be a key regulator of spine structure (Penzes et al., 2001b). Kalirin-7, the most abundant kalirin isoform, is a brain-specific guanine exchange factor for Rac1(Johnson et al., 2000; Penzes et al., 2000). It is expressed in the hippocampus and cortex, in a developmentally dependent manner, coinciding with synaptogenesis (Xie et al., 2007). Kalirin-7 contains a GEF domain, spectrin-like repeats, Sec14p-like domain, and a PDZ binding domain (Johnson et al., 2000; Ma et al., 2008a; Penzes et al., 2001a). Overexpression of Kalirin-7 is leads to axon outgrowth and an increase in spine density (May et al., 2002; Penzes et al., 2001b). Conversely, loss of Kalirin-7 results in decreased spine density and dendritic arborization (Ma et al., 2003; Ma et al., 2008a; May et al., 2002). Kalirin-7 is also positively regulated by CaMKII, where NMDA receptor activation leads to increased Kalirin-7 phosphorylation and GEF activity (Xie et al., 2007). This NMDA dependent activation also leads to Rac1 mediated AMPA receptor clustering and spine enlargement.

Kalirin-7 also appears to serve as scaffold for receptor associated, PDZ-containing proteins (Penzes et al., 2001b). Kalirin-5 (delta-Kalirin-7), a truncated isoform of kalirin-7 lacking the Sec14p domain and 4 spectrin repeats, has been found with similar expression patterns as full-length Kalirin-7(Johnson et al., 2000; McPherson et al., 2002; McPherson et al., 2004). Unlike Kalirin-7, kalirin-5, does not increase spine density, suggesting GEF activity is not absolutely necessary for spine formation (Schiller et al., 2008). Physiological role of the delta isoform is not entirely know; however, it is suspected to play a role in spine structure during periods of chronic cocaine exposure (Mains et al., 2011).

One of the larger functional groups that appeared in the screen for synaptic, ubiquitinated proteins was comprised of cytoskeletal proteins and their effectors (Fig. 3). In fact, the gamma isoform of actin was one of the top 40 proteins out of 279 based on adjusted Tg/WT ratio (Table 2). It has recently been shown that actin can be ubiquitinated and degraded in a proteasome dependent manner (Zhang et al., 2010). The major actin polymerization activators, Arp2/3 and Formin, appeared in the screen, as well as Cofilin, the family of actin disassembly proteins (Table 3 and data not shown). Moreover, the neuronal Rac1-GEF, Kalirin-7 also appeared as a strong hit in the screen (Table 3). With an already strong connection between actin cytoskeletal dynamics and synaptic structure and function, this group of potential targets identified in the screen provided a promising base from which to examine the interplay between neuronal function and ubiquitination.

RESULTS

Actin-based spine motility and the UPS

Recent work has implicated the actin cytoskeleton and its interactors in both the synaptic vesicle cycle and activity-driven synaptic plasticity(Dillon and Goda, 2005; Sudhof, 2004). Real-time examination of spontaneous spine motility was shown to be driven by dynamic actin polymerization (Fischer et al., 1998; Halpain et al., 1998). Interestingly, stimulation of glutamate receptors resulted in a blockade of spine movement, suggesting activation of glutamate receptors results in stabilization of spine motility(Fischer et al., 2000; Halpain et al., 1998). A number of molecular components that have recently been shown to couple spine motility with activity are also known to bind either actin or actin-associated components (Dillon and Goda, 2005). These components have also been shown to be substrates of the proteasome, and their effects on actin dynamics are proteasomal dependent (Aberle et al., 1997; Lynch et al., 2006; Tursun et al., 2005). Furthermore, recent evidence has shown that the stimulation of a glutamatergic synapse results in a sequestration of proteasomes in the spine head, with roughly 50% of the proteasomes being associated with the actin cytoskeleton (Bingol and Schuman, 2006). With actin and many of its regulators appearing in the screen for synaptic ubiquitinated proteins, a simple examination of actin dynamics and proteasome function was a logical first step.

GFP fusions of actin have been shown to accurately monitor actin dynamics in dendritic spines, as it incorporates into actin-containing structures and allows the visualization of actin dynamics in living neurons (Fischer et al., 1998). Moreover, it has become an efficient way to monitor alterations in spine shape and spine motility, as both

processes are highly dependent on actin dynamics. Using a similar approach to monitor actin dynamics, we asked if proteasomal inhibition affected actin dynamics in dendritic spines. Time-lapse imaging of primary hippocampal neurons infected with YFP-actin Sindbis virus show that actin in the spine head is dynamically changing and reflects spine motility as previously demonstrated (Fig. 19 A and B**)(**Fischer et al., 1998**)**. Interestingly, application of the proteasome inhibitor MG-132 produces a significant decrease in spine motility within 30 minutes, and almost a total loss of spine motility after 2 hours of treatment (Fig. 19A and B). A summed difference plot of YFP-actin signal is plotted for control (Fig. 19A, second panel) or 120 minute MG-132 treated neurons (Fig. 19A, fourth panel). The decrease in summed intensity at dendritic spines in the MG-132 treated neurons suggests proteasome-dependent components are involved in the dynamic cycling of F-actin/G-actin ratio. Biochemical comparison of F-actin/G-actin ratios indicates a small but reproducible increase in total F-actin following proteasome inhibition (Fig. 19 C**)**. This suggests targets of the proteasome are involved in either actin polymerization or F-actin stability. Although the mechanisms behind these apparent changes are unclear, this data provides impetus towards future studies examining the role of the UPS in synaptic actin dynamics.

The UPS and synaptic Rho-GEFs, kalirin-5 and kalirin-7

The kalirin family of Rac1neuronal RhoGEFs was highly represented within the screen for synaptic, ubiquitinated proteins. Two isoforms in particular, kalirin-7 and Kalirin-5 (delta-kalirin-7) were very abundant, with high Tg/WT spectral ratios (Fig. 20A). These results strongly suggest that kalirin is readily ubiquitinated within the mammalian synapse. As the name implies, delta-kalirin-7, or kalirin-5, is highly

homologous to kalirin-7. An alternate translation initiation site results in the truncated amino-terminus found in the kalirin-5 isoform (Penzes et al., 2000). Given the fact that both kalirin isoforms are nearly identical, it isn't surprising that both appear to be the predominant ubiquitinated forms of kalirin. Kalirin-5 and kalirin-7 ubiquitination was validated in heterologous cells, using tagged kalirin constructs and overexpressed ubiquitin (Fig 20 B). Immunoprecipitation of either kalirin-5 or kalirin-7, and subsequent analysis of ubiquitin immunoreactivity reveals canonical, higher molecular weight laddering, indicative of poly-ubiquitinated kalirin (Fig. 20 B, Lane 1 and 3). In an overexpression system, in heterologous cells, it appears both kalirin isoforms are readily poly-ubiquitinated.

A number of reports have drawn a connection between kalirin-7 phosphorylation, PP1 and PKA activity, and the effects on GEF activity (Shioda et al., 2011; Xie et al., 2007; Xin et al., 2008). Inhibition of PP1 with okadaic acid leads to an increase in kalirin-7 phosphorylation and GEF activity (Shioda et al., 2011). Moreover, there is an emerging understanding that phosphorylation serves as regulatory precursor to ubiquitination (Brooks and Gu, 2003; Hunter, 2007; Karin and Ben-Neriah, 2000). With this mind, we examined the potential effect of inhibiting known kalirin phospho-effectors on kalirin ubiquitination and stability. Using heterologous system, overexpressing kalirin-7-GFP and HA-ubiquitin, with a panel of PP1 and PKA inhibitors and agonists, we first looked at kalirin-7 ubiquitination (Fig. 21 A). Application of a PP1/2 inhibitor (OA) or PKA inhibitor (H89) leads to a decrease in ubiquitinated kalirin-7 compared to DMSO or MG-132 treated cells (Fig 21 A, Lane 3 and 5). However, concomitant application on proteasome inhibitor (MG-132) and the inhibitors leads to a buildup of

kalirin-7 ubiquitin conjugates (Fig. 21 A, Lane 4 and 6). A crude PKA activator, Forskolin, was also examined, with no observable effect on kalirin-7 ubiquitin conjugates or stability (Fig. 21A, Lane 7). Overall, the data suggests that PP1/2 phosphatase activity and PKA kinase activity may be negative regulators of kalirin-7 ubiquitination. This is a bit strange, as PP1 and PKA have opposing enzymatic activities, suggesting a possible bi-directional mode of kalirin-7 ubiquitination. There is no observable change in total kalirin-7 levels, but this may be due to increased signal-to-noise from the overexpression (Fig. 21A, middle panel). Examination of PP1/2 activity on endogenous kalirin populations reveals that kalirin-5 stability is affected by PP1/2 inhibition, with a dramatic decrease in kalirin-5 levels after 8 hours of PP1/2 inhibition (Fig 21B, bottom panel). Application of proteasome inhibitors stabilizes this population, suggesting that kalirin-5 is targeted to the proteasome in a PP1/2 dependent manner. Strangely, kalirin-7 levels do not decrease as dramatically as kalirin-5, although there is a consistent, observable change (Fig. 21B, top panel). Together, these results suggest that in an overexpression system, kalirin-5 and kalirin-7 are ubiquitinated under similar conditions; however, endogenous PP1/2-dependent ubiquitination seems to be a kalirin-5 specific phenomenon. Closer examination of kalirin-5 stability using a cycloheximide chase in the presence of proteasome inhibitors reveals kalirin-5 is rapidly turned over by the proteasome in a matter of hours (Fig. 21 C, top panel). In addition to PP1 and PKA, CaMKII is a known regulator of kalirin activity. In neurons, phosphorylation of kalirin-7 at thr95 by αCaMKII leads to an increase in GEF activation, and subsequent dendritic spine enlargement (Xie et al., 2007; Xin et al., 2008). When a constitutively active form of αCaMKII (TD) is overexpressed, it leads to a downregulation of kalirin-5 (Fig. 21D,

Lanes 7-9). Moreover, application of proteasome inhibitors can stabilize this population, suggesting that αCaMKII kinase activity can promote proteasomal degradation of kalirin-5 (Fig 21D, Lanes 10-12).

The next logical step in understanding the role of ubiquitination in kalirin-5 function is to identify potential sites of ubiquitination, as well as putative ligases. Identification of either a preferred lysine or an E3 ligase would allow us to ask more specific questions regarding the role of kalirin ubiquitination and stability on neuronal structure and function. Despite the fact that kalirin is a neuronal-specific protein, we knew that because we could produce robust kalirin-5 ubiquitination in non-neuronal cells, there was a good chance the ubiquitin machinery was conserved between cell types (Fig. 20B). Kalirin-5 immunoprecipitates, from HEK293T cells expressing kalirin-5-Myc were analyzed by tandem MS/MS. A E3 ligase, Cullin 4B (Cul4B), as well as two de-ubiquiting enzymes, Usp7 and Usp36, were identified (data not shown). Moreover, DDB1 and RBX1, components of a functional E3 complex with Cul4B also co-precipitated with kalirin-5 (data not shown). When co-expressed with kalirin-5 and HA-ubiquitin, Cul4B was able to promote dramatic ubiquitination of kalirin-5 (Fig. 22A, Lane 1). This ubiquitination is also dependent on the ability of Cul4B to form a functional complex with its E2-E3, as the dominant negative form is unable to promote ubiquitination (Fig. 22A, lane 2). Co-immunprecipitation of either kalirin-5 or Cul4B from lysates expressing both reveals that the two proteins are able to strongly interact (Fig. 22 B). Together, these results suggest that, at least in HEK-293T cells, Cul4B is able to interact with and ubiquitinate kalirin-5. In the search for ubiquitinated kalirin-5 peptides, the expected addition of either of the two most C-terminal tryptic peptides of

human ubiquitin (GG or LRGG, of 114.05 or 383.22 Da, respectively) was identified on Lys-58 and Lys-89 (Fig. 22C). Unfortunately, neither of these sites appears to be preferred, either individually or in tandem, as examination of kalirin-5 ubiquitination using K58R, K89R , or K58,89R mutants produces no change in ubiquitination when compared to wild-type (data not shown). These results reinforce the often documented promiscuity that ligases have for ubiquitination sites holds true for kalirin-5.

DISCUSSION

The actin cytoskeleton is vital to nearly every eukaryotic biological process. In addition to its scaffolding and structural properties, the actin cytoskeleton functions in such dynamic processes as cell division, cell motility, and organelle trafficking (Dominguez and Holmes, 2010). Thus it is not surprising that actin plays a role in numerous neuronal processes. In addition to being the major structural component of the synapse, enriched in both the pre- and post-synaptic terminals, actin has long been implicated in both axon guidance and synaptogenesis (Dillon and Goda, 2005; Fifkova and Delay, 1982). Previous studies speak strongly towards a role of the UPS in synaptic plasticity. There are currently only a handful of validated UPS targets in the synapse. At the beginning of this project, we hypothesized that there is a large, yet unidentified population of ubiquitinated proteins residing in the synapse. Moreover, we also hypothesized that the synaptic actin cytoskeleton is dynamically regulated by the UPS. Attesting to this hypothesis many targets from the first pass mass spectrometry screen fell into the actin-cytoskeleton classification group.

Actin-based spine motility is quite dynamic in both young and mature neurons (Fischer et al., 1998). Studies have found that the vast majority of actin in the spine is dynamic and turned over in less than one minute (Star et al., 2002). Increases in neuronal activity, through the application of or NMDA/AMPA receptor agonists, leads to a dramatic increase in the stable actin population, and subsequent decrease in motility (Fischer et al., 2000; Star et al., 2002). Since proteasome inhibition causes such similar, robust decrease in motility, it would be possible to imagine that similar pathways are being perturbed. Given the numerous targets identified in the screen, as well as the

number of additional actin-regulators already established as targets of the UPS, it is not at all surprising that global blockade of proteasome activity has such profound effects (Fig. 19A and B). The effect is also quite rapid, with visible downregulation of actin-based motility seen within 5 minutes (data not shown). These treatments also correspond to a small, let reproducible change in F-actin levels (Fig. 19C). Induction of LTP and activation of glutamate receptors correlate with increases in spine size and number, both requiring actin polymerization and F-actin levels(Honkura et al., 2008; Matsuzaki et al., 2004; Okamoto et al., 2004). Stabilizing effectors of actin polymerization, or actin itself, through inhibition of proteasome-dependent degradation could explain these results. In fact, actin, as well as an actin effector, Rac1 were recently found to be degraded by the proteasome (Lynch et al., 2006; Zhang et al., 2010).

The neuronal Rac1 regulator, kalirin, was one of the many actin-related proteins identified in the screen (Fig 20A). This target is promising, not only because it is a target of the UPS, but also because it has profound effects on activity-based synaptic structure. Of the two isoforms identified, kalirin-5 seems to be a more tractable target of the UPS. It shows context-specific changes in stability not readily observed with kalirin-7. It seems that inhibition of PP1/2 or PKA results in robust ubiquitination and proteasomal degradation in heterologous cells (Fig. 21A). However, only PP1/2 inhibition causes any change in proteasome-dependent stability of endogenous kalirin-5 populations (Fig. 21 D). PP1 is of particular interest in that it interacts with numerous receptors and components of the PSD, the actin cytoskeleton, and inhibits master plasticity regulator, CaMKII (Mauna et al., 2010; Munton et al., 2004; Westphal et al., 1999). Inhibition of PP1 activity is akin to constitutive activation of αCaMKII at Thr286 (Munton et al.,

2004). Since CaMKII has already been shown to enhance kalirin-7 GEF activity through phosphorylation, examination of a potential role in kalirin-5 stability seemed prudent (Xie et al., 2007). The fact that constitutively active CaMKII-TD can lead to a proteasome-dependent downregulation of kalirin-5 is quite exciting. This suggests that other plasticity pathways that lead to both CaMKII activation and spine plasticity may converge at kalirin-5. To date, very little is known about kalirin-5 function in neurons. Kalirin-5 does not exert the same effects as kalirin-7, where only kalirin-7 overexpression can lead to increases in spine size and number (Ma et al., 2010; Ma et al., 2008b; Schiller et al., 2008). Due to such high sequence homology, teasing apart the effects of kalirin-5 versus kalirin-7 can be difficult with current technologies. For example, RNAi mediated-knockdown of kalirin-5 cannot be performed without concurrent loss of kalirin-7. Re-introduction of RNAi-resistant kalirin-7 is a possible , albeit complicated, solution. Until the technology becomes more tractable, the role of kalirin-5 may be elusive. Direct analysis may not be feasible at the moment, but examination of effectors of kalirin-5 ubiquitination and stability may provide a promising avenue of study. The putative E3 ligase for kalirin-5, Cul4B, has recently been implicated in X-linked mental retardation, which has disease-correlates relating to dendritic spine morphology(Svitkina et al., 2010; Zou et al., 2007) (Fig. 22) . It would stand to reason that Cul4B may play a role in dendritic spine remodeling through kalirin-5. Ongoing studies are examining the possible role of Cul4B in synaptic function.

Chapter III, in part, contains material previously published in Keil, JM, Shen Z, Briggs SP, Patrick GP**.** (2010). Regulation of STIM1 and SOCE by the ubiquitin proteasome system (UPS). *PloS One*. 5(10):e13465.

MATERIALS AND METHODS

DNA and Sindbis constructs.

YFP-actin was generous gift from the Halpain lab. For production of recombinant Sindbis virions, RNA was transcribed using the SP6 mMessage mMachine (Ambion, Austin, TX), and electroporated into BHK cells using a BTX ECM 600 at 220V, 129 Ω, and 1050 μF. Virion were collected after 24-32 hours and stored at -80°C until use. For Sindbis infection of hippocampal cultures YFP-actin virion were added directly to the culture media, with expression carried out for 12 – 18 hours prior to treatment and/or fixation.

Western blot analysis.

For western blot analysis, all lysates were electrophoresed on SDS-polyacrylamide gels, transferred onto nitrocellulose membranes (Biorad, Hercules, CA), blocked with 5% fat-free milk in TBS/0.1% Tween20 (TBST), and incubated with primary antibodies in TBST +2%BSA overnight at 4^{o}C. Membranes were then washed in TBST, and incubated with the appropriate HRP-conjugated secondary antibody in TBST +2%BSA, and developed with HyGlo ECL (Denville Scientific Inc, South Plainfield, NJ).

Immunoprecipitations.

For all immunoprecipitations, cells were scraped and lysed in PB buffer plus 1% TritonX-100, 0.1% SDS, Complete protease inhibitors, 25 μM MG132, 100 μM NEM. Lysates were cleared at 18,000 X g for 30', and the resulting supernatant was incubated with 2 μg of antibody overnight. Immune complexes were precipitated using Protein

A/G agarose beads (Pierce). Beads were washed 3 X in PB buffer and resuspended in 2X Laemelli sample buffer prior to western blotting.

Immunostaining and confocal microscopy.

For all imaging purposes, we used a Leica (Wetzlar, Germany) DMI6000 inverted microscope outfitted with a Yokogawa (Tokyo, Japan) Spinning disk confocal head, an Orca ER High Resolution B&W Cooled CCD camera (6.45 μm/pixel at 1X) (Hamamatsu, Sewickley, PA), Plan Apochromat 40X/1.25 na and 63X/1.4 na objective, and a Melles Griot (Carlsbad, CA) Argon/Krypton 100 mW air-cooled laser for 488/568/647 nm excitations. Confocal z-stacks were acquired in all experiments. For fixed cell imaging following treatments, hippocampal cultures (4 – 21 DIV) were fixed in 4% paraformaldehyde/4% sucrose (PFA) for 10 minutes at room temperature, and blocked and permeabilized in PBS-MC (phosphate buffered saline with 1 mM MgCl2 and 0.1 M CaCl2) with Triton X-100 (0.2%) and BSA (2%) for 15 minutes. Cells were incubated overnight at 4^{o}C with primary antibody in PBS-MC and 2%BSA. Primary antibodies were visualized with appropriate secondary antibodies (1:1000): Cy3 goat anti-chicken IgG (Jackson Immuno Research, West Grove, PA); goat anti-mouse Alexa 488, goat anti-rabbit Alexa 568, goat anti-mouse Alexa 568, and goat anti-mouse Alexa 647 (Invitrogen, Carlsbad, CA). Cells were then washed and coverslips were mounted in Aqua Poly/Mount (Polysciences, Warrington, PA). For live-labeling of surface STIM1-GFP, HEK293 cells were plated on poly-D-lysine (1 mg/ml) coated 35 mm glass coverslips and transfected with 1 μg of STIM1-GFP with Lipofectamine2000 (Invitrogen, Carlsbad, CA) according to the manufacturer's instructions. Prior to fixation and permeabilization, rabbit anti-GFP AlexaFluor 594 conjugated antibody (0.02 μg/μl final)

was added directly to the cells in culture media and incubated 20 min at 37°C. Cells were washed 3X in PBS-MC, fixed in 4%PFA/4%Sucrose at room temp for 10 min, washed 3X in PBS-MC and mounted in Aqua/Poly mount.

Antibodies, Reagents, and Drugs.

α-actin (mAb, 1:2000) antibody was purchased from BD Biosciences (Franklin Lakes, NJ); α-ubiquitin (pAb, 1:2000) antibody was purchased from Dakocytomation (Kyoto, Japan) α-kalirin (pan) (rAb, 1:1000) antibody was purchased from Upstate Biotechnologies (Lake Placid, NY); α-Cul4B (mAb, 1:2000) antibody was purchased from BD Biosciences (Franklin Lakes, NJ); α-CamKII α (mAb, 1:1000) antibody was purchased from Upstate Biotechnologies (Lake Placid, NY); The following pharmacological reagents were used: MG132 from Peptide Institute (Osaka, Japan); cycloheximide, Okadaic acid, H-89, Forskolin, cytochalasinD, Phalloidin, from Sigma-Aldrich (St. Louis, MO).

Image Analysis.

All imaging was acquired in the dynamic range of 8 bit (0-255) with Simple PCI (Hamamatsu) imaging software. Summed difference analysis and plots were created as described by Fisher et al., 1998. Pooled, average values within each experiment were normalized to control and plotted as mean length ± SEM. Statistical significance was determined by unpaired Student's t-test or ANOVA with *post hoc* Bonferroni's multiple-comparison test as indicated.

Mass Spectrometry

As described in Chapter 1, pages 20 through 22.

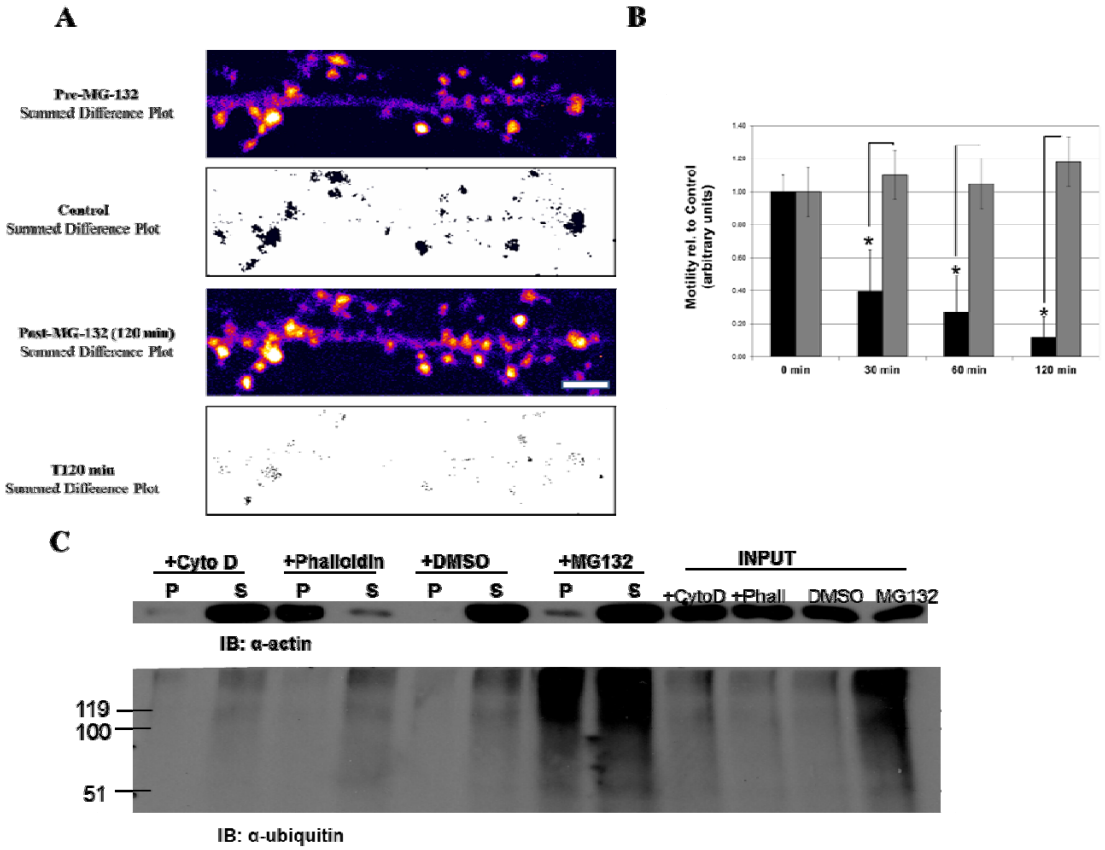

Figure 19. Actin based spine motility is proteasomal-dependent. (A)Primary hippocampal neurons (>21 DIV) were infected with YFP-actin virus. 5 min time-lapse images (20-15s intervals) were taken over a period of 2 hours following treatment with DMSO vector control (Top panel) or 5 uM MG132 (third panel). Difference plots (second, fourth panel) represent the summed change in fluorescence over time. (B) Plot of the spine motility relative to control. Gray represents control/DMSO and black is MG132 treated neurons. (N=3, *P<0.05). Error bars represent ±SEM. Scale bar = 5 µm. (C) Changes in the amount of G-actin and F-actin were examined in cultured hippocampal neurons treated with proteasome inhibitor MG132 (25uM) or vector control (DMSO). P=pellet (F-actin); S=supernatant (G-actin). Cytochalasin D and Phalloidin serve as negative and positive controls, respectively. A significant increase in F-actin levels is observed following proteasome inhibition. N=2

A

ID	Tg/WT Ratio	WT SPEC	TG SPEC	% Coverage	Predicted Protein
Kalrn	12	7	81	30	PREDICTED: kalirin, RhoGEF kinase isoform 3 (Delta kalirin-7)
Kalrn	11	7	79	27	PREDICTED: similar to kalirin, RhoGEF kinase isoform 2 (Delta kalirin-7)
Kalrn	9	6	56	28	Delta kalirin-7 homolog
Kalrn	42	1	42	16	PREDICTED: kalirin, RhoGEF kinase isoform 6 (Delta kalirin-7)
Kalrn	3	5	13	28	PREDICTED: kalirin, RhoGEF kinase isoform 2 (kalirin-7)
Kalrn	7	0	7	10	PREDICTED: kalirin, RhoGEF kinase isoform 4 (kalirin-7)
Kalrn	6	0	6	8	KALIRIN-12A homolog
Kalrn	1	5	6	25	PREDICTED: kalirin, RhoGEF kinase isoform 7

B

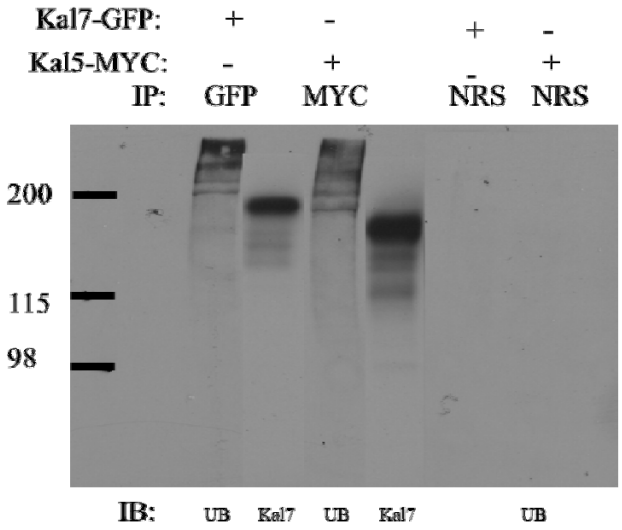

Figure 20. **Kalirin-5 and Kalirin-7 are ubiquitinated.** (A) Kalirin isoform peptide summary from mass spectrometry screen for synaptic ubiquitinated protein. Kalirin-5 (delta-Kalirin-7) hits are highlighted in yellow. Average kalirin ratio and kalirin-5 ratio are calculated and highlighted in gray. (B) HEK-293T cells co-expressing kalirin-7GFP or kalirin-5-Myc along with HA-ubiquitin were precipitated with α-GFP or α-Myc antibodies. Myc immunoprecipitates were analyzed via western blot with α-ubiquitin or α-myc antibodies.

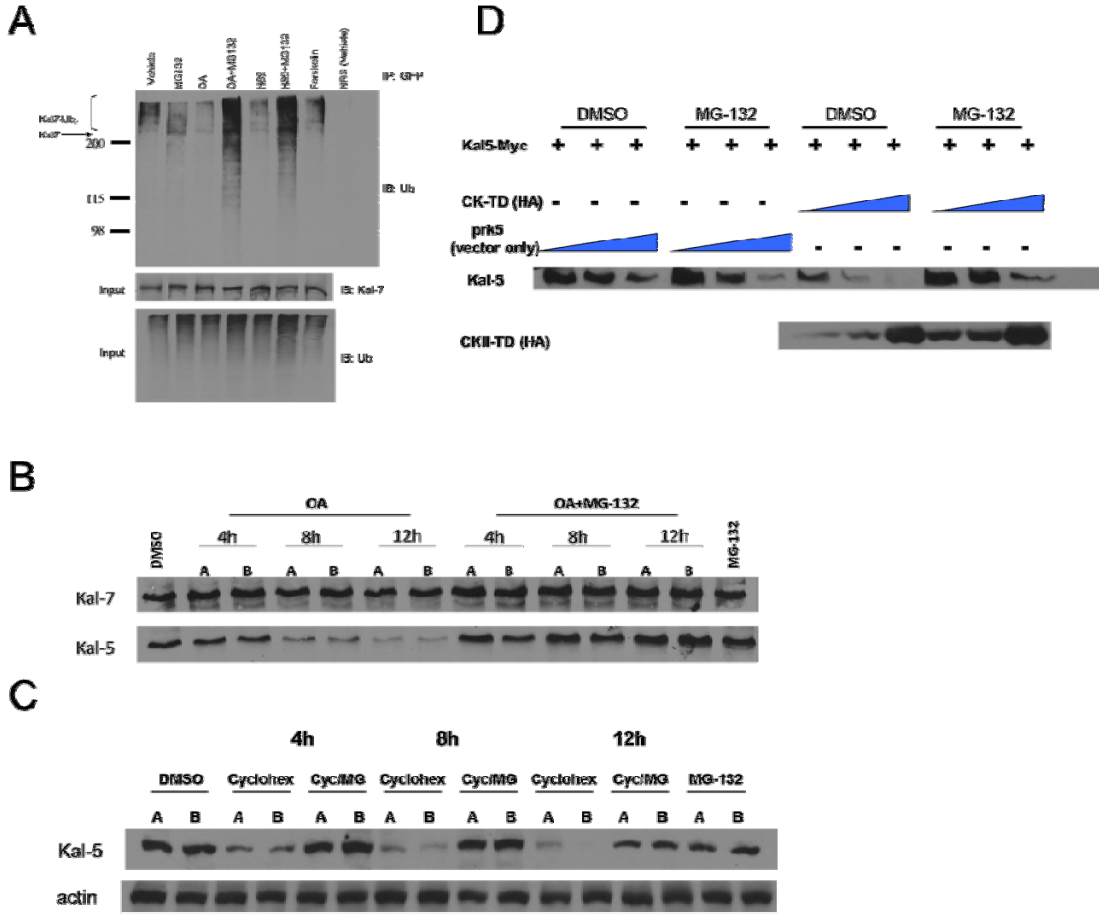

Figure 21. PP1/2 and PKA activity affect the ubiquitination and stability of Kalirin-7 and Kalirin-5. (A) HEK-293T cells co-expressing Kal7-GFP and HA-ubiquitin are treated with PP1/2 inhibitor okadaic acid (OA - 1μM), PKA inhibitor H-89 (2 μM), or PKA agonist Forskolin (10 μM) with or without MG-132 (10 μM) for 8 hours. Lysates are immunoprecipitated with α-GFP and examined via western blot using α-ubiquitin (Top, Bottom) and Kalirin-7 (Middle). Representative blot of 3 independent experiments. (B) Cultured rat cortical neurons (DIV 18) were treated with okadaic acid (1μM) for 4, 8, or 12h with and without MG-132 (10 μM). Lysates were analyzed via western blot, with α-pan Kalirin antibody. Representative blot from 3 independent experiments. (C) Cultured rat cortical neurons (DIV 18) were treated with cycloheximide (50 μM) for 4, 8, or 12h with and without MG-132 (10 μM). Lysates were analyzed via western blot, with α-pan Kalirin antibody. Representative blot from 2 independent experiments. (D) HEK293T cells co-expressing Kal5-Myc with HA-αCaMKII-TD or pRK5 vector at 50 ng, 150 ng, or 500ng were treated with DMSO or MG-132 (10 μM) for 4 hours. Lysates were examined via western blot with α-Myc or α-HA antibodies. Representative blot from 3 independent experiments.

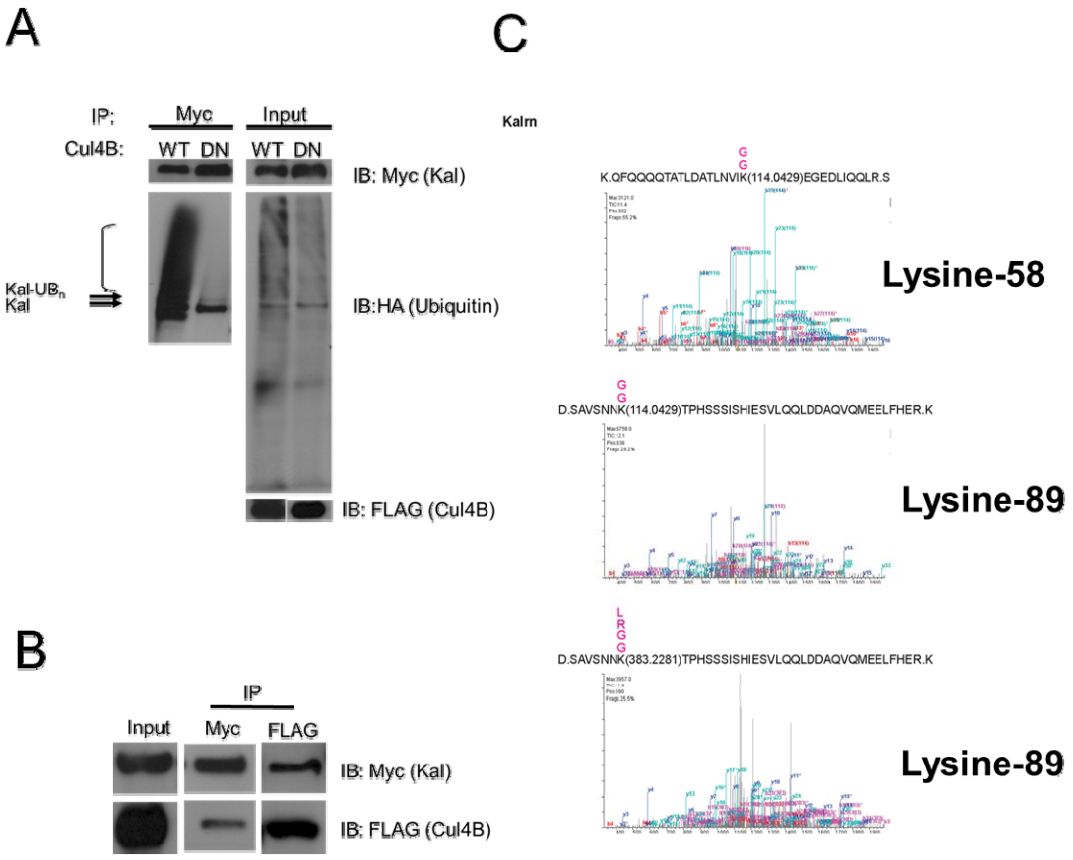

Figure 22. Kalirin-5 is ubiquitinated by Cul4B. (A) HEK293T cells expressing Kal5-Myc, HA-ubiquitin, and wild-type (WT) or dominant-negative (DN) Cul4B-FLAG are immunoprecipitated with α-Myc and analyzed via western blot using α-HA. (B) Using the conditions as in (A), lysates are immunoprecipitated for kalirin-5 (Myc) or Cul4B (FLAG) and analyzed with α-Myc (Top panel) or α-FLAG (Bottom panel) antibodies. Representative blots from 2 independent experiments. (C) α-Myc immunoprecipitates from HEK 293T cells expressing Kal5-Myc were analyzed via MS/MS. Spectra for 2 ubiquitin-modified lysines (K58 and K89) are presented

REFERENCES

Aberle, H., A. Bauer, J. Stappert, A. Kispert, and R. Kemler. 1997. beta-catenin is a target for the ubiquitin-proteasome pathway. *EMBO J*. 16:3797-3804.

Alicia, S., Z. Angelica, S. Carlos, S. Alfonso, and L. Vaca. 2008. STIM1 converts TRPC1 from a receptor-operated to a store-operated channel: moving TRPC1 in and out of lipid rafts. *Cell Calcium*. 44:479-491.

Alroy, I., S. Tuvia, T. Greener, D. Gordon, H.M. Barr, D. Taglicht, R. Mandil-Levin, D. Ben-Avraham, D. Konforty, A. Nir, O. Levius, V. Bicoviski, M. Dori, S. Cohen, L. Yaar, O. Erez, O. Propheta-Meiran, M. Koskas, E. Caspi-Bachar, I. Alchanati, A. Sela-Brown, H. Moskowitz, U. Tessmer, U. Schubert, and Y. Reiss. 2005. The trans-Golgi network-associated human ubiquitin-protein ligase POSH is essential for HIV type 1 production. *Proc Natl Acad Sci U S A*. 102:1478-1483.

Alvarez, V.A., and B.L. Sabatini. 2007. Anatomical and physiological plasticity of dendritic spines. *Annu Rev Neurosci*. 30:79-97.

Aspenstrom, P., A. Fransson, and J. Saras. 2004. Rho GTPases have diverse effects on the organization of the actin filament system. *Biochem J*. 377:327-337.

Baba, A., T. Yasui, S. Fujisawa, R.X. Yamada, M.K. Yamada, N. Nishiyama, N. Matsuki, and Y. Ikegaya. 2003. Activity-evoked capacitative Ca2+ entry: implications in synaptic plasticity. *J Neurosci*. 23:7737-7741.

Baba, Y., K. Hayashi, Y. Fujii, A. Mizushima, H. Watarai, M. Wakamori, T. Numaga, Y. Mori, M. Iino, M. Hikida, and T. Kurosaki. 2006. Coupling of STIM1 to store-operated Ca2+ entry through its constitutive and inducible movement in the endoplasmic reticulum. *Proc Natl Acad Sci U S A*. 103:16704-16709.

Bern, M., D. Goldberg, W.H. McDonald, and J.R. Yates, 3rd. 2004. Automatic quality assessment of peptide tandem mass spectra. *Bioinformatics*. 20 Suppl 1:i49-54.

Berna-Erro, A., A. Braun, R. Kraft, C. Kleinschnitz, M.K. Schuhmann, D. Stegner, T. Wultsch, J. Eilers, S.G. Meuth, G. Stoll, and B. Nieswandt. 2009. STIM2 regulates capacitive Ca2+ entry in neurons and plays a key role in hypoxic neuronal cell death. *Sci Signal*. 2:ra67.

Berridge, M.J., P. Lipp, and M.D. Bootman. 2000. The versatility and universality of calcium signalling. *Nat Rev Mol Cell Biol*. 1:11-21.

Bingol, B., and E.M. Schuman. 2006. Activity-dependent dynamics and sequestration of proteasomes in dendritic spines. *Nature*. 441:1144-1148.

Bingol, B., and M. Sheng. 2011. Deconstruction for reconstruction: the role of proteolysis in neural plasticity and disease. *Neuron*. 69:22-32.

Bird, G.S., S.Y. Hwang, J.T. Smyth, M. Fukushima, R.R. Boyles, and J.W. Putney, Jr. 2009. STIM1 is a calcium sensor specialized for digital signaling. *Curr Biol*. 19:1724-1729.

Bishop, A.L., and A. Hall. 2000. Rho GTPases and their effector proteins. *Biochem J*. 348 Pt 2:241-255.

Blanchard, A., V. Ohanian, and D. Critchley. 1989. The structure and function of alpha-actinin. *J Muscle Res Cell Motil*. 10:280-289.

Bourne, J., and K.M. Harris. 2007. Do thin spines learn to be mushroom spines that remember? *Curr Opin Neurobiol*. 17:381-386.

Brandman, O., J. Liou, W.S. Park, and T. Meyer. 2007. STIM2 is a feedback regulator that stabilizes basal cytosolic and endoplasmic reticulum Ca2+ levels. *Cell*. 131:1327-1339.

Brooks, C.L., and W. Gu. 2003. Ubiquitination, phosphorylation and acetylation: the molecular basis for p53 regulation. *Curr Opin Cell Biol*. 15:164-171.

Cahalan, M.D. 2009. STIMulating store-operated Ca(2+) entry. *Nat Cell Biol*. 11:669-677.

Calloway, N., M. Vig, J.P. Kinet, D. Holowka, and B. Baird. 2009. Molecular clustering of STIM1 with Orai1/CRACM1 at the plasma membrane depends dynamically on depletion of Ca2+ stores and on electrostatic interactions. *Mol Biol Cell*. 20:389-399.

Carlin, R.K., D.J. Grab, R.S. Cohen, and P. Siekevitz. 1980. Isolation and characterization of postsynaptic densities from various brain regions: enrichment of different types of postsynaptic densities. *J Cell Biol*. 86:831-845.

Carlisle, H.J., and M.B. Kennedy. 2005. Spine architecture and synaptic plasticity. *Trends Neurosci*. 28:182-187.

Cheng, D., C.C. Hoogenraad, J. Rush, E. Ramm, M.A. Schlager, D.M. Duong, P. Xu, S.R. Wijayawardana, J. Hanfelt, T. Nakagawa, M. Sheng, and J. Peng. 2006. Relative and absolute quantification of postsynaptic density proteome

isolated from rat forebrain and cerebellum. *Mol Cell Proteomics*. 5:1158-1170.

Chesarone, M.A., A.G. DuPage, and B.L. Goode. 2010. Unleashing formins to remodel the actin and microtubule cytoskeletons. *Nat Rev Mol Cell Biol*. 11:62-74.

Cho, K.O., C.A. Hunt, and M.B. Kennedy. 1992. The rat brain postsynaptic density fraction contains a homolog of the Drosophila discs-large tumor suppressor protein. *Neuron*. 9:929-942.

Ciani, B., R. Layfield, J.R. Cavey, P.W. Sheppard, and M.S. Searle. 2003. Structure of the ubiquitin-associated domain of p62 (SQSTM1) and implications for mutations that cause Paget's disease of bone. *J Biol Chem*. 278:37409-37412.

Cingolani, L.A., and Y. Goda. 2008. Actin in action: the interplay between the actin cytoskeleton and synaptic efficacy. *Nat Rev Neurosci*. 9:344-356.

Cline, H. 2005. Synaptogenesis: a balancing act between excitation and inhibition. *Curr Biol*. 15:R203-205.

Colledge, M., E.M. Snyder, R.A. Crozier, J.A. Soderling, Y. Jin, L.K. Langeberg, H. Lu, M.F. Bear, and J.D. Scott. 2003. Ubiquitination regulates PSD-95 degradation and AMPA receptor surface expression. *Neuron*. 40:595-607.

Collins, M.O., L. Yu, M.P. Coba, H. Husi, I. Campuzano, W.P. Blackstock, J.S. Choudhary, and S.G. Grant. 2005. Proteomic analysis of in vivo phosphorylated synaptic proteins. *J Biol Chem*. 280:5972-5982.

Csutora, P., K. Peter, H. Kilic, K.M. Park, V. Zarayskiy, T. Gwozdz, and V.M. Bolotina. 2008. Novel role for STIM1 as a trigger for calcium influx factor production. *J Biol Chem*. 283:14524-14531.

Danielsen, J.M., K.B. Sylvestersen, S. Bekker-Jensen, D. Szklarczyk, J.W. Poulsen, H. Horn, L.J. Jensen, N. Mailand, and M.L. Nielsen. 2010. Mass spectrometric analysis of lysine ubiquitylation reveals promiscuity at site level. *Mol Cell Proteomics*.

Daou, S., N. Mashtalir, I. Hammond-Martel, H. Pak, H. Yu, G. Sui, J.L. Vogel, T.M. Kristie, and B. Affar el. 2011. Crosstalk between O-GlcNAcylation and proteolytic cleavage regulates the host cell factor-1 maturation pathway. *Proc Natl Acad Sci U S A*. 108:2747-2752.

Delahunty, C.M., and J.R. Yates, 3rd. 2007. MudPIT: multidimensional protein identification technology. *Biotechniques*. 43:563, 565, 567 passim.

Denis, N.J., J. Vasilescu, J.P. Lambert, J.C. Smith, and D. Figeys. 2007. Tryptic digestion of ubiquitin standards reveals an improved strategy for identifying ubiquitinated proteins by mass spectrometry. *Proteomics*. 7:868-874.

Dent, E.W., E.B. Merriam, and X. Hu. 2010. The dynamic cytoskeleton: backbone of dendritic spine plasticity. *Curr Opin Neurobiol*.

Deshaies, R.J., and C.A. Joazeiro. 2009. RING domain E3 ubiquitin ligases. *Annu Rev Biochem*. 78:399-434.

Deveraux, Q., V. Ustrell, C. Pickart, and M. Rechsteiner. 1994. A 26 S protease subunit that binds ubiquitin conjugates. *J Biol Chem*. 269:7059-7061.

Dillon, C., and Y. Goda. 2005. The actin cytoskeleton: integrating form and function at the synapse. *Annu Rev Neurosci*. 28:25-55.

Dominguez, R., and K.C. Holmes. 2010. Actin Structure And Function. *Annu Rev Biophys*.

Ehlers, M.D. 2003. Activity level controls postsynaptic composition and signaling via the ubiquitin-proteasome system. *Nat Neurosci*. 6:231-242.

Emptage, N.J., C.A. Reid, and A. Fine. 2001. Calcium stores in hippocampal synaptic boutons mediate short-term plasticity, store-operated Ca2+ entry, and spontaneous transmitter release. *Neuron*. 29:197-208.

Eng, J., McCormack, A., and Yates, J. 1994. An Approach to Correlate Tandem Mass Spectral Data of Peptides with Amino Acid Sequences in a Protein Database. *j Am Chem Soc Mass Spectrom*. 5:976-989.

Ethell, I.M., and E.B. Pasquale. 2005. Molecular mechanisms of dendritic spine development and remodeling. *Prog Neurobiol*. 75:161-205.

Fifkova, E., and R.J. Delay. 1982. Cytoplasmic actin in neuronal processes as a possible mediator of synaptic plasticity. *J Cell Biol*. 95:345-350.

Fischer, M., S. Kaech, D. Knutti, and A. Matus. 1998. Rapid actin-based plasticity in dendritic spines. *Neuron*. 20:847-854.

Fischer, M., S. Kaech, U. Wagner, H. Brinkhaus, and A. Matus. 2000. Glutamate receptors regulate actin-based plasticity in dendritic spines. *Nat Neurosci*. 3:887-894.

Flick, K., I. Ouni, J.A. Wohlschlegel, C. Capati, W.H. McDonald, J.R. Yates, and P. Kaiser. 2004. Proteolysis-independent regulation of the transcription factor Met4 by a single Lys 48-linked ubiquitin chain. *Nat Cell Biol*. 6:634-641.

Gibson, D.A., and L. Ma. 2011. Developmental regulation of axon branching in the vertebrate nervous system. *Development*. 138:183-195.

Glickman, M.H., D.M. Rubin, H. Fu, C.N. Larsen, O. Coux, I. Wefes, G. Pfeifer, Z. Cjeka, R. Vierstra, W. Baumeister, V. Fried, and D. Finley. 1999. Functional analysis of the proteasome regulatory particle. *Mol Biol Rep*. 26:21-28.

Grant, S.G. 2006. The synapse proteome and phosphoproteome: a new paradigm for synapse biology. *Biochem Soc Trans*. 34:59-63.

Halpain, S. 2000. Actin and the agile spine: how and why do dendritic spines dance? *Trends Neurosci*. 23:141-146.

Halpain, S., A. Hipolito, and L. Saffer. 1998. Regulation of F-actin stability in dendritic spines by glutamate receptors and calcineurin. *J Neurosci*. 18:9835-9844.

Harris, K.M. 1999. Structure, development, and plasticity of dendritic spines. *Curr Opin Neurobiol*. 9:343-348.

Hauser, C.T., and R.Y. Tsien. 2007. A hexahistidine-Zn2+-dye label reveals STIM1 surface exposure. *Proc Natl Acad Sci U S A*. 104:3693-3697.

Hayden, M.S., and S. Ghosh. 2008. Shared principles in NF-kappaB signaling. *Cell*. 132:344-362.

Heasman, S.J., and A.J. Ridley. 2008. Mammalian Rho GTPases: new insights into their functions from in vivo studies. *Nat Rev Mol Cell Biol*. 9:690-701.

Henley, J.R., K.H. Huang, D. Wang, and M.M. Poo. 2004. Calcium mediates bidirectional growth cone turning induced by myelin-associated glycoprotein. *Neuron*. 44:909-916.

Hershko, A., and A. Ciechanover. 1998. The ubiquitin system. *Annu Rev Biochem*. 67:425-479.

Hewavitharana, T., X. Deng, Y. Wang, M.F. Ritchie, G.V. Girish, J. Soboloff, and D.L. Gill. 2008. Location and function of STIM1 in the activation of Ca2+ entry signals. *J Biol Chem*. 283:26252-26262.

Hicke, L., and R. Dunn. 2003. Regulation of membrane protein transport by ubiquitin and ubiquitin-binding proteins. *Annu Rev Cell Dev Biol*. 19:141-172.

Hochstrasser, M. 2006. Lingering mysteries of ubiquitin-chain assembly. *Cell*. 124:27-34.

Holtmaat, A., and K. Svoboda. 2009. Experience-dependent structural synaptic plasticity in the mammalian brain. *Nat Rev Neurosci*. 10:647-658.

Honkura, N., M. Matsuzaki, J. Noguchi, G.C. Ellis-Davies, and H. Kasai. 2008. The subspine organization of actin fibers regulates the structure and plasticity of dendritic spines. *Neuron*. 57:719-729.

Hoogenraad, C.C., M.I. Feliu-Mojer, S.A. Spangler, A.D. Milstein, A.W. Dunah, A.Y. Hung, and M. Sheng. 2007. Liprinalpha1 degradation by calcium/calmodulin-dependent protein kinase II regulates LAR receptor tyrosine phosphatase distribution and dendrite development. *Dev Cell*. 12:587-602.

Huang da, W., B.T. Sherman, and R.A. Lempicki. 2009a. Bioinformatics enrichment tools: paths toward the comprehensive functional analysis of large gene lists. *Nucleic Acids Res*. 37:1-13.

Huang da, W., B.T. Sherman, and R.A. Lempicki. 2009b. Systematic and integrative analysis of large gene lists using DAVID bioinformatics resources. *Nat Protoc*. 4:44-57.

Hunter, T. 2007. The age of crosstalk: phosphorylation, ubiquitination, and beyond. *Mol Cell*. 28:730-738.

Ikeda, F., and I. Dikic. 2008. Atypical ubiquitin chains: new molecular signals. 'Protein Modifications: Beyond the Usual Suspects' review series. *EMBO Rep*. 9:536-542.

Jaffe, A.B., and A. Hall. 2005. Rho GTPases: biochemistry and biology. *Annu Rev Cell Dev Biol*. 21:247-269.

Johnson, R.C., P. Penzes, B.A. Eipper, and R.E. Mains. 2000. Isoforms of kalirin, a neuronal Dbl family member, generated through use of different 5'- and 3'-ends along with an internal translational initiation site. *J Biol Chem*. 275:19324-19333.

Karin, M., and Y. Ben-Neriah. 2000. Phosphorylation meets ubiquitination: the control of NF-[kappa]B activity. *Annu Rev Immunol*. 18:621-663.

Kennedy, M.B., H.C. Beale, H.J. Carlisle, and L.R. Washburn. 2005. Integration of biochemical signalling in spines. *Nat Rev Neurosci*. 6:423-434.

Kim, J.H., and R.L. Huganir. 1999. Organization and regulation of proteins at synapses. *Curr Opin Cell Biol*. 11:248-254.

Kirkpatrick, D.S., C. Denison, and S.P. Gygi. 2005a. Weighing in on ubiquitin: the expanding role of mass-spectrometry-based proteomics. *Nat Cell Biol.* 7:750-757.

Kirkpatrick, D.S., N.A. Hathaway, J. Hanna, S. Elsasser, J. Rush, D. Finley, R.W. King, and S.P. Gygi. 2006. Quantitative analysis of in vitro ubiquitinated cyclin B1 reveals complex chain topology. *Nat Cell Biol.* 8:700-710.

Kirkpatrick, D.S., S.F. Weldon, G. Tsaprailis, D.C. Liebler, and A.J. Gandolfi. 2005b. Proteomic identification of ubiquitinated proteins from human cells expressing His-tagged ubiquitin. *Proteomics.* 5:2104-2111.

Landis, D.M., and T.S. Reese. 1983. Cytoplasmic organization in cerebellar dendritic spines. *J Cell Biol.* 97:1169-1178.

Layfield, R., D. Tooth, M. Landon, S. Dawson, J. Mayer, and A. Alban. 2001. Purification of poly-ubiquitinated proteins by S5a-affinity chromatography. *Proteomics*. 1:773-777.

Lee, H.K. 2006. Synaptic plasticity and phosphorylation. *Pharmacol Ther.* 112:810-832.

Lee, S.H., J.H. Choi, N. Lee, H.R. Lee, J.I. Kim, N.K. Yu, S.L. Choi, S.H. Lee, H. Kim, and B.K. Kaang. 2008. Synaptic protein degradation underlies destabilization of retrieved fear memory. *Science.* 319:1253-1256.

Lee, S.H., and R. Dominguez. 2010. Regulation of actin cytoskeleton dynamics in cells. *Mol Cells.* 29:311-325.

Lewis, R.S. 2007. The molecular choreography of a store-operated calcium channel. *Nature.* 446:284-287.

Li, W., and Y. Ye. 2008. Polyubiquitin chains: functions, structures, and mechanisms. *Cell Mol Life Sci.* 65:2397-2406.

Liou, J., M. Fivaz, T. Inoue, and T. Meyer. 2007. Live-cell imaging reveals sequential oligomerization and local plasma membrane targeting of stromal interaction molecule 1 after Ca2+ store depletion. *Proc Natl Acad Sci U S A.* 104:9301-9306.

Liou, J., M.L. Kim, W.D. Heo, J.T. Jones, J.W. Myers, J.E. Ferrell, Jr., and T. Meyer. 2005. STIM is a Ca2+ sensor essential for Ca2+-store-depletion-triggered Ca2+ influx. *Curr Biol.* 15:1235-1241.

Lisman, J., H. Schulman, and H. Cline. 2002. The molecular basis of CaMKII function in synaptic and behavioural memory. *Nat Rev Neurosci.* 3:175-190.

Lisman, J.E. 1985. A mechanism for memory storage insensitive to molecular turnover: a bistable autophosphorylating kinase. *Proc Natl Acad Sci U S A*. 82:3055-3057.

Long, J., T.R. Gallagher, J.R. Cavey, P.W. Sheppard, S.H. Ralston, R. Layfield, and M.S. Searle. 2008. Ubiquitin recognition by the ubiquitin-associated domain of p62 involves a novel conformational switch. *J Biol Chem*. 283:5427-5440.

Luik, R.M., B. Wang, M. Prakriya, M.M. Wu, and R.S. Lewis. 2008. Oligomerization of STIM1 couples ER calcium depletion to CRAC channel activation. *Nature*. 454:538-542.

Lynch, E.A., J. Stall, G. Schmidt, P. Chavrier, and C. D'Souza-Schorey. 2006. Proteasome-mediated degradation of Rac1-GTP during epithelial cell scattering. *Mol Biol Cell*. 17:2236-2242.

Ma, X.M., J. Huang, Y. Wang, B.A. Eipper, and R.E. Mains. 2003. Kalirin, a multifunctional Rho guanine nucleotide exchange factor, is necessary for maintenance of hippocampal pyramidal neuron dendrites and dendritic spines. *J Neurosci*. 23:10593-10603.

Ma, X.M., J.P. Huang, E.J. Kim, Q. Zhu, G.A. Kuchel, R.E. Mains, and B.A. Eipper. 2010. Kalirin-7, an important component of excitatory synapses, is regulated by estradiol in hippocampal neurons. *Hippocampus*.

Ma, X.M., D.D. Kiraly, E.D. Gaier, Y. Wang, E.J. Kim, E.S. Levine, B.A. Eipper, and R.E. Mains. 2008a. Kalirin-7 is required for synaptic structure and function. *J Neurosci*. 28:12368-12382.

Ma, X.M., Y. Wang, F. Ferraro, R.E. Mains, and B.A. Eipper. 2008b. Kalirin-7 is an essential component of both shaft and spine excitatory synapses in hippocampal interneurons. *J Neurosci*. 28:711-724.

Mabb, A.M., and M.D. Ehlers. 2010. Ubiquitination in postsynaptic function and plasticity. *Annu Rev Cell Dev Biol*. 26:179-210.

MacCoss, M.J., C.C. Wu, and J.R. Yates, 3rd. 2002. Probability-based validation of protein identifications using a modified SEQUEST algorithm. *Anal Chem*. 74:5593-5599.

Mains, R.E., D.D. Kiraly, J.E. Eipper-Mains, X. Ma, and B.A. Eipper. 2011. Kalrn promoter usage and isoform expression respond to chronic cocaine exposure. *BMC Neurosci*. 12:20.

Manji, S.S., N.J. Parker, R.T. Williams, L. van Stekelenburg, R.B. Pearson, M. Dziadek, and P.J. Smith. 2000. STIM1: a novel phosphoprotein located at the cell surface. *Biochim Biophys Acta*. 1481:147-155.

Mansuy, I.M., and S. Shenolikar. 2006. Protein serine/threonine phosphatases in neuronal plasticity and disorders of learning and memory. *Trends Neurosci*. 29:679-686.

Marotti, L.A., Jr., R. Newitt, Y. Wang, R. Aebersold, and H.G. Dohlman. 2002. Direct identification of a G protein ubiquitination site by mass spectrometry. *Biochemistry*. 41:5067-5074.

Matsuzaki, M., N. Honkura, G.C. Ellis-Davies, and H. Kasai. 2004. Structural basis of long-term potentiation in single dendritic spines. *Nature*. 429:761-766.

Mattson, M.P., H. Zhu, J. Yu, and M.S. Kindy. 2000. Presenilin-1 mutation increases neuronal vulnerability to focal ischemia in vivo and to hypoxia and glucose deprivation in cell culture: involvement of perturbed calcium homeostasis. *J Neurosci*. 20:1358-1364.

Matus, A. 2000. Actin-based plasticity in dendritic spines. *Science*. 290:754-758.

Mauna, J.C., T. Miyamae, B. Pulli, and E. Thiels. 2010. Protein phosphatases 1 and 2A are both required for long-term depression and associated dephosphorylation of cAMP response element binding protein in hippocampal area CA1 in vivo. *Hippocampus*.

May, V., M.R. Schiller, B.A. Eipper, and R.E. Mains. 2002. Kalirin Dbl-homology guanine nucleotide exchange factor 1 domain initiates new axon outgrowths via RhoG-mediated mechanisms. *J Neurosci*. 22:6980-6990.

McPherson, C.E., B.A. Eipper, and R.E. Mains. 2002. Genomic organization and differential expression of Kalirin isoforms. *Gene*. 284:41-51.

McPherson, C.E., B.A. Eipper, and R.E. Mains. 2004. Kalirin expression is regulated by multiple promoters. *J Mol Neurosci*. 22:51-62.

Muik, M., M. Fahrner, I. Derler, R. Schindl, J. Bergsmann, I. Frischauf, K. Groschner, and C. Romanin. 2009. A Cytosolic Homomerization and a Modulatory Domain within STIM1 C Terminus Determine Coupling to ORAI1 Channels. *J Biol Chem*. 284:8421-8426.

Munton, R.P., S. Vizi, and I.M. Mansuy. 2004. The role of protein phosphatase-1 in the modulation of synaptic and structural plasticity. *FEBS Lett*. 567:121-128.

Newey, S.E., V. Velamoor, E.E. Govek, and L. Van Aelst. 2005. Rho GTPases, dendritic structure, and mental retardation. *J Neurobiol*. 64:58-74.

Newton, K., M.L. Matsumoto, I.E. Wertz, D.S. Kirkpatrick, J.R. Lill, J. Tan, D. Dugger, N. Gordon, S.S. Sidhu, F.A. Fellouse, L. Komuves, D.M. French, R.E. Ferrando, C. Lam, D. Compaan, C. Yu, I. Bosanac, S.G. Hymowitz,

R.F. Kelley, and V.M. Dixit. 2008. Ubiquitin chain editing revealed by polyubiquitin linkage-specific antibodies. *Cell*. 134:668-678.

Okamoto, K., T. Nagai, A. Miyawaki, and Y. Hayashi. 2004. Rapid and persistent modulation of actin dynamics regulates postsynaptic reorganization underlying bidirectional plasticity. *Nat Neurosci*. 7:1104-1112.

Okamoto, K., R. Narayanan, S.H. Lee, K. Murata, and Y. Hayashi. 2007. The role of CaMKII as an F-actin-bundling protein crucial for maintenance of dendritic spine structure. *Proc Natl Acad Sci U S A*. 104:6418-6423.

Olofsson, B. 1999. Rho guanine dissociation inhibitors: pivotal molecules in cellular signalling. *Cell Signal*. 11:545-554.

Pak, D.T., and M. Sheng. 2003. Targeted protein degradation and synapse remodeling by an inducible protein kinase. *Science*. 302:1368-1373.

Parekh, A.B., and J.W. Putney, Jr. 2005. Store-operated calcium channels. *Physiol Rev*. 85:757-810.

Park, C.Y., P.J. Hoover, F.M. Mullins, P. Bachhawat, E.D. Covington, S. Raunser, T. Walz, K.C. Garcia, R.E. Dolmetsch, and R.S. Lewis. 2009. STIM1 clusters and activates CRAC channels via direct binding of a cytosolic domain to Orai1. *Cell*. 136:876-890.

Patrick, G.N. 2006. Synapse formation and plasticity: recent insights from the perspective of the ubiquitin proteasome system. *Curr Opin Neurobiol*. 16:90-94.

Peng, J. 2008. Evaluation of proteomic strategies for analyzing ubiquitinated proteins. *BMB Rep*. 41:177-183.

Peng, J., J.E. Elias, C.C. Thoreen, L.J. Licklider, and S.P. Gygi. 2003a. Evaluation of multidimensional chromatography coupled with tandem mass spectrometry (LC/LC-MS/MS) for large-scale protein analysis: the yeast proteome. *J Proteome Res*. 2:43-50.

Peng, J., D. Schwartz, J.E. Elias, C.C. Thoreen, D. Cheng, G. Marsischky, J. Roelofs, D. Finley, and S.P. Gygi. 2003b. A proteomics approach to understanding protein ubiquitination. *Nat Biotechnol*. 21:921-926.

Penzes, P., R.C. Johnson, M.R. Alam, V. Kambampati, R.E. Mains, and B.A. Eipper. 2000. An isoform of kalirin, a brain-specific GDP/GTP exchange factor, is enriched in the postsynaptic density fraction. *J Biol Chem*. 275:6395-6403.

Penzes, P., R.C. Johnson, V. Kambampati, R.E. Mains, and B.A. Eipper. 2001a. Distinct roles for the two Rho GDP/GTP exchange factor domains of kalirin in regulation of neurite growth and neuronal morphology. *J Neurosci.* 21:8426-8434.

Penzes, P., R.C. Johnson, R. Sattler, X. Zhang, R.L. Huganir, V. Kambampati, R.E. Mains, and B.A. Eipper. 2001b. The neuronal Rho-GEF Kalirin-7 interacts with PDZ domain-containing proteins and regulates dendritic morphogenesis. *Neuron*. 29:229-242.

Penzes, P., and K.A. Jones. 2008. Dendritic spine dynamics--a key role for kalirin-7. *Trends Neurosci*. 31:419-427.

Pickart, C.M. 2004. Back to the future with ubiquitin. *Cell*. 116:181-190.

Pickart, C.M., and M.J. Eddins. 2004. Ubiquitin: structures, functions, mechanisms. *Biochim Biophys Acta*. 1695:55-72.

Pocklington, A.J., J.D. Armstrong, and S.G. Grant. 2006a. Organization of brain complexity--synapse proteome form and function. *Brief Funct Genomic Proteomic*. 5:66-73.

Pocklington, A.J., M. Cumiskey, J.D. Armstrong, and S.G. Grant. 2006b. The proteomes of neurotransmitter receptor complexes form modular networks with distributed functionality underlying plasticity and behaviour. *Mol Syst Biol*. 2:2006 0023.

Putney, J.W., Jr. 2007. New molecular players in capacitative Ca2+ entry. *J Cell Sci*. 120:1959-1965.

Radivojac, P., V. Vacic, C. Haynes, R.R. Cocklin, A. Mohan, J.W. Heyen, M.G. Goebl, and L.M. Iakoucheva. 2010. Identification, analysis, and prediction of protein ubiquitination sites. *Proteins*. 78:365-380.

Renner, M., C.G. Specht, and A. Triller. 2008. Molecular dynamics of postsynaptic receptors and scaffold proteins. *Curr Opin Neurobiol*. 18:532-540.

Ris, L., I. Dewachter, D. Reverse, E. Godaux, and F. Van Leuven. 2003. Capacitative calcium entry induces hippocampal long term potentiation in the absence of presenilin-1. *J Biol Chem*. 278:44393-44399.

Roos, J., P.J. DiGregorio, A.V. Yeromin, K. Ohlsen, M. Lioudyno, S. Zhang, O. Safrina, J.A. Kozak, S.L. Wagner, M.D. Cahalan, G. Velicelebi, and K.A. Stauderman. 2005. STIM1, an essential and conserved component of store-operated Ca2+ channel function. *J Cell Biol*. 169:435-445.

Sadygov, R.G., J. Eng, E. Durr, A. Saraf, H. McDonald, M.J. MacCoss, and J.R. Yates, 3rd. 2002. Code developments to improve the efficiency of automated MS/MS spectra interpretation. *J Proteome Res*. 1:211-215.

Schiller, M.R., F. Ferraro, Y. Wang, X.M. Ma, C.E. McPherson, J.A. Sobota, N.I. Schiller, R.E. Mains, and B.A. Eipper. 2008. Autonomous functions for the Sec14p/spectrin-repeat region of Kalirin. *Exp Cell Res*. 314:2674-2691.

Schmidt, A., and A. Hall. 2002. Guanine nucleotide exchange factors for Rho GTPases: turning on the switch. *Genes Dev*. 16:1587-1609.

Schrimpf, S.P., V. Meskenaite, E. Brunner, D. Rutishauser, P. Walther, J. Eng, R. Aebersold, and P. Sonderegger. 2005. Proteomic analysis of synaptosomes using isotope-coded affinity tags and mass spectrometry. *Proteomics*. 5:2531-2541.

Schubert, V., and C.G. Dotti. 2007. Transmitting on actin: synaptic control of dendritic architecture. *J Cell Sci*. 120:205-212.

Sheng, M., and C.C. Hoogenraad. 2007. The postsynaptic architecture of excitatory synapses: a more quantitative view. *Annu Rev Biochem*. 76:823-847.

Shioda, N., H. Beppu, T. Fukuda, E. Li, I. Kitajima, and K. Fukunaga. 2011. Aberrant calcium/calmodulin-dependent protein kinase II (CaMKII) activity is associated with abnormal dendritic spine morphology in the ATRX mutant mouse brain. *J Neurosci*. 31:346-358.

Skaug, B., X. Jiang, and Z.J. Chen. 2009. The role of ubiquitin in NF-kappaB regulatory pathways. *Annu Rev Biochem*. 78:769-796.

Smith, I.F., J.P. Boyle, P.F. Vaughan, H.A. Pearson, R.F. Cowburn, and C.S. Peers. 2002. Ca(2+) stores and capacitative Ca(2+) entry in human neuroblastoma (SH-SY5Y) cells expressing a familial Alzheimer's disease presenilin-1 mutation. *Brain Res*. 949:105-111.

Smyth, J.T., W.I. Dehaven, G.S. Bird, and J.W. Putney, Jr. 2008. Ca2+-store-dependent and -independent reversal of Stim1 localization and function. *J Cell Sci*. 121:762-772.

Smyth, J.T., J.G. Petranka, R.R. Boyles, W.I. DeHaven, M. Fukushima, K.L. Johnson, J.G. Williams, and J.W. Putney, Jr. 2009. Phosphorylation of STIM1 underlies suppression of store-operated calcium entry during mitosis. *Nat Cell Biol*. 11:1465-1472.

Soderling, S.H., and J.D. Scott. 2006. WAVE signalling: from biochemistry to biology. *Biochem Soc Trans*. 34:73-76.

Spassova, M.A., J. Soboloff, L.P. He, W. Xu, M.A. Dziadek, and D.L. Gill. 2006. STIM1 has a plasma membrane role in the activation of store-operated Ca(2+) channels. *Proc Natl Acad Sci U S A*. 103:4040-4045.

Star, E.N., D.J. Kwiatkowski, and V.N. Murthy. 2002. Rapid turnover of actin in dendritic spines and its regulation by activity. *Nat Neurosci*. 5:239-246.

Stathopulos, P.B., G.Y. Li, M.J. Plevin, J.B. Ames, and M. Ikura. 2006. Stored Ca2+ depletion-induced oligomerization of stromal interaction molecule 1 (STIM1) via the EF-SAM region: An initiation mechanism for capacitive Ca2+ entry. *J Biol Chem*. 281:35855-35862.

Stossel, T.P., J. Condeelis, L. Cooley, J.H. Hartwig, A. Noegel, M. Schleicher, and S.S. Shapiro. 2001. Filamins as integrators of cell mechanics and signalling. *Nat Rev Mol Cell Biol*. 2:138-145.

Sudhof, T.C. 2004. The synaptic vesicle cycle. *Annu Rev Neurosci*. 27:509-547.

Svitkina, T., W.H. Lin, D.J. Webb, R. Yasuda, G.A. Wayman, L. Van Aelst, and S.H. Soderling. 2010. Regulation of the postsynaptic cytoskeleton: roles in development, plasticity, and disorders. *J Neurosci*. 30:14937-14942.

Tabb, D.L., W.H. McDonald, and J.R. Yates, 3rd. 2002. DTASelect and Contrast: tools for assembling and comparing protein identifications from shotgun proteomics. *J Proteome Res*. 1:21-26.

Tada, T., and M. Sheng. 2006. Molecular mechanisms of dendritic spine morphogenesis. *Curr Opin Neurobiol*. 16:95-101.

Tamarina, N.A., A. Kuznetsov, and L.H. Philipson. 2008. Reversible translocation of EYFP-tagged STIM1 is coupled to calcium influx in insulin secreting beta-cells. *Cell Calcium*. 44:533-544.

Tan, J.M., E.S. Wong, D.S. Kirkpatrick, O. Pletnikova, H.S. Ko, S.P. Tay, M.W. Ho, J. Troncoso, S.P. Gygi, M.K. Lee, V.L. Dawson, T.M. Dawson, and K.L. Lim. 2008. Lysine 63-linked ubiquitination promotes the formation and autophagic clearance of protein inclusions associated with neurodegenerative diseases. *Hum Mol Genet*. 17:431-439.

Tang, F., and K. Kalil. 2005. Netrin-1 induces axon branching in developing cortical neurons by frequency-dependent calcium signaling pathways. *J Neurosci*. 25:6702-6715.

Taylor, J., K.H. Chung, C. Figueroa, J. Zurawski, H.M. Dickson, E.J. Brace, A.W. Avery, D.L. Turner, and A.B. Vojtek. 2008. The scaffold protein POSH regulates axon outgrowth. *Mol Biol Cell*. 19:5181-5192.

Tsirigotis, M., S. Thurig, M. Dube, B.C. Vanderhyden, M. Zhang, and D.A. Gray. 2001. Analysis of ubiquitination in vivo using a transgenic mouse model. *Biotechniques*. 31:120-126, 128, 130.

Tursun, B., A. Schluter, M.A. Peters, B. Viehweger, H.P. Ostendorff, J. Soosairajah, A. Drung, M. Bossenz, S.A. Johnsen, M. Schweizer, O. Bernard, and I. Bach. 2005. The ubiquitin ligase Rnf6 regulates local LIM kinase 1 levels in axonal growth cones. *Genes Dev*. 19:2307-2319.

Tuvia, S., D. Taglicht, O. Erez, I. Alroy, I. Alchanati, V. Bicoviski, M. Dori-Bachash, D. Ben-Avraham, and Y. Reiss. 2007. The ubiquitin E3 ligase POSH regulates calcium homeostasis through spatial control of Herp. *J Cell Biol*. 177:51-61.

Waldron, R.T., A.D. Short, and D.L. Gill. 1997. Store-operated Ca2+ entry and coupling to Ca2+ pool depletion in thapsigargin-resistant cells. *J Biol Chem*. 272:6440-6447.

Wang, B., H. Suzuki, and M. Kato. 2008. Roles of mono-ubiquitinated Smad4 in the formation of Smad transcriptional complexes. *Biochem Biophys Res Commun*. 376:288-292.

Washburn, M.P., D. Wolters, and J.R. Yates, 3rd. 2001. Large-scale analysis of the yeast proteome by multidimensional protein identification technology. *Nat Biotechnol*. 19:242-247.

Wayman, G.A., Y.S. Lee, H. Tokumitsu, A.J. Silva, and T.R. Soderling. 2008. Calmodulin-kinases: modulators of neuronal development and plasticity. *Neuron*. 59:914-931.

Westphal, R.S., S.J. Tavalin, J.W. Lin, N.M. Alto, I.D. Fraser, L.K. Langeberg, M. Sheng, and J.D. Scott. 1999. Regulation of NMDA receptors by an associated phosphatase-kinase signaling complex. *Science*. 285:93-96.

Whittaker, V.P., I.A. Michaelson, and R.J. Kirkland. 1964. The separation of synaptic vesicles from nerve-ending particles ('synaptosomes'). *Biochem J*. 90:293-303.

Williams, R.T., P.V. Senior, L. Van Stekelenburg, J.E. Layton, P.J. Smith, and M.A. Dziadek. 2002. Stromal interaction molecule 1 (STIM1), a transmembrane protein with growth suppressor activity, contains an extracellular SAM domain modified by N-linked glycosylation. *Biochim Biophys Acta*. 1596:131-137.

Witze, E.S., W.M. Old, K.A. Resing, and N.G. Ahn. 2007. Mapping protein post-translational modifications with mass spectrometry. *Nat Methods*. 4:798-806.

Wooten, M.W., T. Geetha, J.R. Babu, M.L. Seibenhener, J. Peng, N. Cox, M.T. Diaz-Meco, and J. Moscat. 2008. Essential role of sequestosome 1/p62 in regulating accumulation of Lys63-ubiquitinated proteins. *J Biol Chem*. 283:6783-6789.

Wu, M.M., J. Buchanan, R.M. Luik, and R.S. Lewis. 2006. Ca2+ store depletion causes STIM1 to accumulate in ER regions closely associated with the plasma membrane. *J Cell Biol*. 174:803-813.

Wyszynski, M., J. Lin, A. Rao, E. Nigh, A.H. Beggs, A.M. Craig, and M. Sheng. 1997. Competitive binding of alpha-actinin and calmodulin to the NMDA receptor. *Nature*. 385:439-442.

Xie, Z., D.P. Srivastava, H. Photowala, L. Kai, M.E. Cahill, K.M. Woolfrey, C.Y. Shum, D.J. Surmeier, and P. Penzes. 2007. Kalirin-7 controls activity-dependent structural and functional plasticity of dendritic spines. *Neuron*. 56:640-656.

Xin, X., Y. Wang, X.M. Ma, P. Rompolas, H.T. Keutmann, R.E. Mains, and B.A. Eipper. 2008. Regulation of Kalirin by Cdk5. *J Cell Sci*. 121:2601-2611.

Xu, G., J.S. Paige, and S.R. Jaffrey. 2010. Global analysis of lysine ubiquitination by ubiquitin remnant immunoaffinity profiling. *Nat Biotechnol*. 28:868-873.

Xu, P., and J. Peng. 2008. Characterization of polyubiquitin chain structure by middle-down mass spectrometry. *Anal Chem*. 80:3438-3444.

Xu, Z., N.V. Kukekov, and L.A. Greene. 2003. POSH acts as a scaffold for a multiprotein complex that mediates JNK activation in apoptosis. *EMBO J*. 22:252-261.

Yao, I., H. Takagi, H. Ageta, T. Kahyo, S. Sato, K. Hatanaka, Y. Fukuda, T. Chiba, N. Morone, S. Yuasa, K. Inokuchi, T. Ohtsuka, G.R. Macgregor, K. Tanaka, and M. Setou. 2007. SCRAPPER-dependent ubiquitination of active zone protein RIM1 regulates synaptic vesicle release. *Cell*. 130:943-957.

Yates, J.R., 3rd. 2004. Mass spectral analysis in proteomics. *Annu Rev Biophys Biomol Struct*. 33:297-316.

Yeromin, A.V., S.L. Zhang, W. Jiang, Y. Yu, O. Safrina, and M.D. Cahalan. 2006. Molecular identification of the CRAC channel by altered ion selectivity in a mutant of Orai. *Nature*. 443:226-229.

Yi, J.J., and M.D. Ehlers. 2007. Emerging roles for ubiquitin and protein degradation in neuronal function. *Pharmacol Rev*. 59:14-39.

Yoo, A.S., I. Cheng, S. Chung, T.Z. Grenfell, H. Lee, E. Pack-Chung, M. Handler, J. Shen, W. Xia, G. Tesco, A.J. Saunders, K. Ding, M.P. Frosch, R.E. Tanzi, and T.W. Kim. 2000. Presenilin-mediated modulation of capacitative calcium entry. *Neuron*. 27:561-572.

Yuste, R., and T. Bonhoeffer. 2001. Morphological changes in dendritic spines associated with long-term synaptic plasticity. *Annu Rev Neurosci*. 24:1071-1089.

Zhang, F., S. Saha, S.A. Shabalina, and A. Kashina. 2010. Differential arginylation of actin isoforms is regulated by coding sequence-dependent degradation. *Science*. 329:1534-1537.

Zhang, S.L., Y. Yu, J. Roos, J.A. Kozak, T.J. Deerinck, M.H. Ellisman, K.A. Stauderman, and M.D. Cahalan. 2005. STIM1 is a Ca2+ sensor that activates CRAC channels and migrates from the Ca2+ store to the plasma membrane. *Nature*. 437:902-905.

Zigmond, S.H. 2004. Formin-induced nucleation of actin filaments. *Curr Opin Cell Biol*. 16:99-105.

Zou, Y., Q. Liu, B. Chen, X. Zhang, C. Guo, H. Zhou, J. Li, G. Gao, Y. Guo, C. Yan, J. Wei, C. Shao, and Y. Gong. 2007. Mutation in CUL4B, which encodes a member of cullin-RING ubiquitin ligase complex, causes X-linked mental retardation. *Am J Hum Genet*. 80:561-566.